DEVELOPMENT OF LIGHT-RESPONSIVE ACTUATORS BASED ON CONJUGATED POLYMERS/LIQUID CRYSTAL ELASTOMERS THROUGH PHOTOPOLYMERIZATION

HUANG ZHENJIA

PhD

The Hong Kong Polytechnic University

2024

The Hong Kong Polytechnic University

Department of Industrial and Systems Engineering

Development of light-responsive actuators based on conjugated polymers/liquid crystal elastomers through photopolymerization

Huang Zhenjia

A thesis submitted in partial fulfillment of the requirements for the degree of Doctor of Philosophy

August 2023

CERTIFICATE OF ORIGINALITY

I hereby declare that this thesis is my own work and that, to the best of my knowledge and belief, it reproduces no material previously published or written, nor material that has been accepted for the award of any other degree or diploma, except where due acknowledgement has been made in the text.

_____(Signed)

Huang Zhenjia (Name of student)

Abstract

Near-infrared (NIR) light-triggered liquid crystal elastomers (LCEs) actuators based on the photothermal effect have attracted tremendous scientific attention in biomedical devices and untethered robotics. By incorporating light-absorbing components in LCEs, the absorbed light can be converted into heat to induce the phase transition. By designing the mesogen alignment, reversible deformations from simple to complex modes can be realized. Most studies use inorganic nanoparticles as photothermal agents in LCEs; however, compatibility always complicates the LCE preparation and fabrication. This calls for developing organic photothermal agents filled LCEs, such as organic conjugated polymers (CPs)/LCEs, for addressing the material issues. There is no report on fabricating macro- and micro-actuators based on photothermal CPs for light-triggered actuation. It is highly appealing to develop new LCEs-based materials to fabricate different scales of actuators with fast response time. The microfabrication of LCE photoresists with room-temperature liquid crystal phases remains a challenge. Meanwhile, the applications of the inorganic nanoparticle-filled LCE macro-actuators are limited by relatively weaker actuation response due to the uneven distribution of nanoparticles in LCEs. Therefore, this thesis aimed to develop a method combining synthesis of photothermal CPs, photopolymerization techniques, and optimization of fabrication parameters for designing and fabricating light-triggered CPs/LCEs-based macro-actuators and micro-actuators for achieving controllable actuation.

To overcome the material issue, organic CPs were proposed as photothermal materials for photoresponsive LCEs. Based on molecular design strategies and Stille cross-coupling polymerization, photothermal DPP58-TBZ12 CPs were designed and synthesized to achieve NIR light absorption ability (around 746 nm), high photothermal conversion efficiency (52.7%), and photostability. As the CPs display good solubility in tetrahydrofuran and compatibility with LCEs, they were incorporated into the LCEs homogeneously with arbitrary concentrations. This presented an effective method to prepare light-responsive CPs/LCEs for actuator manufacturing.

With the CPs incorporated in the LCEs and through tailoring the mesogen alignment, 2D light-triggered macro-actuators were fabricated through one-pot UV photopolymerization for realizing various shape changes and 3D locomotion. Under NIR light irradiation, the film macro-actuators achieved multimodal shape morphing, including bending, “Swiss” rolling, and helical twisting, by controlling the alignment angles to the film's long axis. The macro-actuators had an ultrafast response time within 3 s when exposed to NIR light. With reversible and continuous helical twisting, the macro-actuators possessed locomotion ability with a high velocity of 0.47 mm/s under successive NIR light illumination.

In addition to fabricating macro-actuators, micro-actuators were fabricated through direct laser writing based on two-photon polymerization (DLW-TPP) to demonstrate the applicability of the CPs/LCEs at the microscale. It is a powerful fabrication technology to achieve the sub-micrometer resolution of 3D structures

with design freedom. To prepare DLW-TPP compatible LCE-based photoresists, the compositions were carefully tailored to make the photoresists maintain room-temperature liquid crystal phases. Moreover, incorporating CPs could lower the nematic-to-isotropic temperature of the photoresist, which would alleviate the crystallization occurrence during the printing process. To determine writing windows for producing the micro-structure with good structural fidelity, optimizing printing parameters was also performed. Through designing planar alignment and parameter optimization, the microactuator showed a large actuation strain (25.0%) within 5 s upon NIR light stimulation.

In all, this thesis presents the work for developing novel CPs as photothermal agents for LCEs-based actuators and realizing the fabrication of CPs/LCEs actuators in different dimensions and scales through different photopolymerization technologies coupled with optimization of fabrication parameters. The diverse actuation modes and fast response speed of these actuators demonstrated the great potential of CPs/LCEs for boosting the design of light-responsive LCEs and the fabrication of LCEs-based actuators at macroscale and microscale. These CPs/LCEs actuators show great prospects in 3D dynamic cell culture platforms and soft robotics.

Publications

Journal papers

1. **Huang, Z.,** Tsui, G. C. P., Yeung, K. W., Li, C., Tang, C. Y., Yang, Zhang, M., & Wong, W. Y. (2023). 4D direct laser writing of photo-triggered liquid crystal elastomer microactuators with large actuation strain. *Materials & Design*, 232, 112101.

2. Huang, Z., Tsui, G. C. P., Deng, Y., Tang, C. Y., Yang, M., Zhang, M., & Wong, W. Y. (2022). Bioinspired near-infrared light-induced ultrafast soft actuators with tunable deformation and motion based on conjugated polymers/liquid crystal elastomers. *Journal of Materials Chemistry C*. 10, 12731-12740.

3. **Huang, Z.**, Tsui, G. C. P., Deng, Y., & Tang, C. Y. (2020). Two-photon polymerization nanolithography technology for fabrication of stimulus-responsive micro/nano-structures for biomedical applications. *Nanotechnology Reviews*, *9*(1), 1118-1136.

4. Huang, W. F., Xiao, Y. L., **Huang, Z. J.**, Tsui, G. C., Yeung, K. W., Tang, C. Y., & Liu, Q. (2020). Super-hydrophobic polyaniline-TiO2 hierarchical nanocomposite as anticorrosion coating. *Materials Letters*, *258*, 126822.

5. Deng, Y., Xie, K., Zhong, S., Cai, J., Tsui, G. C. P., **Huang, Z**., Guo, Z., & Huang, Z. (2023). Study on surface of polydimethylsiloxane irradiated by laser with assistance of pre-strain and its regulation on cell alignment. *Journal of Micromechanics and Microengineering*, *33*(4), 045004.

Conference papers

1. **Huang, Z.**, Tsui, C. P., Deng, Y., Tang, C. Y., & Yeung, K. W. (2019). Regulation of MG63 Cell Alignment through Micro- and nano-patterned Substrates Directly Fabricated by Two-Photon Polymerization. In D. Hui (Ed.), *Conference proceedings of 27th Annual International Conference on Composites/Nano Engineering*

Acknowledgements

First and foremost, I would like to express my deepest gratitude to my chief supervisor, Dr. Gary Chi-Pong Tsui, who gave me his full support in my research and life. His great patience, valuable guidance, and positive encouragement of great help to complete my Ph.D. study. During my studies, I learned a lot of knowledge about how to perform academic research strictly and how to write an academic paper. His obliging soul and positive attitude toward life will be a precious memory in my future career. Besides, I am grateful to my co-supervisor Prof. Mo Yang in the Dept. of BME for his continuous guidance and support.

Besides my supervisor and co-supervisor, I am thankful for the experimental support and materials characterizations from Prof. Raymond Wai-Yeung Wong and Dr. Miao Zhang in the Dept. of ABCT. I would like to express my thanks to my group members and friends, Dr. Ka Wai Yeung, Dr. Yuqing Dong, Dr. Ling Chen, and Dr. Tengfei Yin, for their valuable advice and kind help in my research and life. They gave me lots of technical support in experiment issues.

Finally, I wish to express my deep gratitude to my parents for their selfless love, understanding, and support throughout my study.

Table of Contents

List of Figures

List of Table

Chapter 1 Introduction

1.1 Background of Research

Shape change and motion are common features of biological systems, exemplified by phenomena like muscle contractions and animal heartbeats. To mimic various biological behaviors, scientists have devoted tremendous efforts towards the creation of devices known as "actuators" capable of undergoing similar movements and alterations in shape (Ilami et al., 2021). In recent years, there has been a growing fascination with flexible photoresponsive soft actuators due to their distinct advantages, including flexibility, contactless operation, spatiotemporal control capability, and their wide range of technological applications (Zhang et al., 2022, Zhao et al., 2021c, Zhao et al., 2021b). Light-responsive soft robots offer a distinct advantage over traditional electric power-driven rigid robots in terms of their ability to interact with humans in a more friendly and safe manner. The adjustment of irradiation parameters, including light intensity and irradiation duration, allows for precise regulation of the dosage of irradiation and, consequently, the extent of photoreactions. Spatial control can be manipulated in 2D and 3D structures by switching the light on or off. Additionally, they excel at handling delicate and fragile objects with precision and care without complex serial-parallel circuits (Apsite et al., 2022, Stoychev et al., 2019). Researchers and engineers have been exploring different materials and structures to create light-responsive soft robotic systems. Consequently, the rational design

and efficient production of novel light-responsive materials have gained significant importance in this field.

To date, different soft photoresponsive materials and deformable structures have been developed to create soft robotics. For example, Fe-nanoparticles-doped poly(N-isopropyl acrylamide) nanocomposite hydrogels show shrinking-swelling deformation behavior under NIR light illumination due to the generated localized heating (Zheng et al., 2020, Wei et al., 2023). Multi-walled carbon nanotubes filled shape memory polymers can also be actuated by external light (Bi et al., 2020). Liquid crystal elastomers containing azobenzene groups can undergo a photomechanical response when UV light is applied (Ceamanos et al., 2023). Despite extensive endeavors dedicated to the advancement of these smart polymers and structures, certain constraints have also been recognized. Hydrogels require an aqueous environment for deformation utilizing diffusion of water and have low elastic modulus. Most hydrogel-based actuators have slow actuation speeds (Wang et al., 2020b). Shape memory polymers need post-mechanical programming after manufacturing for temporarily deformed shapes (Zhang et al., 2019b). They exhibit a one-way response, meaning that they cannot undergo cycling between the actuated state and the unactuated state upon switching on/off external stimuli. In comparison, smart materials based on liquid crystal elastomers (LCEs) have emerged as attractive candidates for developing high-performance photoresponsive actuators. They can display quick, reversible, pre-programmed anisotropic shape deformations in different environments.

In LCEs-based actuators, the incorporation of longer-wavelength NIR photothermal agents is one emerging effective approach to impart LCEs with light-responsiveness compared with traditional UV light-responsive azobenzene moieties (Zhang and Serpe, 2017, Dong and Zhao, 2018). Fast local heating generated by the photothermal fillers leads to phase transitions of LCEs, thus offering remote light stimulation to manipulate the performance of LCE actuators. These LCEs possess lots of advantages, including fast photo-to-heat speed, suitability in biological tissue, and precise spatial manipulation. Photothermal agents, such as carbon nanotubes (CNTs), graphene oxide (GO), and gold nanoparticles (AuNPs), have been widely investigated. However, these inorganic materials inherently possess obvious problems. Most of them have limited compatibility with organic polymeric networks, which restricts their incorporation within the LCEs-based actuators. When the quantity of photothermal reagents is decreased, it causes a decline in actuation speed. Conversely, increasing the amount results in uneven doping and further unpredictable deformation behaviors of the soft actuator. In contrast, organic photothermal agents, including small molecule dyes and conjugated polymers, exhibit favorable compatibility with LCEs, enabling tunable concentrations to be achieved. Organic photothermal materials demonstrate excellent light-harvesting properties and high efficiency in converting light into heat. Particularly, the molecular structures of conjugated polymers can be rationally designed for specific wavelength absorption and light-to-heat conversion efficiency. As a result, photothermal conjugated polymers are

becoming increasingly favored in the design and fabricating of LCE-based actuators and devices as a component for photothermal conversion. In comparison to certain photothermal nanomaterials, the incorporation of photothermal conjugated polymers does not cause substantial disruption to the alignment of liquid crystal (LC) molecules, and it also helps prevent excessive aggregation of dopants within the LCEs matrix. To date, just a few studies have been conducted to incorporate polyaniline into LCEs and investigate their photo-actuation performance. To the best of our knowledge, only polyaniline nanoparticles were used to develop light-responsive LCEs (Liu et al., 2016, Li et al., 2017a). and most of them use conventional two-step polymerization to fabricate actuators with simple structures. To fulfill the great potential and application of the conjugated polymers for photoresponsive actuators, new conjugated polymers with alternating donor-acceptor backbones were synthesized to prepare CPs/LCEs materials.

The actuation modes of LCEs are determined by the liquid crystal mesogen alignment, which can be predesigned in different fabrication methods. Traditional LCE-based actuators are fabricated by two-step crosslinking. The methods use stretching force to align mesogens and can produce large areas of thin monodomain LCE films (Zhang et al., 2022). Initially, a polymer network with partial polymerization and weak crosslinking is created. Subsequently, by employing mechanical stretching and other techniques, monodomain LCEs can be achieved with the desired shape. The shape and orientation of the LCEs are then permanently fixed through a second-step reaction (Liu et al., 2016). These

processes tend to take several days to complete the process (Liu et al., 2017). One-pot UV photopolymerization is another effective method to produce thin film LCE actuators, which use liquid crystal cells to achieve mesogen alignment. This method only requires one step to finish polymerization and crosslinking, which usually requires several minutes to several hours.

3D printing techniques integrated with stimuli-responsive LCEs generate a new term, “4D printing”. 3D structures with complex architectures and dynamic properties can be directly fabricated by 4D printing technologies, such as Direct laser writing based on two-photon polymerization (DLW-TPP) and UV-assisted direct ink writing (DIW) (Ambulo et al., 2017b, Peng et al., 2022). Currently, DLW-TPP is a powerful tool for additive manufacturing of 2D and 3D micro/nanostructures with submicron resolutions and desired functional properties (Huang et al., 2020). It is effective in initiating targeted polymerization within different stimuli-responsive materials, providing exceptional resolution and significant flexibility in structural design. Various polymer microstructures have been fabricated and show their application in soft actuators (Martella et al., 2017b, Ma et al., 2020), tissue engineering (Seo et al., 2020), and drug delivery (Faraji Rad et al., 2021). Nevertheless, most commercial DLW-TPP equipment does not have a heating stage to heat the photoresists with liquid crystalline phases for CCD-virtual printing. The LC photoresists with room temperature liquid crystalline phases need to be further formulated to advance the LCE-based microdevices.

DIW is an extrusion-based technique that enables the creation of complex 3D structures with precise architectures and compositions at the meso- and microscale (Saadi et al., 2022a). Unlike the aforementioned technologies, where the resin is in a bath, this technique extrudes viscoelastic LCE inks consisting of liquid crystal oligomers that have not yet undergone crosslinking. As the ink is extruded from the nozzle, the shear stress generated during the process guides the mesogens to align along the computer-designed printing path spontaneously. Curing or drying of the extruded inks can be done during the printing process after each is deposited. This also can be performed after the whole structure is printed. By controlling the spatial alignment of these liquid crystal mesogens, structures with diverse actuation modes can be engineered. Most importantly, it allows simultaneous multi-material printing by using multiple extrusion nozzles (Rocha et al., 2020).

Despite considerable efforts that have been devoted to materials design for developing fast, responsive, and large-degree actuators, it remains a challenge to prepare stable and homogenous LCE materials containing functional agents with a facile method. LCE photoresists with room-temperature liquid crystal phases are uncommon and challenging to formulate for DLW-TPP microfabrication. This problem hinders the fabrication process and application of stimuli-responsive LCE micro-structures.

1.2 Research Gap, Objectives, and Significance

Based on the above-mentioned issues, this research aims to design and synthesize novel photothermal CPs with D-A alternating backbone structures for

developing CPs/LCEs photoresists, which are suitable for diverse photopolymerization technologies. Then, NIR light-responsive 2D and 3D actuators will be manufactured by photopolymerization technologies, including one-pot UV photopolymerization and two-photon polymerization. The actuators are expected to realize different shape deformations by designing the mesogen alignment. Moreover, the scale of LCEs-based actuators will be controlled in large and micro sizes by these technologies. The main objectives are listed as follows:

(1) To design and synthesize DPP58-TBZ12 CPs with high photothermal conversion efficiency and good photostability as photothermal dopants for photothermal LCE-based actuators with enhanced response performance and multimodal deformation.

(2) To develop 2D bioinspired NIR photo-triggered soft macro-actuators based on CPs/LCEs using one-pot UV photopolymerization for realizing multimodal deformation and ultrafast response time.

(3) To develop 3D NIR photo-triggered CPs/LCEs micro-actuators with large actuation strain through DLW-TPP technology with optimization of the composition and printing parameters.

(4) To investigate the actuation performance and underlying actuation and locomotion mechanisms of the fabricated CPs/LCEs micro- and macro-actuators under the influence of the mesogen alignment in LCEs networks.

This study first introduced conjugated polymers with D-A alternating backbone structures into liquid crystal elastomers for NIR light-responsive soft

actuators. Actuators with dimensions from 2D to 3D and sizes from micrometer to centimeter are manufactured by different photopolymerization technologies. Influence factors for actuation performance, including exposure time and light power intensity, are carefully evaluated. The actuation speed and strain under NIR light irradiation have been improved largely. This work can provide useful guidance for developing LCE material systems with simple processes and fabrication of untethered, battery-free, small-scaled NIR light-responsive LCE-based actuators.

1.3 Overview of Methodology

This is a pioneering work to develop a method combining photopolymerization techniques, synthesis of photothermal CPs, and optimization of fabrication parameters for designing and fabricating light-triggered CPs/LCEs-based macro-actuators and micro-actuators for achieving controllable actuation. Based on molecular design strategies and the Stille cross-coupling polymerization technique, photothermal CPs were designed and synthesized to achieve high photothermal conversion efficiency and homogeneous dispersion in LCEs. By incorporation of the CPs in the LCEs and through tailoring the mesogen alignment in LCEs, 2D bioinspired NIR photo-triggered macro-actuators were fabricated through one-pot UV photopolymerization method for realizing various shape changes and 3D locomotion, which cannot be easily achieved in other macro-actuators reported in the open literature. In addition to the preparation of the macro-actuators, precise micro-actuators were fabricated through the DLW-TPP

technique to demonstrate the applicability of the developed CPs/LCEs material at a micro-scale level. To determine the best writing windows for producing the micro-structure with good structural fidelity and contraction/expansion response, optimization of the TPP printing parameters was also performed. Furthermore, underlying actuation and locomotion mechanisms of the actuators under the influence of the mesogen alignment in the LCEs networks were investigated. An overview of the whole research methodology is displayed in **Figure 1.1**. The methodology of this thesis is displayed as follows to realize the potential research issues:

1. **Design and synthesize photothermal CPs through Stille cross-coupling polymerization.**

   CPs have been chosen as the functionally photothermal agents for LCEs-based actuators due to their high photo-to-heat conversion efficiency, favorable solution-processability, easy molecular design, and good compatibility. New DPP58-TBZ12 CPs with alternating D-A structures were designed using molecular design strategies and synthesized by Stille cross-coupling polymerization. The CPs can exhibit optical absorption in the NIR region resulting from the nonradiative relaxation of the rich delocalized π electrons. The DPP58-TBZ12 CPs were dissolved in THF solvent to prepare homogeneous CPs/LCEs materials.

2. **Fabricate 2D film macro-actuators with multimodal deformation and ultrafast response time via one-pot UV photopolymerization.**

The shape deformation mode of the film-like macro-actuators is controlled by the mesogen alignment angle to the long axis of the film. 2D CPs/LCEs films were prepared via one-pot UV photopolymerization. Three macro-actuators with typical three alignment angles were acquired from the films. Then, different types of shape changes were realized under NIR light. The macro-actuator was also driven to move under successive NIR light illumination based on the twisting shape change.

3. **Fabricate 3D porous micro-actuators with large actuation strain via DLW-TPP technology by tuning the photoresist composition and printing parameters.**

   The combination of a deliberately developed photoresist and microfabrication method significantly simplifies the creation of micro-actuators. A systematic study of DLW-TPP-compatible photoresists and printing optimizing processes has been performed. The formulation of the LCE photoresists was rationally tailored to lower the phase transition temperature so that the crystallization could be alleviated during the printing process. A series of laser powers and scanning speeds were investigated to determine the writing windows for micro-structures with good structural fidelity.

4. **Investigate the actuation performance and underlying actuation and locomotion mechanisms of CPs/LCEs actuators under NIR light stimulation.**

The actuation performance of the fabricated CPs/LCEs macro-actuators and micro-actuators under NIR light irradiation was evaluated regarding shape deformation, response speed, and actuation reversibility. The influence of the mesogen alignment angle in the LCEs on the deformation modes was investigated systematically. The response speed and the actuation were compared with previously reported actuators.

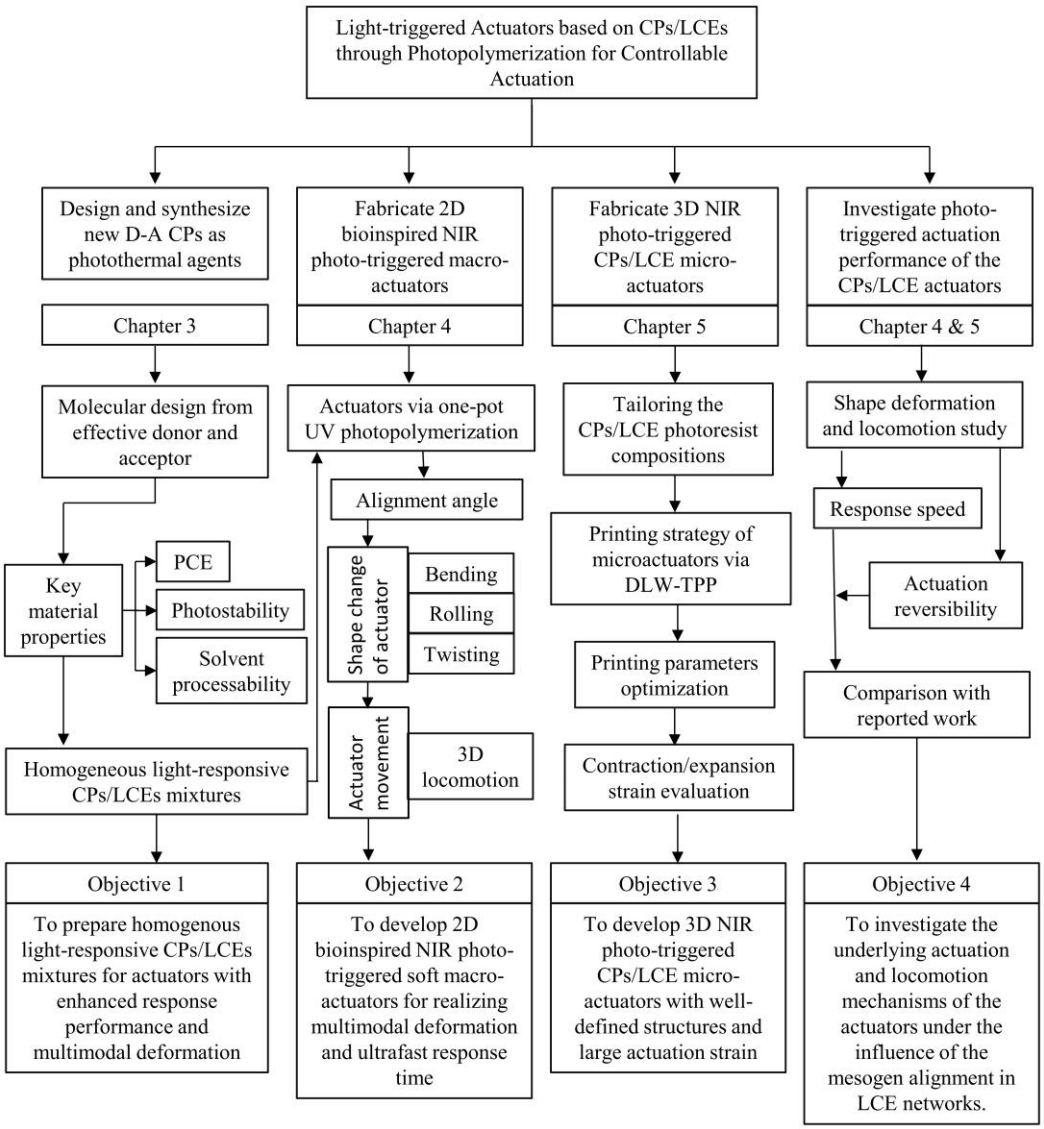

Figure 1.1 Overview of the whole research methodology

1.4 Organization of the Thesis

This thesis is divided into six main chapters, and they are outlined as follows:

Chapter 1 briefly introduces the fundamental knowledge of light-responsive actuators, research objectives, and research significance.

Chapter 2 gives a comprehensive literature review of the related topics, including the light-responsive soft actuators and their applications, light-responsive polymers, actuation mechanisms of light-responsive LCEs, main methods for liquid crystal mesogen alignments, photopolymerization technologies for LCE-based actuators. It compares the properties of current mainstream polymers and points out our purpose to develop novel NIR light-responsive CPs/LCEs materials for actuators.

Chapter 3 describes the design strategy, synthesis route, and characterizations of organic conjugated polymers with high photothermal conversion efficiency. The results of synthesizing DPP58-TBZ12 CPs are presented.

Chapter 4 describes the fabrication of thin film LCE actuators via one-pot UV photopolymerization technology. Thin film actuators are fabricated using the developed DPP58-TBZ12 CPs/LCEs material, which shows reversible shape deformation from 2D to 3D upon NIR light irradiation by controlling the mesogen alignment direction to the axis of the film. The actuator can be actuated to roll in one direction under successive NIR light on/off cycles.

Chapter 5 describes a 3D porous LCE micro-actuator by state-of-the-art technology, DLW-TPP microfabrication. To develop DLW-TPP-compatible

photoresists, the component ratios are carefully optimized to make the CPs/LC photoresists with room-temperature liquid crystal phases. The printing range of the photoresists using DLW-TPP technology is investigated to determine the scanning speed and laser powers. The actuation strains of micro-actuators are evaluated and discussed. The potential biomedical application of the NIR photoresponsive CPs/LCEs micro-actuators is also proposed. The influence of surface topography with micro- and nano-features is discussed.

Chapter 6 summarizes the whole research work, gives the statement of originality and contribution to knowledge, and suggests our future work framework.

Chapter 2 Literature Review

2.1 Introduction

Light-stimulated polymer-based soft actuators have emerged as a fascinating field of research and development in the realm of materials science and engineering (Zhao et al., 2021a, Xiao et al., 2020b). These soft actuators can harvest photon energy from an external light source and then transfer it to other energy for generating reversible shape changes (e.g., contraction, expansion, bending, twisting) and mechanical motions, making them highly versatile and suitable for a wide range of applications under challenging non-contact environments even when small in size (Hu et al., 2019). Acquired inspiration from nature, where light plays a crucial role in biological systems, researchers have focused on developing composite materials that can mimic and replicate these light-responsive functionalities. In recent years, extensive research and innovation have been made in designing and fabricating light-responsive polymer-based soft actuators, paving the way for groundbreaking advancements in fields such as soft robotics (El-Atab et al., 2020, Li et al., 2022), biomedical engineering, microfluidics system (Ter Schiphorst et al., 2018), and beyond. Exciting developments in light-responsive LCEs have highlighted the potential applications.

This chapter aims to review the previous research works on this research topic. An overview of soft actuators is presented, followed by the presentation of different applications of light-responsive actuators. There, representative smart

polymers, including hydrogel, shape memory polymers (SMPs), and LCEs are introduced. LCEs are highlighted and chosen as the research objects by comparing their advantage and disadvantages. Subsequently, the light-induced actuation mechanisms and main alignment approaches of LCEs are summarized. Finally, three polymerization methods for the manufacture of LCE actuators, including one-pot UV photopolymerization, direct laser writing via two-photon polymerization, and direct ink writing, are reviewed.

2.2 Light-responsive Soft Actuators and Their Applications

Light-responsive actuators refer to both materials and devices that can alter their shape when exposed to an external light change in their environment and can perform mechanical tasks at different scales, including nano-, micro-, and macroscales (Apsite et al., 2022, Ionov, 2015a). Conventional rigid actuators adapted for mechanical systems usually comprise rigid materials (e.g., metals and ceramics) with an elastic modulus E in the range of hundreds of megapascals and tens of gigapascals. Their actuation usually relies on relatively small deformations of rigid materials such as shape memory alloys and piezoelectric ceramics. Soft actuators based on the soft matter with a low Young's modulus, unlike traditional hard ones, are pushing the boundaries of conventional robots thanks to their various advantages, such as greater flexibility, adaptability, and reconfigurability, which are similar to those found in living systems.

The properties of soft actuators make them highly promising for a range of applications across various fields., including bionic soft robotics (Wani et al., 2017,

Zeng et al., 2017), microfluidics (Dradrach et al., 2023), drug delivery, light-electric harvester (Zhao and Liu, 2020) (**Figure 2.1**). They are employed in soft robotic systems to achieve compliant and flexible motion. They can enable precise and controlled manipulation, gripping, and locomotion in robots that interact with delicate objects or navigate complex environments. These actuators can mimic biological systems and provide safer human-robot interactions. They are also utilized in microfluidic devices and lab-on-a-chip systems for precise fluid manipulation, mixing, and pumping. By controlling the actuation of microvalves or micropumps with light, complex fluidic processes can be automated, enabling applications in chemical analysis, drug delivery, and diagnostics. LCE cantilevers can perform spontaneous vibration under the irradiation of light. Combined with Faraday's law, light-induced mechanical energy can be transformed into electric energy.

There are several useful metrics commonly used to compare actuator performance. The function of speed, strain, force, and recovery time in LCE actuators is crucial for understanding their performance characteristics and their suitability for various applications. The speed of LCE actuators is particularly important in applications where rapid and precise actuation is required. For example, in soft robotics or microfluidic systems, fast actuation can be essential for achieving responsive and efficient movement. The strain capability of LCE actuators is essential in applications where large deformations are required. In soft robotics or artificial muscles, a high strain allows for a wide range of motion and

flexibility, making these actuators suitable for applications that involve complex movements and shape changes. Force is critical in applications that demand mechanical work, such as lifting or manipulating objects. In soft grippers for robotics, for example, a higher force allows the gripper to grasp objects securely and perform tasks that require a certain level of strength. In applications requiring repetitive actuation, a short recovery time is beneficial. For instance, in devices like adaptive lenses or optical elements, a fast recovery time ensures quick adjustments, making the actuator responsive to dynamic changes in the environment.

In summary, the optimization of speed, strain, force, and recovery time in LCE actuators is essential for tailoring their performance to specific applications. The versatility of LCE actuators makes them suitable for a range of applications, including soft robotics, adaptive optics, and biomedical devices, where these functional characteristics play a crucial role in determining the overall efficiency and effectiveness of the actuator in a given context.

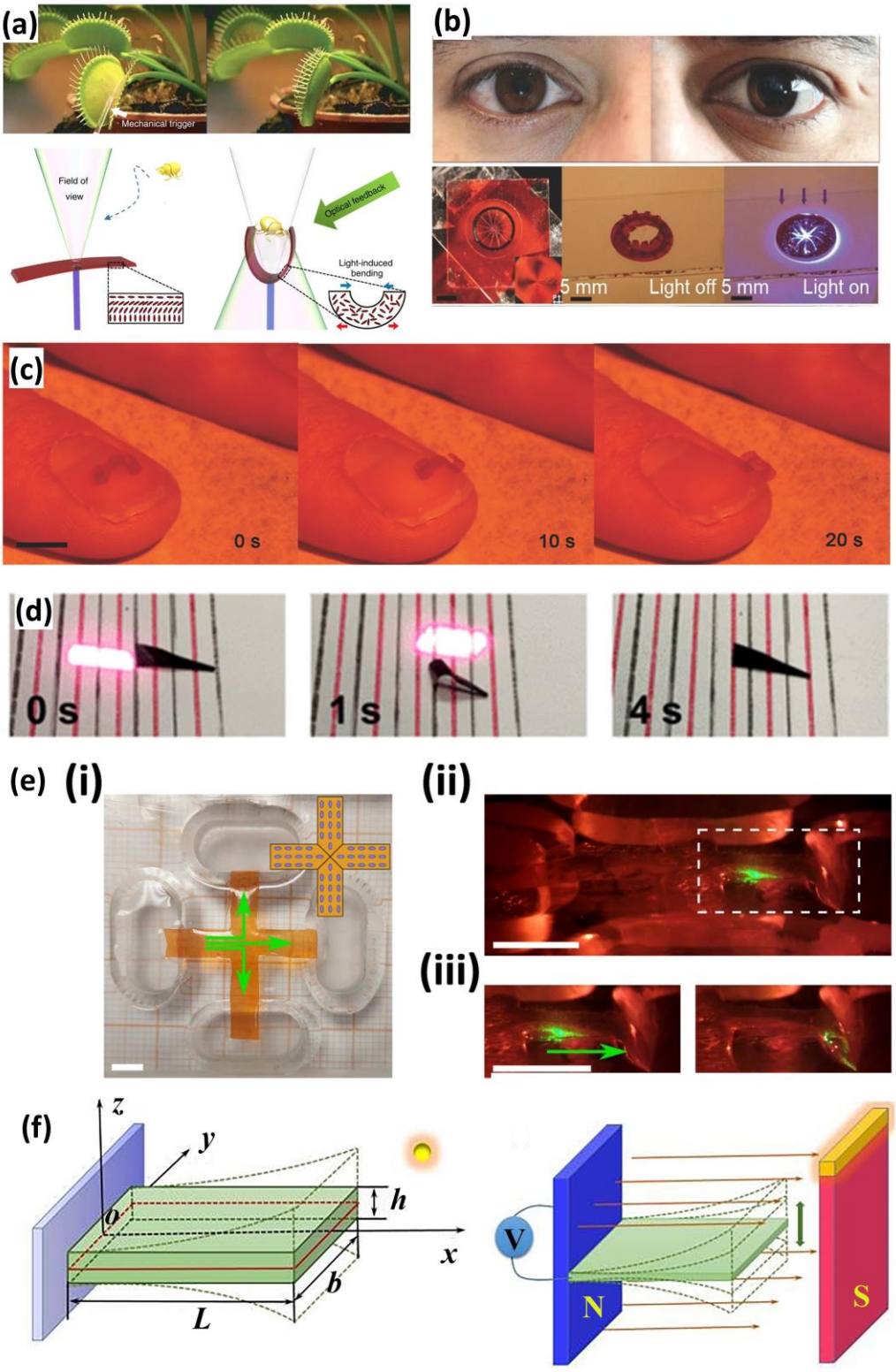

Figure 2.1 (a) Bionic light-triggered LCEs Venus flytrap robot (Wani et al., 2017). (b) Light-powered LCE actuator mimicking human iris and its feedback mechanism (Zeng et al., 2017). (c) The light-induced motion of a

caterpillar robot on the nail of a human finger. Scale bars: 5 mm (Zeng et al., 2018). (d) An LCE trapezoidal soft robot moves forward and backward under alternating NIR light irradiation (Yu et al., 2022b). (e) Photo-peristaltic LCEs pump to demonstrate the transport of water (Dradrach et al., 2023). (f) One model of an LCE cantilever for a light-electric mini-generator (Zhao and Liu, 2020).

2.3 Light-responsive Polymers for Actuators

Smart polymeric materials can provide soft actuators with an additional degree of freedom by altering their structure, macroscopic properties, and shape in response to external signals. The use of such polymeric materials allows devices to be made smaller, which opens numerous applications that cannot be achieved with externally powered systems. Various responsive soft materials, such as LCEs, stimuli-responsive hydrogels, and SMPs, have promoted the development of intelligent actuators due to their ability to change physical properties, such as shape, color, or size, in response to light source changes. These polymers can be engineered by molecular modulation and chemical modification. Each of them has special properties that render it particularly appropriate for specific applications. To enhance the functionalities of actuators in these applications, researchers have committed enormous efforts in light-responsive material system development and structure design. Three main smart polymers are briefly introduced in this section. Their properties, especially advantages and disadvantages are elucidated and compared.

2.3.1 Hydrogels

Hydrogels are prime materials for creating soft actuators due to their ability to undergo significant reversible deformations through swelling and deswelling cycles (Ma et al., 2018, Le et al., 2019, Zhang et al., 2021a). They are three-dimensional polymer networks that contain over 90% water, yet still possess structural integrity and strength. This unique property allows them to exhibit large volume changes, sometimes more than 10 times their original volume, in response to external stimuli, such as temperature, light, pH, and electric and magnetic fields. Different types of deformations of hydrogel actuators can be achieved.

There are two primary approaches to achieving photo-actuation in hydrogels, including the isomerization-based approach and the photothermal effect (Shang et al., 2019a, Wang et al., 2023b). In the former approach, photo-actuation is achieved through isomerization (a process where the arrangement of atoms in a molecule is changed) of light-driven entities within the hydrogel. These entities can be small molecules or functional groups that undergo conformational changes upon exposure to light. The isomerization process can lead to alterations in the gel properties, such as changes in hydrophilicity (water affinity), charging state (electrical properties), or crosslinking density (degree of network formation). These modifications, in turn, can result in substantial changes in the physical and chemical behavior of the hydrogel. In the photo-thermal approach, photo-actuation is achieved through the addition of light-responsive agents into the hydrogel structure. These agents can absorb light energy and convert it into heat, inducing

a temperature increase within the hydrogel. This localized increase in temperature triggers a volume transition of the hydrogel, causing it to expand or contract. By carefully selecting the photo-thermal agents and their concentration, researchers can control the extent and direction of the volume change. This strategy provides a versatile and relatively straightforward method to achieve photo-actuation in hydrogels. The isomerization-based approach often requires the synthesis of complex and laborious light-responsive molecules, which can be a challenging task. On the other hand, the photo-thermal approach offers greater flexibility, as it allows for the use of various combinations of photo-thermal agents to achieve the desired actuation response. This ease of implementation and control makes the photo-thermal approach more accessible for practical applications.

Hydrogels are often biocompatible and exhibit low toxicity, making them suitable for biomedical applications such as tissue engineering, drug delivery, and wound healing (Yao et al., 2023). Additionally, it is easy to manufacture hydrogel actuators with diverse shapes and movements by using photolithography and molding. Nevertheless, hydrogel actuators have a significant drawback: they can only be actuated in aqueous solutions. To overcome this limitation, a high-humidity air supply can be used, but this approach results in significant volume exchange losses and longer actuation times on the order of minutes. Also, hydrogels typically have relatively low mechanical strength compared to other materials, making them unsuitable for specific soft robotics.

2.3.2 Shape Memory Polymers

SMPs are networks of polymers that can temporarily retain a specific shape during a transition period. The concept of shape memory in polymers relies on the material's ability to exist in two distinct states: a temporary (metastable) state and a permanent state (Pilate et al., 2016, Lendlein and Gould, 2019). The permanent shape of SMPs is determined by the crosslinking process step, while the temporary shape is the shape achieved when the deformation is fixed. In detail, the permanent shape of SMPs can be achieved through conventional polymer processing techniques like molding or extrusion. Afterward, the SMPs undergo programming by applying external mechanical stress above a specific transition temperature (T_{trans}), which can be either the glass transition temperature (T_g) or the melting temperature (T_m). When the temperature exceeds T_{trans}, the polymer chains become pliable due to the presence of flexible switching segments, allowing them to be easily deformed by external stress. Upon subsequent cooling below T_{trans}, the SMPs are locked into a temporary shape by restricting the chain flexibility. Finally, the SMPs regain their original shape when heated above T_{trans} (**Figure 2.2**). It should be mentioned that relying solely on heat may not always be practical, especially in scenarios involving electronic devices or when precise control over the shape change is desired. This is where photo-actuation comes into play.

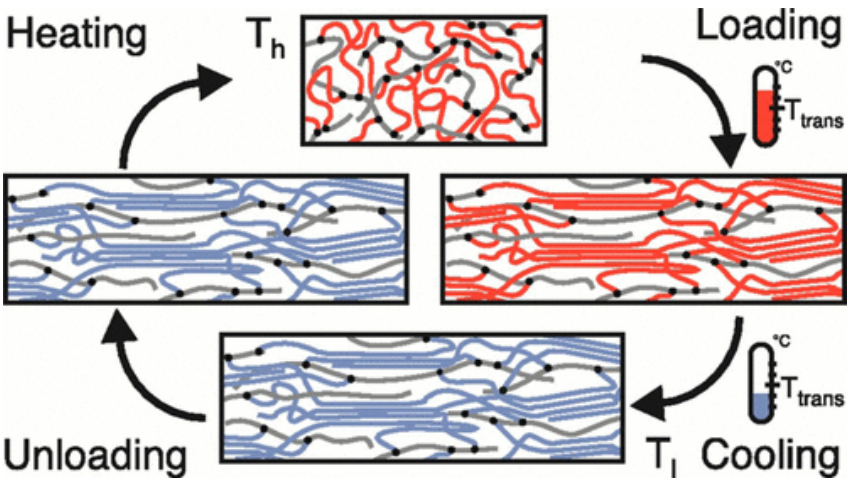

Figure 2.2 Working principle of shape memory polymers (Ionov, 2015b)

To achieve photo-actuation in SMPs, light-responsive elements or additives are incorporated into the polymer matrix. These light-responsive components can be photosensitive molecules, nanoparticles, or other light-absorbing materials (Wang et al., 2022b, Leng et al., 2011). When exposed to light of a specific wavelength or intensity, these components undergo a photochemical or photothermal reaction, leading to changes in the polymer's properties, such as its shape, stiffness, or modulus.

Shape memory polymeric actuators have several advantages compared to hydrogels. They exhibit higher moduli, enabling enhanced specific work performance, and can undergo actuation in both dry and wet environments. These characteristics make them highly appealing for various applications. One advantage is the ability to operate in both dry and wet conditions, providing versatility in different environments. Additionally, the transition temperature of shape memory polymeric actuators can be adjusted by selecting appropriate polymers or modifying their composition, enabling customization for specific

requirements. Another advantage is the availability of biocompatible and biodegradable shape memory polymers, making them suitable for medical applications.

However, it is important to note that most shape memory polymers exhibit "one-way" shape memory behavior, meaning they cannot autonomously cycle between actuated and initial states (Del Pozo et al., 2022b). Their recovery speed is relatively slow from tens of seconds to minutes. After each actuation, reprogramming is required. Only a limited number of shape memory polymers possess "two-way" actuation capabilities, allowing for reversible shape changes without the need for repeated reprogramming.

2.3.3 Liquid Crystal Elastomers

Liquid crystal elastomers have evolved significantly since they were first introduced by Finkelmann et al. in 1981 (Finkelmann et al., 1981). They are a unique class of materials with distinctive properties, unlike liquid crystal polymers (LCPs) that lack crosslinking or highly crosslinked liquid crystal networks (LCNs). LCEs are low-crosslinked liquid crystal polymer networks within which side-chain or main-chain liquid crystal molecule units (also called mesogens) are linked with flexible elastomeric polymer chains (**Figure 2.3**). They display the soft elasticity of polymer networks and the reversible and director-independent property-changing behaviors of liquid crystals (Zhang et al., 2022). The interaction between the mesogens can result in the alignment of polymer chains, which can be disturbed by the introduction of external stimuli, such as heat (Wu et al., 2020a,

Zhai et al., 2021), light (Wang et al., 2020b, Yang et al., 2022b, Zhang et al., 2020), electric and magnetic field (He et al., 2019, Guin et al., 2020, Xiao et al., 2019), humidity (Kim et al., 2021b) and solvent (Boothby et al., 2017). For the photo-actuation of LCE actuators, the strategies are also similar to the light-responsive hydrogels, which utilize photoisomerization or photothermal heating (Wang et al., 2023a). However, organic solvents are necessary to acquire homogenous mixtures for LCEs. Due to the stimuli-responsiveness of the mesogens, LCEs can temporarily become isotropic and display a large and reversible deformation under stimuli without the need for an aqueous environment or tethered power source. These unique properties enable LCEs as potential material candidates for soft actuators, soft robotics, and artificial muscles.

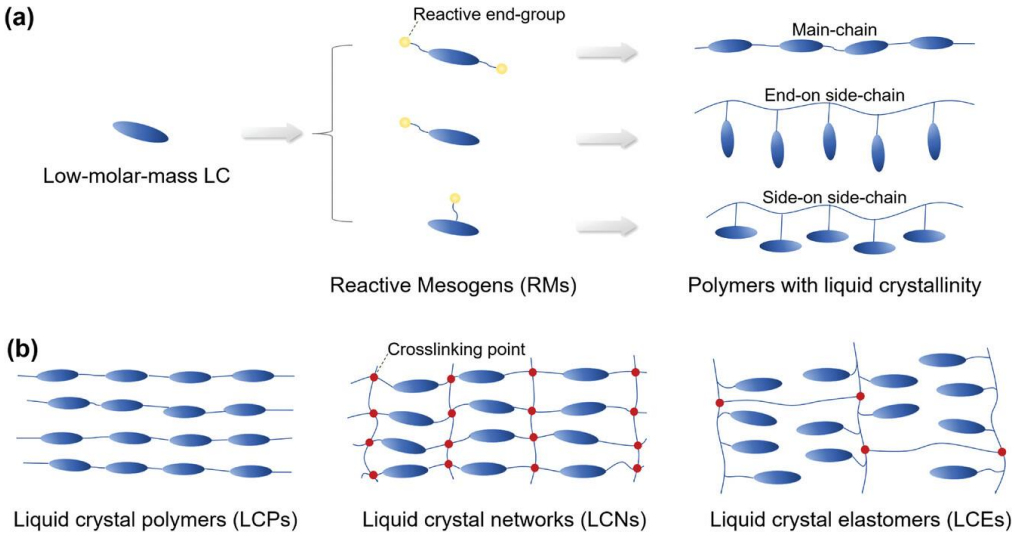

Figure 2.3 Schematic drawings of reactive mesogens and crosslinked polymer networks. a) Visualization of reactive mesogens (di- and mono-substituted) and different polymer chains. (b) Crosslinked liquid crystal networks of LCPs, LCNs, and LCEs (Chen et al., 2022b).

Due to the designability of mesogens in spatial distribution, various shape-morphing modes, including bending (Huang et al., 2022, Ma et al., 2019), twisting (Shahsavan et al., 2020, Ryabchun et al., 2023), oscillating (Deng et al., 2022, Shi et al., 2022), and mechanochromic response (Liu et al., 2022, Sun et al., 2022a), can be realized by LCEs with non-uniform alignment styles. Aligned monodomain LCEs with oriented global mesogens are the only ones capable of exhibiting large, reversible, and anisotropic responses (Merkel et al., 2018). LCEs synthesized without any additional alignment treatment are typically polydomain. Although the mesogens can be locally ordered in sub-domains, the material remains macroscopically isotropic. Hence, the crucial factor for utilizing LCEs in applications is to control their mesogen orientations and distribution, thereby enabling pre-programmed responsiveness behavior to light stimulus.

In contrast to the above smart soft materials, LCE actuators possess a lot of advantages. They can achieve anisotropic and reversible shape deformations easily by alignment manipulation of the mesogens, allowing for programmable complex, large-scale motion. The response time is always very fast, which enables rapid shape changes. The actuation speed is typically on the order of milliseconds to seconds, depending on the specific design and material properties. Most LCE actuators can be actuated easily by NIR light in diverse environments. **Table 2.1** gives a comparison of different smart polymers for actuators.

Table 2.1 Summarized Physical and Actuating Properties of Smart Materials

material	Young's modulus/ actuation stress	actuation time	max actuation amplitude	Actuation environment	References
hydrogels	0.004-0.45 MPa	1-120 min	60-400%	wet	(Francis et al., 2017, Zheng et al., 2015, Yuk et al., 2017)
shape memory polymers	100 MPa-2 GPa (frozen state) 0.1-100 MPa (soft state)	0.003-5 min	150-330%	Dry or wet	(Mao et al., 2016, Ge et al., 2016, Safranski and Gall, 2008)
liquid crystal elastomers	0.1-2000 MPa	0.1-5s	20-1700%	Dry or wet	(Palagi et al., 2016, Shahsavan et al., 2020, Guan et al., 2022, Stoychev et al., 2019)

2.4 Actuation Mechanism of Light-responsive LCE-based Actuators

Among the various external stimuli, light possesses several desirable properties for actuation, making it an appealing stimulus option. It enables convenient, non-contact, and spatiotemporal manipulation of actuators without complex wired equipment. It also allows for precise control over spatial and temporal aspects, facilitating high-resolution manipulation. Light's properties,

such as intensity, wavelength, and exposure time, are easily adjustable. Additionally, it serves as a clean and safe energy source, eliminating the need for substantial heating. Light-driven actuation also offers the advantage of pausing and resuming processes as needed. Consequently, light-driven polymeric materials have gained considerable attention in recent years. To date, the design strategy for the photoresponsive LCEs can be classified into two main categories: photoisomerization and the photothermal effect (Wang et al., 2023a, Qin et al., 2021). Both of them require the volume change resulting from the order-disorder phase transition of LC mesogens.

2.4.1 Photoisomerization Effect-based Actuation

Photoisomerization effect-based actuation is a prominent mechanism utilized in light-responsive liquid crystal elastomer actuators. This mechanism relies on the ability of specific photoresponsive chromophores (e.g., azobenzene) incorporated within the LCE matrix to undergo reversible isomerization upon exposure to light (Leanza et al., 2023). The isomerization process involves the rearrangement of molecular bonds and results in a change in the shape or conformation of the photoresponsive molecules. The photoisomerization effect-based actuation in LCE actuators typically involves two key components: the photoresponsive chromophore and the LCE matrix. The photoresponsive molecule, also known as the photoswitch, is carefully selected to exhibit reversible isomerization in response to specific wavelengths or intensities of light.

In most photoisomerizable LCEs, UV light exposure induces a transition in azobenzene molecules, shifting them from the energetically favorable trans-state to the cis-state. The azobenzene can act as the photo-responsive dopant and the mesogen simultaneously. The cis-state can subsequently return to the trans-state through blue/green light exposure or thermal relaxation. The trans isomer, with its rod-like structure, stabilizes the phase structure of the liquid crystal (LC), while the bent cis isomer tends to disrupt the alignment of the LC. This molecular configuration change disrupts the alignment of mesogens, resulting in a transition from a liquid crystal (ordered) phase to an isotropic (disordered) phase (**Figure 2.4 a**). As a consequence, the phase change can be greatly amplified by utilizing various deformations in LCEs, such as shrinking, bending, or other changes, depending on the design and configuration of the LCE actuator. Azobenzene moieties can also be covalently bonded into the polymer network for the light-fueled deformation of LCEs due to the cooperative effect.

Lots of important works about UV photoresponsive LCE systems containing azobenzene have been reported. For example, an LCEs-based belt assembled from an LCEs film containing azobenzene, which could serve as a light-driven plastic motor by irradiating the belt with UV light and green light in different directions simultaneously, has been reported (Yamada et al., 2008). Various simple or assembled actuators containing azobenzene, like a flower-like actuator (Lu et al., 2021), spiral ribbons (Iamsaard et al., 2014), and wave transporter (Gelebart et al., 2017), have also been studied widely.

Nevertheless, certain inherent drawbacks in these photoisomerizable LCE systems cannot be overlooked. Deformed LCEs under UV light need illumination with visible light to recover their shape. The restricted penetration depth of UV light poses challenges for certain LCE applications, and there is a limited range of useful photochemical reactions available (Sun et al., 2022b, Qin et al., 2021). Furthermore, long-term stability remains a persistent issue due to photodegradation and side reactions in these systems. As a result, alternative approaches for developing photoresponsive LCEs have become increasingly significant. In the biological applications of light-responsive actuators, a light source with low energy, especially NIR light, is preferred because of less damage to bio-samples and penetration of depth into tissues.

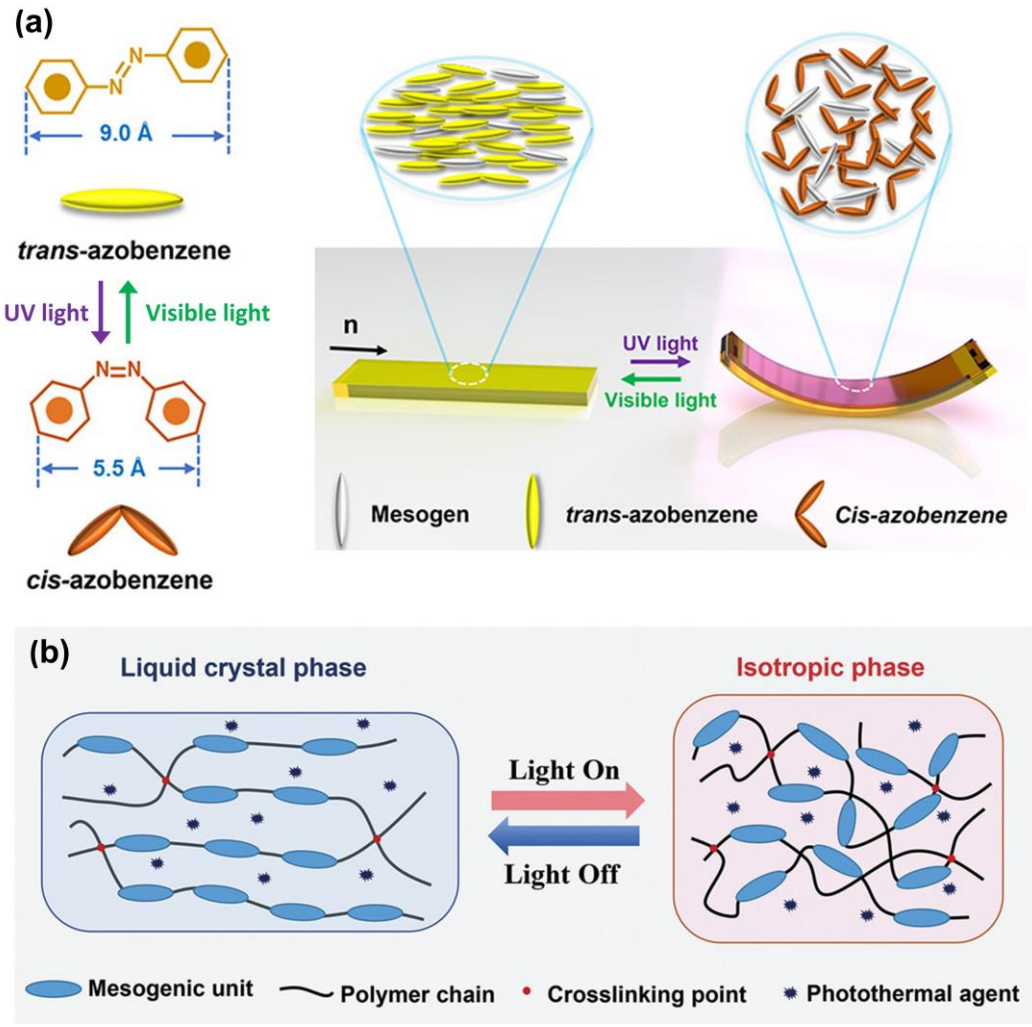

Figure 2.4 Schematic illustration of photoisomerization and photothermal effect triggered reversible macroscopic shape deformation of LCEs (Pang et al., 2019b). (a) Trans-cis photoisomerization of azobenzene moiety. (b) The photothermal effect of incorporated dopants (Wang et al., 2023a).

2.4.2 Photothermal Effect-based Actuation

Photothermal effect-based actuation is another significant mechanism employed in light-responsive LCEs to achieve effective actuation in response to light stimuli. This mechanism exploits the generation of localized heat within the LCE material when exposed to light, leading to changes in its shape, orientation, or mechanical properties. The photothermal effect-based actuation in LCEs

involves the incorporation of photothermal materials within the elastomer matrix. These materials are specifically selected to have high absorption coefficients at the desired wavelength of light. Upon absorbing light, the materials undergo an electronic excitation, converting the light energy into heat energy through non-radiative processes such as internal conversion or vibrational relaxation. The localized heating generated by the absorbed light raises the temperature of the LCEs beyond the LC-to-isotropic phase transition point. Then the aligned mesogens will lose their orientation and become randomly aligned, triggering reversible macroscopic shape deformations in the LCEs (**Figure 2.4 b**). The extent and direction of actuation can be controlled by optimizing the composition of the LCEs matrix and the distribution of the light-absorbing dopants within it.

Within the realm of photothermal-responsive LCEs, NIR light has garnered significant focus. This is primarily attributed to its ability to penetrate deeper into most polymer materials and its tendency to cause less damage compared to UV light. Additionally, a diverse range of photothermal agents, both inorganic and organic, can absorb NIR light and produce heat. Different types of photothermal dopants have been added inside or on the surface of LCEs for photothermal effect-based actuation, including carbon-based materials, metallic nanoparticles, and organic photothermal materials. The choice of dopants depends on factors such as the absorption wavelengths of light, photothermal conversion efficiency, thermal stability, and compatibility with the LCE matrix. The actuation response in photothermal effect-based LCEs can be tailored by adjusting parameters such as

the light intensity, duration of illumination, and the thermal conductivity of the elastomer matrix. The localized heating induced by the absorbed light can result in various actuation modes.

Carbon-Based Photothermal Materials

Carbon-based photothermal materials primarily include graphene and CNTs. When exposed to NIR light, these carbon materials absorb a significant portion of the photons, causing the electrons within them to undergo energy-level transitions (Ji et al., 2010). The advantage of carbon-based photothermal materials primarily stems from their consistent and stable photothermal properties. Even after prolonged exposure to laser radiation, carbon materials retain their effective photothermal effects.

Graphene, a two-dimensional material composed of carbon rings, exhibits strong optical absorption and heat generation properties when exposed to NIR light. Its excellent photothermal effect is attributed to surface plasmon resonance, which leads to the generation of heat through electron-electron and electron-phonon scattering. CNTs, including single-walled carbon nanotubes (SWCNTs) and multi-walled carbon nanotubes (MWCNTs), are tubular materials with remarkable chemical, electrical, mechanical, and photothermal properties. CNTs can absorb light across a wide range of wavelengths, including visible and NIR light, without any absorption threshold. The photoabsorption characteristics of CNTs can be fine-tuned by adjusting parameters like length-width ratio and winding direction.

However, the self-aggregation tendency of graphene sheets hinders uniform mixing with the polymer matrix, resulting in low load transfer efficiency and compatibility issues between graphene and LCEs. Incorporating carbon-based photothermal materials, such as graphene and CNTs, into LCEs presents challenges in terms of fabrication. Achieving a homogeneous dispersion and alignment of these fillers within the LCEs is crucial but difficult, impacting the overall actuation performance and reliability. The complex fabrication processes involved may limit scalability and reproducibility in practical applications.

Metal Photothermal Materials

The photothermal properties of noble metal photothermal nanomaterials, such as Au, Cu, and Pd, are attributed to the localized surface plasmon resonance effect. This effect occurs when the vibration frequency of the delocalized electrons in the noble metal matches the frequency of incident light, resulting in collective excitation and resonance. The vibrating electrons dissipate their kinetic energy as thermal energy, leading to local heating and temperature increase throughout the metal via thermal conduction. The surface plasmon resonance effect is influenced by the morphology of the noble metals, enabling the control of photothermal materials by manipulating their microscopic structure. Examples include gold nanorods, gold nanospheres, gold nanocages, and palladium nanosheets. Among these, gold nanomaterials have a large absorption cross-section, adjustable light absorption in the near-infrared (NIR) region based on particle size and shape, as well as stability, and low toxicity.

However, it is essential to consider the compatibility between the fillers and the LCEs matrix to ensure the effective loading of nanofillers in LCEs. Aggregation of AuNRs within the LCEs can lead to increased light scattering and reflection, resulting in decreased photothermal conversion efficiency and response speed of LCEs. Furthermore, particle aggregation causes uneven heating of the LCEs, negatively affecting their mechanical and actuation properties. Surface modification of AuNRs offers a viable solution to address these issues and enhance the performance of the LCE-based photothermal systems.

Organic Photothermal Materials

Organic photothermal substances have also found application in the realm of photoresponsive LCEs because of their favorable biocompatibility and remarkable photothermal conversion efficiency. These organic photothermal materials used in photoresponsive LCEs can be broadly categorized into two groups: organic small molecule dyes and conjugated polymers. To achieve appropriate absorption of light across a wide range of wavelengths from UV to NIR and achieve high efficiency in converting light into heat, all these materials should possess π-conjugated structures for nonradiative relaxation.

Organic small-molecule photothermal dyes have been widely used in photothermal therapy due to their good biocompatibility, easy synthesis, and optical properties. Some of them have attracted research interest in NIR light-responsive LCEs. For example, commercially available Lumogen IR788, Dye1002, synthesized croconaine dye YHD796 and N,Ndialkylimidazolidine-

2,4,5-trithone nickel complex with 2- butyloctyl chains (imNi8(4)) have been introduced into the LCE matrix for NIR light-triggered actuation (Kohlmeyer and Chen, 2013b, de Haan et al., 2012, Guo et al., 2016a, Ge et al., 2018) (**Figure 2.5**). While small molecular dyes possess a narrow spectrum of light absorption, granting them a certain level of light selectivity, their photothermal conversion efficiency falls short for certain applications. In most cases, organic small-molecule photothermal materials are physically doped into LCE systems, which can result in phase separation between the LCE matrix and the added fillers. Additionally, the development of NIR light-responsive small-molecule dyes remains a challenging task.

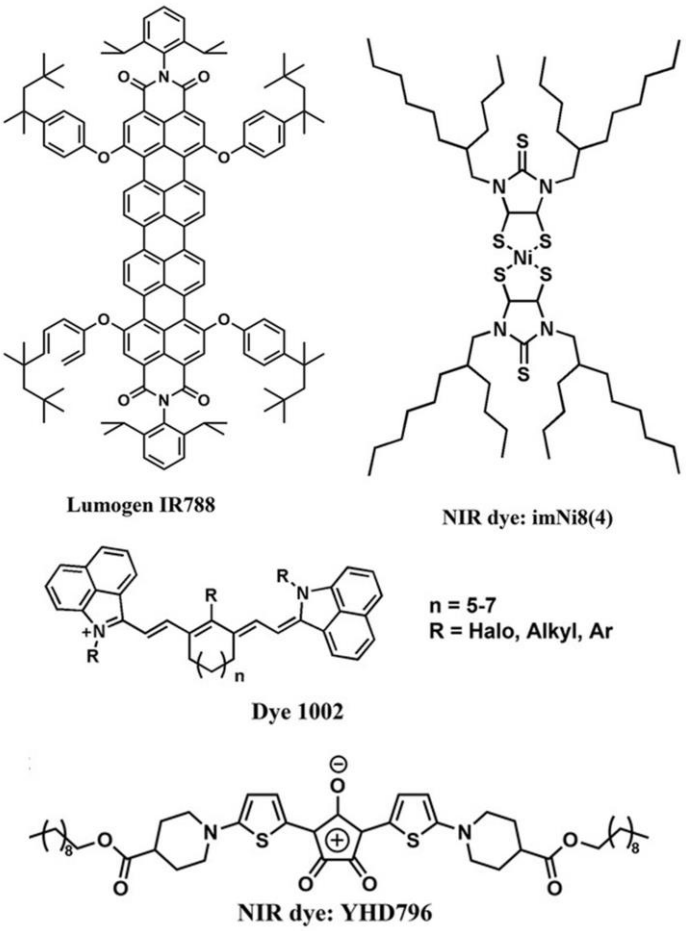

Figure 2.5 Molecular structures of NIR-light responsive small molecule dye, including Lumogen IR788 (Kohlmeyer and Chen, 2013b), imNi8(4) (de Haan et al., 2012), Dye 1002 (Guo et al., 2016a)and Dye YHD796 (Ge et al., 2018).

Conjugated polymers (CPs), one kind of macromolecules, have emerged as a novel class of photothermal materials due to their versatile molecular designs, strong NIR light absorption, high stability and efficiency in converting light to heat, and favorable biocompatibility (Wang et al., 2020c). They are characterized by their conjugated bond structures and repetitive chemical units that contain delocalized π-electron systems. To date, CPs have been widely used in photothermal therapy (Gupta et al., 2020), clean water harvesting (Gao et al., 2019), organic electronics (Pirotte et al., 2018), and energy harvesting (Lu et al.,

2019). Examples of such as polyaniline (PANI) and polydopamine (PDA) with π-conjugated structures have also been introduced into LCEs for actuation by dispersion in the matrix (Liu et al., 2016, Li et al., 2017b) or surface coating (Tian et al., 2018, Lan et al., 2020). By closely stacking their monomeric units, the intermolecular collisions within these polymers are strengthened. The construction of conjugated polymers can partially suppress molecular fluorescence and enhance nonradiative relaxation, resulting in efficient photothermal conversion. Furthermore, the adoption of donor-acceptor (D-A) strategies has been proposed to develop a new range of conjugated polymers, aiming to broaden the absorption of light and enhance the conversion of light into heat.

Conjugated polymers possess desirable characteristics that make them a promising type of polymer-based photothermal material suitable for near-infrared (NIR) light-responsive LCEs. However, most conjugated polymers are combined with nonparticipation methods to create nanoparticles for *in vivo* phototherapy. Amphiphilic polymers with functional groups are used to coprecipitate with CPs to generate nanoparticles. The nanoparticles can stay stable distribution in water, but not in organic solvent. Limited research has been performed to combine D-A-type conjugated polymers with LCEs by organic solvents directly.

2.5 Main Methods for Liquid Crystal Mesogen Alignment

The quality of the anisotropic properties of LCs and their response to external stimuli are directly affected by the mesogen orientation, making it an essential characteristic to consider (Zhao et al., 2021a, Guan et al., 2022). Therefore, it is

imperative to control the mesogen alignment during the fabrication process for the desired actuators. Mesogens, also known as LC molecules, represent an intermediate state of matter that is characterized by both liquid-like fluidity and solid-like crystalline order. The intrinsic anisotropy of mesogens, which is due to their elongated molecular shape, enables them to exhibit flowability with long-range order, as well as large birefringence. Under the influence of the surface anchoring effect, external field, or mechanical stress, the long axes of the mesogens can be oriented along the desired direction. Aligned LCEs are acquired after the photopolymerization and crosslinking.

Several fabrication approaches have been developed to enable the fabrication of aligned LCEs. To attain a uniform alignment of mesogenic molecules on a larger scale, various techniques can be employed to impose boundary conditions. These techniques include chemically modifying the surface of the substrate, applying electric or magnetic fields, or utilizing mechanical forces such as shear or elongation. In additive manufacturing techniques where the LC is in a vat, treated surfaces or electric/magnetic fields are commonly used to achieve the desired boundary conditions. In extrusion-based direct ink writing, ink alignment is mainly controlled by the shear force generated by the extruding nozzle. An appropriate alignment approach should be selected during the fabrication process.

2.5.1 Surface Anchoring Effect-induced Alignment

The surface anchoring effect can be utilized to align the mesogens through methods such as surface rubbing (Guo et al., 2016b, Wani et al., 2019), and

photolithography (Guo et al., 2020a, Ambulo et al., 2020) (**Figure 2.6**), and photoalignment (Wani et al., 2018). Surface anchoring is a complex phenomenon that involves the LC material and coating material. LC molecules near a treated surface can be aligned due to the combination of interaction with the specific coating material on the treated surface and geometrical factors. The intermolecular forces between surface-coated polymers (e.g., polyimide, poly(vinyl alcohol)) and the mesogens, can the micro-/nano-scale channels generated by the mechanical rubbing, jointly induce the surface anchoring effect for mesogen alignment.

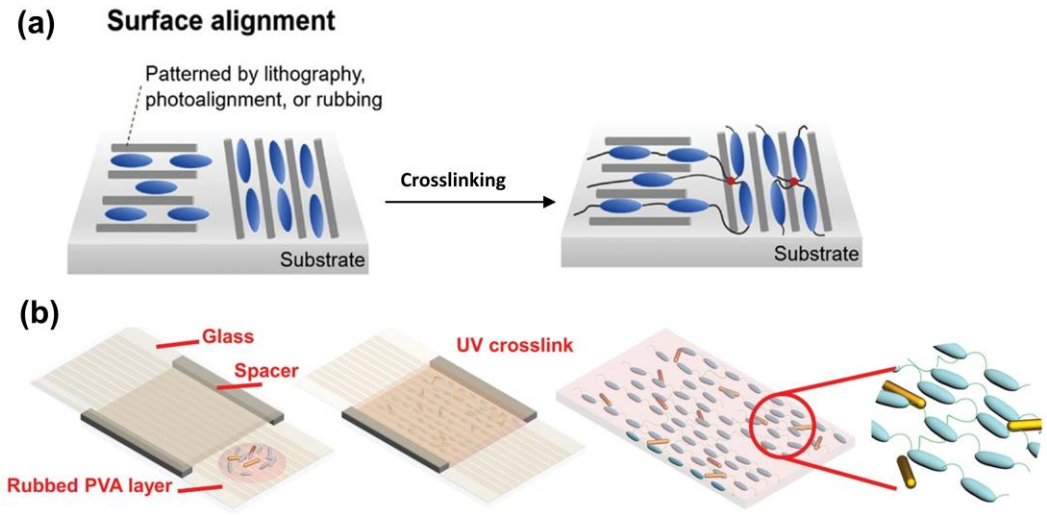

Figure 2.6 Surface alignment of mesogens in LCEs. (a) Creating surface patterns on the substrate (Chen et al., 2022b). (b) Construction of a typical liquid crystal cell with predefined rubbing direction for mesogen alignment (Wang et al., 2020b).

A popular method involves assembling a sandwich-like liquid crystal cell with alignment layers on both the top and bottom substrate surfaces. Due to the fact that mesogens tend to minimize surface energy by forming a state that is well-organized on aligned surfaces, surface alignment is commonly employed to induce

mesogen alignment in thin LCEs (Ware et al., 2015). The substrate such as glass is coated with a material like polyimide and then mechanically rubbed to create microgrooves along the target nematic direction. The cell is then filled at the isotropic temperature and cooled down to the LC phase, followed by slow cooling to room temperature. Due to the boundary conditions imposed by the alignment layers, the mesogens undergo predetermined self-organization during the phase transition from isotropic to LC and are crosslinked to form a network by a subsequent polymerization reaction. The alignment of mesogens can vary determined by the type of alignment layer(s) employed in the liquid crystal cells. There are several alignment types including (1) planar alignment in which mesogens align parallel at both sides and in one direction, (2) homeotropic alignment in which mesogens align homeotropic at both sides, (3) splay alignment in which mesogens align parallel to the surface plane at one side and (4) perpendicular at the other, and twisted alignment in which mesogens pointing in different directions at different surfaces (Del Pozo et al., 2022b).

The surface anchoring effect of mesogens is limited by its weakness. This means that only mesogens close to the treated surface can be effectively aligned, thereby restricting the thickness of the fabricated LCE films to approximately 100 μm. Surface treatment alignment has only been reported to be used to a limited extent in manufacturing technology, such as direct laser writing via two-photon polymerization (DLW-TPP) and one-pot UV photopolymerization.

2.5.2 External Electric/Magnetic Field-assisted Alignment

Apart from the surface anchoring effect, external electric or magnetic fields also allow for the manipulation of the alignment of mesogens (Ryabchun et al., 2023) (**Figure 2.7**). To achieve this, LC cells commonly employ transparent electrodes, such as indium tin oxide (ITO), along with an alignment layer. The alignment layer induces a planar alignment of benzene-containing mesogens, but when a sufficient voltage is applied between the electrodes, the resulting electric field causes the positive dielectric molecules to reorient from a planar to a tilted alignment at intermediate potentials, and a near-homeotropic alignment at high potentials (You et al., 2019). This allows for real-time control of the alignment of the LC. Additionally, the ITO electrode can be of an interdigitated design, which can create more complex alignments. Nevertheless, an extremely high voltage is required to achieve mesogen alignment.

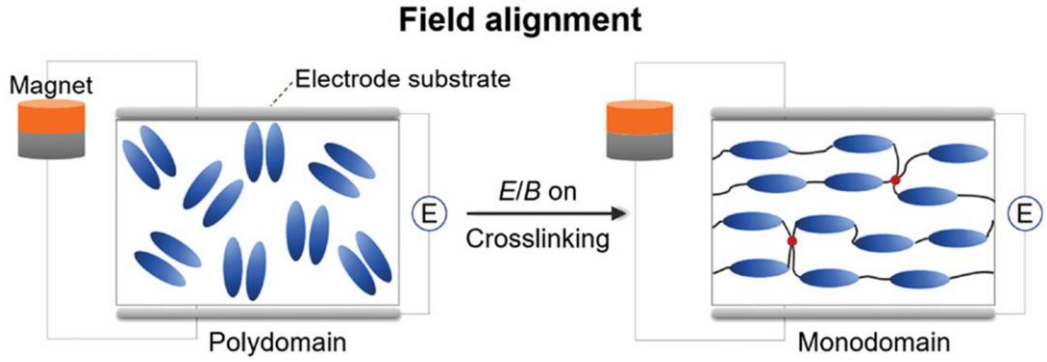

Figure 2.7 External electric/magnetic field alignment method for mesogen in LCEs (Chen et al., 2022b). Here, *E* represents the electric field intensity, and *B* represents the magnetic induction intensity.

The anisotropic molecular structure of mesogens brings about a highly anisotropic magnetic susceptibility of LC molecules. The external magnetic fields

can also be applied to manipulate the orientation of LC molecules in a non-contact manner (Tabrizi et al., 2019). It is important to consider that to achieve magnetic alignment, mesogens must be in a nematic state with high molecular mobility and magnetic susceptibility anisotropy of LC molecules. Typically, a strong magnetic field of several hundreds of millitesla is necessary for the magnetic alignment of mesogens. While Helmholtz coils can provide a uniform magnetic field with controllable field strength, as the required field strength increases, the experimental setup for electromagnets becomes progressively larger and more expensive. Additionally, thermal management is another factor that should be taken into account, which can further add to the overall system cost.

2.5.3 Mechanical Stress-induced Alignment

Mechanical force fields, including tensile and shear stress, can also be used to control the long axes of mesogens (**Figure 2.8**). This method is only capable of aligning the LC mesogen parallel to the mechanical field (Bauman et al., 2022). Splay or twisted nematic alignment is hard to acquire. This approach is widely used to prepare large-scale LCE films or fibers due to its simple operation and equipment. Two-step crosslinking reactions occur in the stretching process. When a weakly crosslinked LCE network (called polydomain) in the first-step reaction is uniaxial-mechanically extended, it causes the mesogens which are randomly oriented, to rotate and align themselves in the direction of the stretch. Afterward, a second stage of photopolymerization is carried out to permanently fix the LC alignment in the crosslinked polymeric network (known as monodomain) by

further crosslinking the remaining reactive groups in the stretched network (Yakacki et al., 2015). The technique is straightforward and efficient in creating LCEs in bulk form with substantial deformation capabilities, which has led to its widespread application in the production of LCE-based devices. Additionally, by regulating the ratio of elastomeric polymer chains to mesogens, the transition temperature T_{NI} can be customized (Shaha et al., 2021).

By applying the same principle, more intricate deformation of LCEs has been achieved through multi-axial mechanical stretching. For instance, biaxial stretching of laser-cut LCEs followed by UV photopolymerization has produced LCE metamaterials that exhibit macroscopic biaxial actuation strain (Wu et al., 2021, Li et al., 2021). Complex LCE morphing has been demonstrated by utilizing sophisticated mechanical programming techniques such as twisting, stamping, and embossing (Barnes et al., 2020). Although mechanical stretching has proven to be a simple and effective means of creating various LCE structures, it remains challenging to encode complex orientational arrangements of mesogens in LCEs, which is crucial for diversifying the range of possible LCE actuation modes.

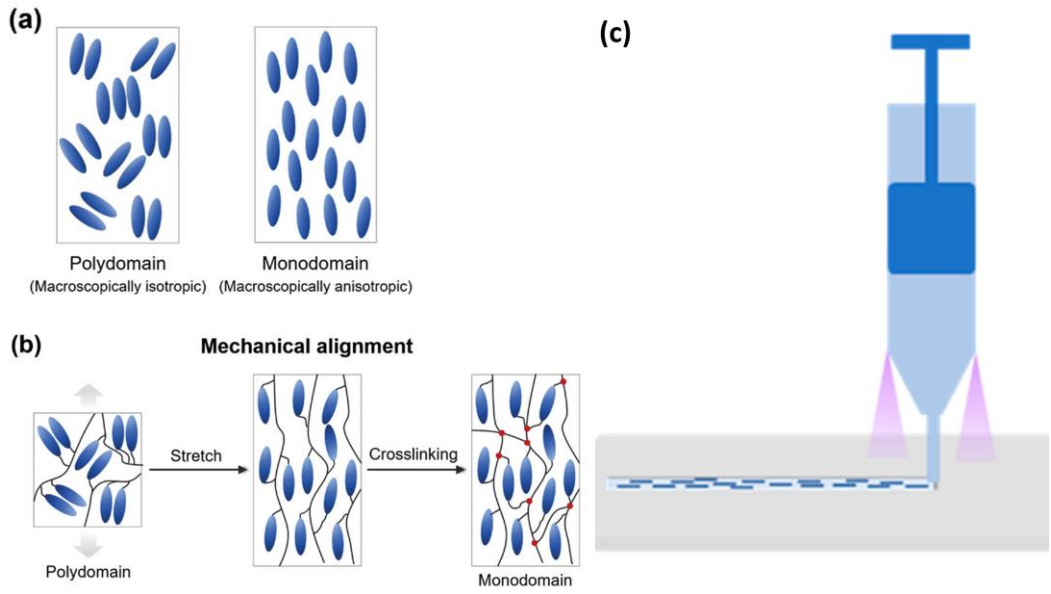

Figure 2.8 Mechanical alignment of mesogens in LCEs. (a) Illustrations of the mesogen alignment in polydomain and monodomain LCEs. (b) Mechanical stretching for mesogen alignment (Chen et al., 2022b), (c) Schematic illustration of the mesogen alignment in the DIW printing direction and fixing this alignment using UV photopolymerization (Wang et al., 2022d).

Shear stress in a viscous flow can also align the LCE precursor solutions or thermoplastic LCEs. This method utilizes the viscous shear flow of a nematic LCE ink with suitable rheological properties instead of mechanically extending lightly crosslinked LCEs. The LC molecules are aligned in the direction of flow when passing through a small gap or a nozzle, where they are exposed to strong shear stress in extensional flow. This principle is widely used in the direct ink writing of LCEs, allowing for complex LC orientation programming by designing printing paths and producing LCEs in 3D geometries (Guan et al., 2022, Saadi et al., 2022a). However, the disadvantage of this approach is that the alignment direction of mesogens is always determined by the printing path.

2.6 Photopolymerization Technologies for LCE-based Actuators

2.6.1 One-pot UV Photopolymerization for Thin Film-like Actuators

The light-responsive film has become the main structure of the LCE actuator in the reported research. They can be fabricated using a one-pot UV photopolymerization technology which allows for convenient and efficient production in a single step, without the need for complex multi-step processes (Yang et al., 2022b, Wang et al., 2020b). During the one-pot polymerization process, the liquid crystal monomers, photoinitiators, and crosslinkers are combined. This allows for the mesogens to be aligned in a specific manner during the reaction. The alignment can be achieved through various methods such as surface rubbing, magnetic fields, or electric fields (Dong and Zhao, 2018). When the mesogens are properly aligned, UV light, typically in the range of 300-400 nm, is applied to induce the photopolymerization reaction under controlled temperature and exposure time. Once the reaction is completed, the resulting LCEs exhibit a well-defined alignment of mesogens. And the arrangement of mesogens can be precisely controlled in this process.

The fabricated LCE film exhibits anisotropic mechanical properties due to the liquid crystal alignment. Upon actuation, the film can undergo significant shape changes, such as bending, twisting, or stretching, in response to external stimuli. The one-pot UV photopolymerization offers several advantages for the fabrication of thin film-like LCE actuators. It simplifies the production process by eliminating the need for multiple steps and reduces the overall processing time. It also allows

for the scalability of production, making it suitable for large-scale manufacturing. Furthermore, precise control over the curing conditions enables the fine-tuning of the mechanical properties of the LCE film, making it customizable for specific applications.

2.6.2 Direct Laser Writing via Two-photon Polymerization for Micro-scale Actuators

Among all additive manufacturing technologies, DLW-TPP provides both sub-micrometer resolution and freedom of structural design (Huang et al., 2020, O'Halloran et al., 2022). It is based on the principles of two-photon absorption, which were first described by Goeppert-Mayer from theory in her doctoral dissertation and experimentally demonstrated by Kaiser and Garrett until the invention of ultrafast lasers. Femtosecond laser fabrication of micro/nanostructures by DLW-TPP can create computer-designed 3D structures with sub-diffraction limit resolution, which is an impossible task for traditional lithographic techniques. Unlike other additive manufacturing technologies, two-photon polymerization microfabrication can fabricate arbitrary and ultraprecise 3D microstructures with high resolution not only on the microscopic scale but also on the nanoscale (Yeung et al., 2020). The distribution of liquid crystal mesogens can be manipulated by the LC cell with designed alignment. Its exceptional capacity to produce 3D structures with high resolution using LCEs has resulted in its specific applications in micro-actuators (del Pozo et al., 2021, Huang et al., 2023), micro-walkers (Zeng et al., 2015), micro-grippers (Chen et al., 2019a, Hsu et al.,

2022, Martella et al., 2017b), and different photonic micro-devices (Del Pozo et al., 2020, Guo et al., 2020b, Guo et al., 2020a).

During the TPP process, liquid LC photoresists are cured into a solid phase upon exposure to femtosecond laser light. Focused ultra-short laser pulses are absorbed by the negative tone photoresists based on two-photon absorption, resulting in a selective polymerization and crosslinking of the photopolymerizable resins, which renders the exposed volume insoluble to the development solvent. In this way, the micro-sized focal volume provided by high numeric aperture focusing enables the direct writing of the required structure by generating the sample via the laser beam using computer-controlled motion stages.

Two-photon absorption (TPA)

In standard photolithography processes, photoresist initiation is triggered by the absorption of a high-energy photon (UV wavelength). There is a linear correlation between the photon density and the reaction speed for single-photon excitation. Unlike the single photon absorption process (**Figure 2.9 a**), to trigger the TPA process, one atom or molecule must absorb simultaneously two photons to arrive at an excited state from the ground stage to induce the transition, which can be realized by an ultrafast laser beam with a high intensity of pulse peak. After immediate excitation, the TPA process occurs within a small focal point in the photosensitive materials to ensure a high resolution. The chemical polymerization between the initiators and monomers will happen. TPA can be classified into two types, sequential and simultaneous absorption. For sequential absorption, a

photosensitive molecule, namely a photosensitizer or photoinitiator, is excited to a real intermediate state after absorbing one photon. Then, a second photon is absorbed by the first-stage species (**Figure 2.9 b**). However, no real intermediate energy state exists in the simultaneous absorption process. This process can be considered as an initial interaction between a photon and a molecule to form a temporary energy state above the ground state, which only exists for an extremely short time interval. If another photon arrives and interacts with the foregoing molecules during the virtual state period, it can be excited to a higher energy state (**Figure 2.9 c**). From the point of the uncertainty principle, the virtual energy state lifetime for the photon in a visible or NIR light source is estimated to be 10^{-16} to 10^{-15} s.

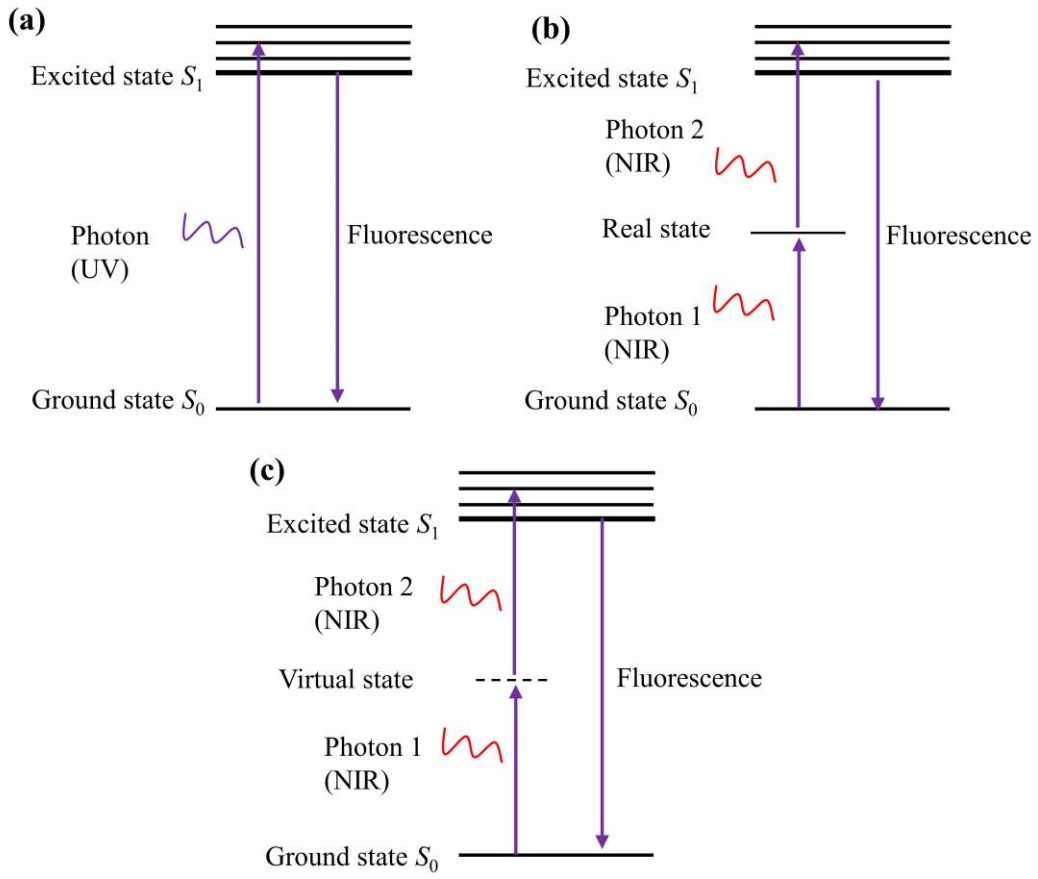

Figure 2.9 Schematic diagram of single photon absorption from a UV source (a) and two-photon absorption from a NIR source including a sequential absorption process (b) and a simultaneous absorption process.

The TPA absorption process that happens in a confined focal volume of the laser beam also shows the chemical reaction induced by TPA concentrates in the vicinity of the focus. Based on this process, photosensitive monomers with active moieties can react with reactive species (e.g., free radicals or cations) generated by photosensitive molecules to form 3D micro-/nano-structures. A typical photoresist system contains 1) one or more photoinitiator(s) or photosensitizer(s) with absorption near two-photon excitation wavelength; 2) transparent photocurable polymeric monomers with functional groups in NIR wavelength; 3) other modification materials to tailor special properties if needed; and 4) Organic or inorganic solvent with ability to dissolve and dilute above individual components for liquid-based photoresists with controlled viscosity, if needed. The overall photopolymerization procedure can be divided into three steps. The highly photoactive initiators (PIs) first conduct localized TPA from the high-energy laser to arrive at an excited state ($PI*$) and generate radicals ($R\cdot$) (initiation). Subsequently, a charge transfer process between the initiators and monomers or oligomers is activated by the radicals to start a free radical-based polymerization between the monomer (M) chains in the confined spot by monomer radical ($RM\cdot$). The polymerization repeats to create 3D extended polymeric networks (propagation). The presence of a crosslinker will help build up the structural

networks between the polymeric chains via covalent bonds. Therefore, the mechanical response and structural integrity of the final structures can be tailored by changing the crosslinker concentration and bonding strength. Finally, the process will end when two monomer radicals are combined (termination). The whole procedure can be depicted by following three steps:

1) Initiation: $PI \xrightarrow{\boldsymbol{2hv}} PI* \rightarrow R\cdot + R\cdot$

2) Propagation: $R\cdot + M \rightarrow RM\cdot \xrightarrow{+M} RMM\cdot\cdots \xrightarrow{+M} RM_n\cdot$

Where *hv* represents Planck's Equation energy for the single absorbed photon.

3) Termination: The termination mechanism typically involves various processes depending on the reaction conditions.

   3-1) Bimolecular Termination:

   Combination Reaction: In bimolecular termination, two polymer radicals combine to form a non-radical species, effectively terminating the polymerization process. This can be expressed as follows:

$$RM_n\cdot + RM_m\cdot \rightarrow RM_{n+m}R$$

   Disproportionation Reaction: This involves the transfer of an electron from one polymer radical to another, resulting in the formation of a non-radical species and an ion. The reaction can be represented as:

$$RM_n\cdot + RM_m\cdot \rightarrow RM_{n+m}R + ion$$

   3-2) Primary Radical Termination:

In primary radical termination, the polymerization process is halted through the reaction of a polymer radical with a non-radical species. This can be described as:

$$RM_n \cdot + non - radical \rightarrow RM_n$$

3-3) Monomolecular Termination (Radical Trapping by Occlusion):

In this mechanism, the polymerization is terminated by trapping the radicals within the growing polymer chains. This can occur through the occlusion of radicals by nearby molecules or functional groups in the polymer structure. The trapped radicals are effectively removed from the polymerization process, preventing further chain growth.

Printing Mechanism and Configuration for DLW-TPP

In the past decades, several commercial DLW-TPP systems have been manufactured for research studies, such as Nanoscribe Professional GT (2007, Germany), Multiphoton Optics GmbH (2013, Germany), and Femtika (2013, Lithuania). There are minor differences in components between these systems. Since most photoresists absorb strongly around 400 nm wavelength, common 780 nm wavelength Ti: Sapphire femtosecond lasers are ideal choices for driving TPA. The setup utilized in current machines for DLW-TPP is similar to the prototype invented by Maruo and colleagues. Essentially, a Ti: sapphire oscillator that is mode-locked is employed to produce stable light at a wavelength of approximately 780 nm, with a repetition rate of 80 MHz. Subsequently, the light is directed through an acoustic-optic modulator that functions as an optical shutter to generate

a periodic laser pulse lasting roughly 100 fs. This brief pulse duration creates a highly concentrated laser beam, minimizing the risk of damaging the material. The laser beam then passes through a neutral density filter and a beam expander before being focused onto preloaded photosensitive materials via a high numerical aperture objective lens (**Figure 2.10**).

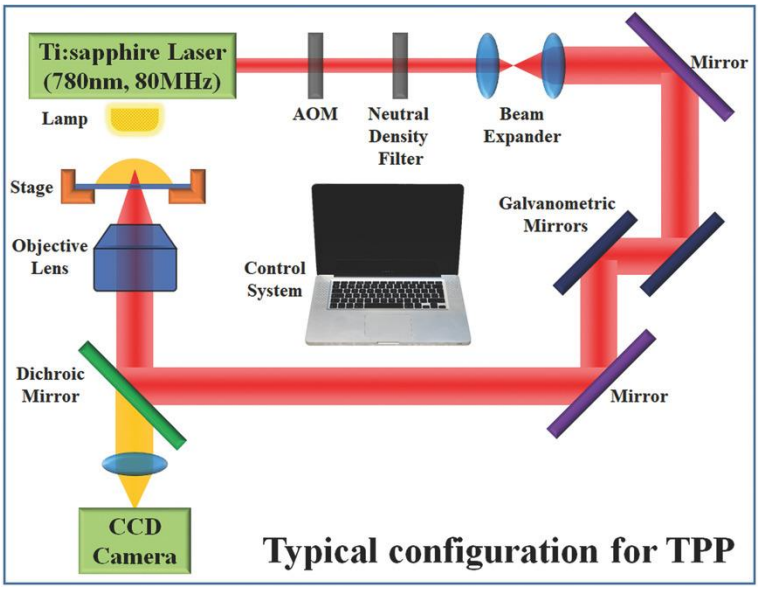

Figure 2.10 A typical schematic TPP setup for the fabrication of 3D structures.

During the fabrication process, two printing configurations including oil immersion configuration and dip-in laser lithography (DiLL) are usually used. The choice of printing configurations generally depends on material properties and printing height. Under DiLL configuration, the objective lens is dipped into the photoresist directly. When the photoresists do not damage the microscope objective lens and have an ideal index, it is recommended to choose DiLL because of no interface limit and wide structural height range. For the oil immersion mode, the lens must be dipped into the immersion oil and then the laser beam is focused into the photoresist through the transparent substrate with a suitable refractive

index. The manufacturing platform can be operated by moving the 3D *XYZ*-stage with a fixed laser beam or moving the laser beam with a stable sample holder. Both approaches have been demonstrated to be effective for manufacturing 3D micro/nano-architectures by different works. Meanwhile, the whole printing process is monitored by a real-time charge-coupled device (CCD) camera and displayed on the computer screen so that the printing parameters can be modified at any time for a more favorable demand.

DLW-TPP printing configurations for LCEs differ from traditional ones that have a free surface, as they use an LC cell consisting of two micropatterned or conductive substrates to induce mesogen alignment instead of a resin vat. A fine laser beam guided by an optic system is focused on any 3D space within the LC cell. The resin focused by the laser is then polymerized point-by-point through the simultaneous absorption of two photons, typically achieved using ultrashort laser pulses (**Figure 2.11**). After laser writing, the unpolymerized monomers are removed with a development bath by opening the cell.

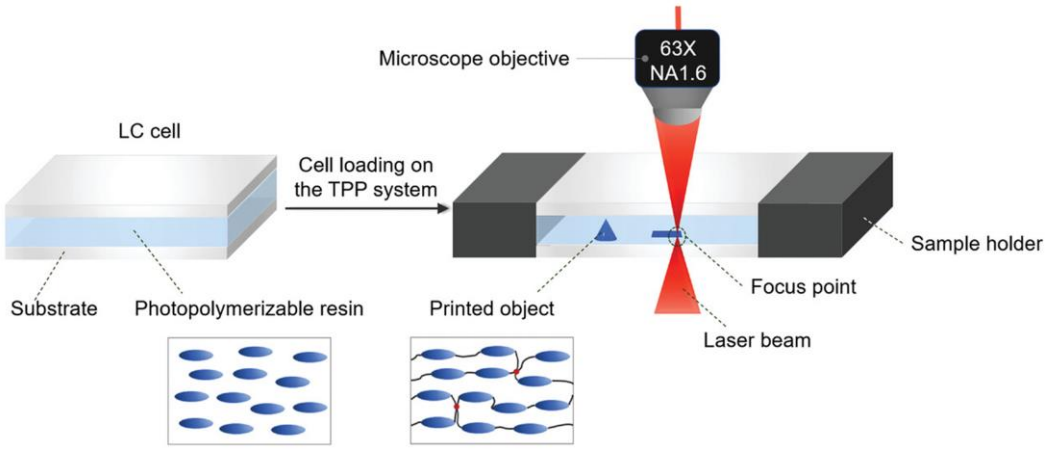

Figure 2.11 Schematic diagram of the DLW-TPP fabrication of LC photoresists loaded in an LC cell (Chen et al., 2022a).

Preparation of LC Photoresists for DLW-TPP

For DLW-TPP, an LC photoresist must meet several requirements. It should contain difunctional mesogens to act as crosslinkers, monofunctional mesogens to add flexibility to the network, and a two-photon photoinitiator. In addition, the material must maintain a stable LC phase at room temperature without the need for a heating stage, which is a fourth requirement imposed by DLW-TPP equipment. While many LC mixtures meet the first three requirements, their LC phases are often unstable at or above room temperature, leading to crystallization within a few minutes and limiting the printing time. Therefore, these mixtures are not suitable for printing in most cases.

The addition of dopants into an LCE photoresist can enhance its optical properties, functionalities, and mechanical performance, as discussed in Section 2.3. When selecting a dopant, two key factors must be considered. Firstly, the dopant should not disrupt the molecular alignment of the photoresist. Secondly, the dopant should be transparent for a 780 nm femtosecond laser, or at least not interfere with TPA. The former requirement can be easily fulfilled by selecting a dopant with dimensions and shapes similar to that of rod-like LC mesogens. The latter consideration depends on the chemical makeup of the dopant and requires careful evaluation.

DLW-TPP Printed LCE-based Micro-structures

Various LCE-based microstructures have been fabricated by DLW-TPP. Much research is aimed at developing micro-actuators that respond to light,

enabling remote, instant, localized, and accurate manipulation at the microscale. In 2015, Zeng et al. successfully created a micro-walker, which was the first light-driven LCE micro-actuator produced using DLW-TPP printing (Zeng et al., 2015) (**Figure 2.12 a**). The micro-walker consisted of a body made of planar-aligned LCEs with azobenzene and four conical legs made of commercial passive acrylate resin. The LCE-based body of the micro-walker could undergo a reversible and anisotropic contraction/expansion upon exposure to successive laser illumination with a λ = 532 nm (green) laser, which brought about its walking on a polyimide-coated microscope glass. Another study developed an autonomous light-responsive micro-hand, which was constructed by combining two splay-aligned LCE strips. When exposed to light, the strips bent and caused the hand to close, and the hand returned to its original state once the light was turned off. The micro-hand was able to move autonomously because objects in its path would alter the direction of the light, causing the hand to react and enabling it to grasp objects independently (**Figure 2.12 b**). Apart from photochemically induced photo-isomerization responses of azobenzene moiety, LCE-based micro-actuators that rely on the photothermal effects of photothermal components have also been fabricated by DLW-TPP. Chen et al. successfully created printable AuNRs/LCEs composite resins and exhibited the light-controlled anisotropic actuating deformation of an LCE micro-woodpile (Chen et al., 2019a) (**Figure 2.12 c**).

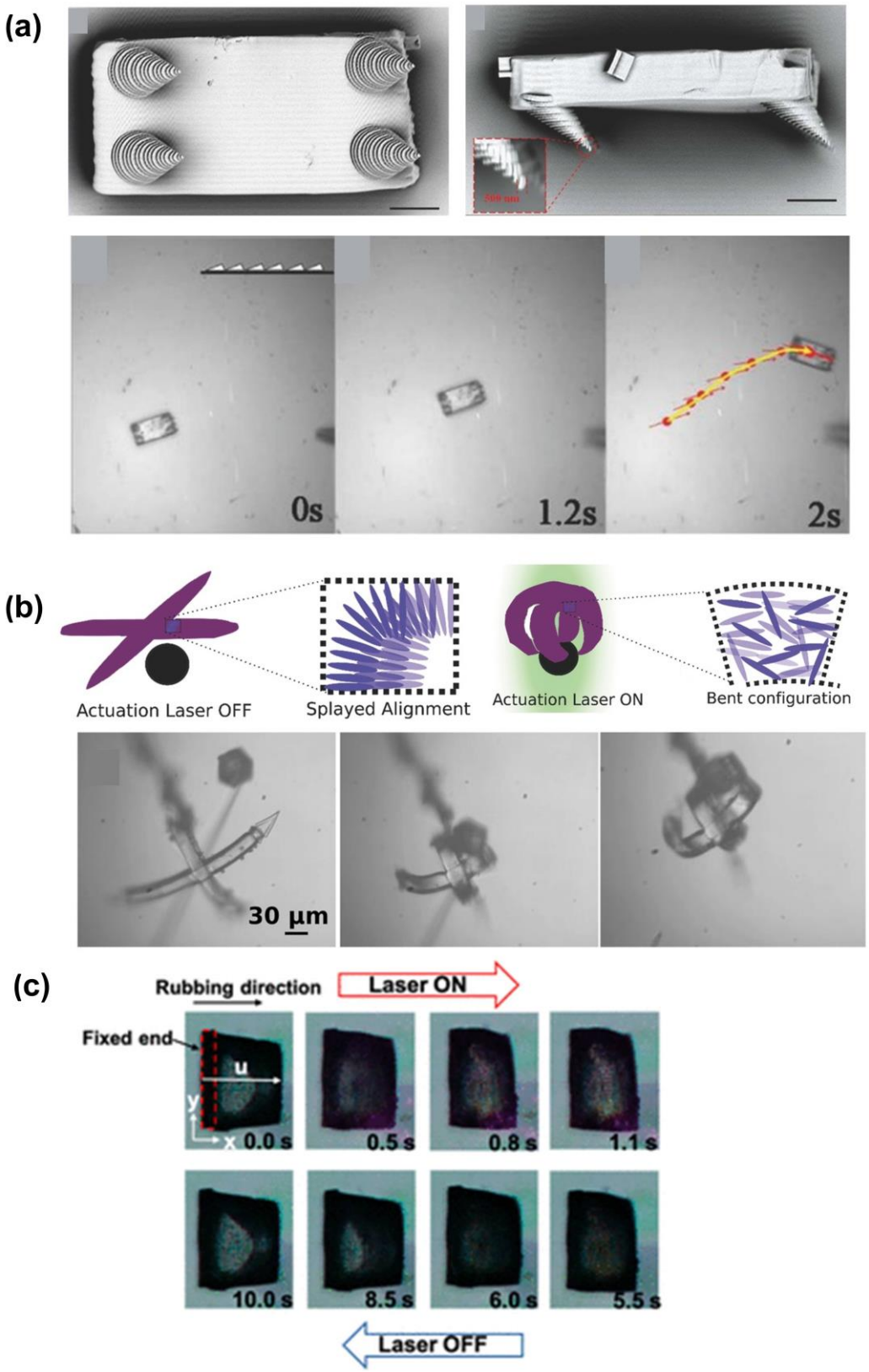

Figure 2.12 (a) a light-driven micro-walker (Scale bar: 10 µm) and its locomotion behavior on a grooved-patterned surface under a 532 nm laser

source. (b) Mechanism illustration of the mesogen orientation change from an open state to a closed state of the micro-hand, and the catching ability of micro-hand for the small object activated with a green laser. (c) Reversible contraction/expansion deformation of an AuNRs/LCEs micro-woodpile upon NIR laser on/off.

2.6.3 UV-assisted Direct Ink Writing for Millimeter to Centimeter-scale Actuators

UV-assisted direct ink writing (DIW) is a type of additive manufacturing method that enables the production of complex 3D structures with varying architectures and compositions at the millimeter and centimeter. In this technique, a viscoelastic ink is extruded under pressure through a deposition nozzle to form a continuous filament, which is then deposited onto the building platform along the designed paths to build a 3D geometry in a layer-by-layer (Saadi et al., 2022b, Rocha et al., 2020) (**Figure 2.13 a**). Then the 3D scaffolds and other 3D geometries are solidified by proper post-processing, resulting in a structure with the desired features and properties (Lewis, 2006) (**Figure 2.13 b-e**). Unlike other additive manufacturing methods, direct ink writing (DIW) is not restricted by the type of material used, as long as the precursor ink demonstrates suitable rheological properties, including apparent viscosity, yield stress under compression and shear, and viscoelastic behavior (i.e., elastic and loss moduli) (Hu et al., 2022).

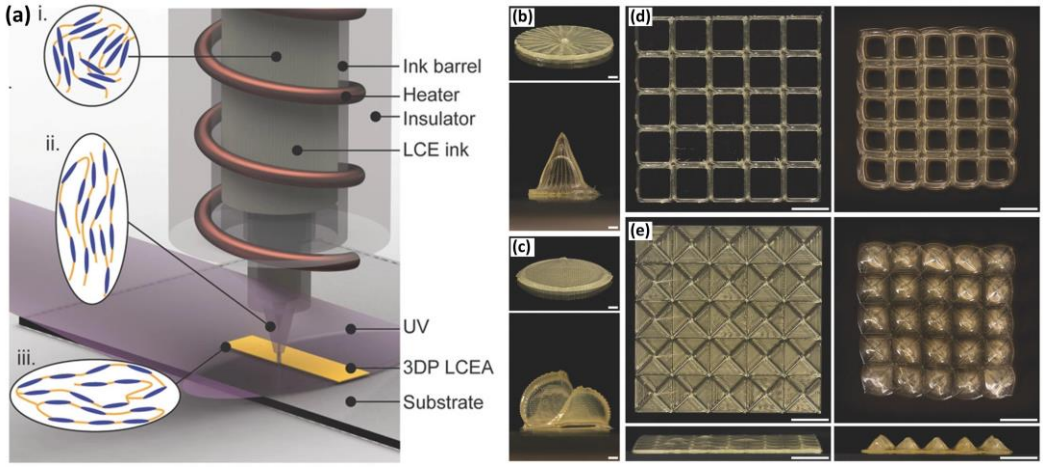

Figure 2.13 (a) Schematic illustration of heater-equipped DIW of the LCE ink, (i) the LCE ink with disorder orientation inside the heated reservoir, (ii) ordered morphology that emerges due to shear-induced alignment within the nozzle, and (iii) programmed mesogen alignment in printed and crosslinked LCE filaments, (b)-(e) DIW printed LCE structures with spatially programmed directors and their shape morphing (Kotikian et al., 2018a).

Oligomeric LCE precursors possess viscoelastic properties. As a result, DIW enables the effective printing of virtually any LCE ink as a 3D structure with programmable stimuli-responsive behaviors and desirable 3D geometry in the centimeter scale thanks to the shear-force-induced mesogen alignment along the printing direction. The utilization of DIW printing technology in designing LCE structures offers significant flexibility in both geometric structure and mesogen alignment. In contrast to conventional methods for creating thin LCE films, 3D LCE structures are anticipated to yield amplified reactions and exhibit intricate alterations in their properties when subjected to stimuli.

Formulating an LC ink for DIW

The widely used DIW-compatible viscous ink with un-crosslinked liquid crystal oligomers is formulated by amine-acrylate "aza-Michael" and thiol acrylate "thiol-Michael" addition reactions (**Figure 2.14**) (Del Pozo et al., 2022b, López-Valdeolivas et al., 2018). The ink is composed mainly of four components: (1) bifunctional RMs that create the polymer network, (2) chain extender or isotropic cross-linker that controls the cross-linking density, (3) photoinitiator that starts the photopolymerization process, and (4) thermal catalyst that speeds up the thiol-acrylate Michael addition. Other components can also be added to the ink for specific functionality, which should not influence the viscoelastic properties. If the molar quantity of the diacrylate mesogen is higher than that of the chain extender, the resulting main-chain LCE mixture can be acrylate-terminated and subsequently photo-crosslinked using a free radical photoinitiator. When an aligned LC phase is photopolymerized, such as through mechanical stretching or direct printing, the printed material exhibits macroscopic alignment and responds to external stimuli by contracting along the molecular director, which is attributed to the order to disorder transition around the T_{NI} of the LCEs.

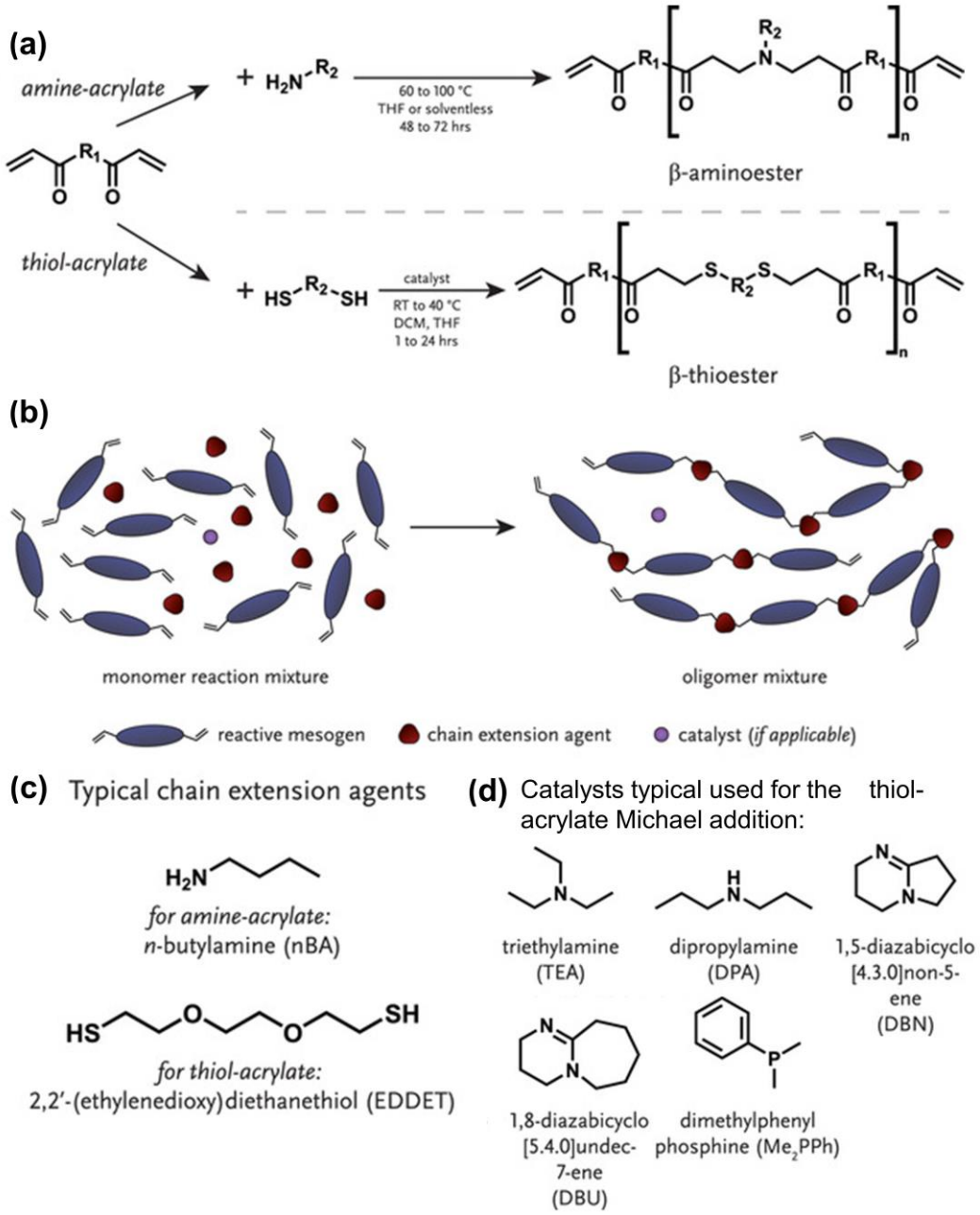

Figure 2.14 (a) Schematic illustrations of the two widely used synthesis routines used for LC oligomers: amine-acrylate (aza-Michael) and thiol-acrylate (thiol-Michael). (b) Schematic representation of the conversion of reactive mesogens to low-weight LC oligomers. (c) Two common chain extension agents are often used in the literature for the two different reaction schemes. (d) Common catalysts used for the thiol-acrylate reaction.

Main printing parameters for DIW

The DIW process typically involves three main steps: 1) Generating 3D structures through Computer-Aided-Design (CAD) software, 2) Creating a 3D movement path for the nozzle using slicing software, and 3) Depositing the ink to generate continuous filament (Tsang et al., 2022, Wang et al., 2022c). A typical DIW printer for LCEs usually consists of an extrusion nozzle and an *X-Y-Z* platform that is motion-controlled, as well as an auxiliary photocuring setup. DIW's key advantage is its ability to customize inks more extensively, enabling the printing of precise 3D structures at the meso- and microscales. DIW can be customized by modifying key variables such as printing temperature and speed, nozzle diameter, and nozzle to printing bed distance. These variables can largely influence the print quality and the mesogen alignment, ultimately affecting the stimuli-response properties of the device (Del Pozo et al., 2022b, Kotikian et al., 2018b, Davidson et al., 2020). Thus, by fine-tuning the printing parameters and utilizing modeling techniques to program the printing path, it is expected that spatially diverse alignment, coupled with enhanced alignment quality, will become achievable. This, in turn, will pave the way for the realization of desired property-changing behaviors in the DIW-printed LCE structures.

As the printing temperature rises, the viscosity of LCEs decreases, reducing the pressure needed for ink extrusion. Conversely, lower printing temperatures are preferable for achieving well-defined structures with strong shear-thinning properties (Kotikian et al., 2018b, López-Valdeolivas et al., 2018). Studies indicate

that printing LCE structures at temperatures within the nematic phase of oligomeric LCE inks results in better alignment of the mesogens along the printing direction, resulting in a higher-order parameter. Additionally, both the order parameter and actuation strain of printed LCEs increase as the printing temperature decreases within mesophases. To achieve a balance between molecular alignment and viscosity, oligomeric LCE ink is typically used for printing in which the ink reservoir is generally heated to approximately 10-20 °C below its T_{NI}.

The molecular alignment of the extruded LC filaments can also be increased with the printing speed because of the strengthened director orientation. This will increase the contraction strain along the printing path. Complex actuated deformation fabricated by a single LC ink can also be realized by programming the spatial printing speed throughout the printing process (Zhang et al., 2019a). Molecular alignment differences can be created throughout the printed structures. Currently, the reported printing speed is in the range of 0.5-28 mm/s (López-Valdeolivas et al., 2018, Kotikian et al., 2019, Ceamanos et al., 2020).

The nozzle diameter is also a parameter that can influence the resolution and mesogen alignment. Although the impact of nozzle diameter on the uniaxial orientation of mesogens in deposited LC oligomer ink hasn't been thoroughly investigated, it has been noted that smaller diameters result in better molecular order (Wang et al.), whereas larger diameters lead to reduced order (Ambulo et al., 2017a). Nozzle diameters typically range between 150-350 μm, and layer heights between 75-190 μm. However, decreasing the nozzle diameter requires a greater

force to extrude the material, and some diameters may not be suitable, depending on the equipment or ink viscosity.

2.7 Summary

This chapter has given a brief review from smart polymeric materials to related fabrication technology for photoresponsive actuators. Widely used polymers, including hydrogels, SMPs, and LCEs, are introduced and explain choosing LCEs as the research material first. The features, advantages, and disadvantages are summarized and compared. Photo-actuation mechanisms of LCEs, including photoisomerization and photothermal effects, are elaborated in detail. The photoisomerizable moieties and photothermal agents using LCEs are listed, followed by an emphasis on the necessity of developing organic conjugated polymers. Common methods to align liquid crystal mesogens, and photopolymerization technologies to fabricate different scales of actuators are reviewed.

Chapter 3 Photothermal Conjugated Polymers for Photo-responsive LCEs

3.1 Introduction

Photothermal CPs are a class of materials that exhibit unique properties, making them attractive for LCE actuator applications. They have been widely applied in photothermal therapeutics recently (Men et al., 2020a). They have obvious advantages over inorganic dopants and low-molecular organic dyes. These polymers possess both conjugated π-electron systems and efficient light absorption capabilities, enabling them to convert light energy into localized heat. Long electron donor-acceptor (D-A) backbones that contain contiguous sp^2- hybridized carbon atoms endow the CPs with a broad absorption in the NIR range, prominent photothermal effect, and high photothermal conversion efficiency (Kim et al., 2021a). This photothermal effect can be harnessed to induce controlled actuation in various systems. The photothermal properties of CPs arise from their unique molecular structure, which typically consists of alternating single and double bonds along the polymer chain. This conjugation leads to extended π-electron delocalization, allowing the polymers to absorb light across a wide range of wavelengths, including visible and near-infrared regions. When exposed to light, the absorbed photons excite the polymer's electrons to higher energy levels. Through nonradiative relaxation processes, the excess energy is dissipated as heat within the LCE matrix.

The choice of photothermal conjugated polymer is crucial for optimizing the actuation performance of LCE actuators. Factors such as the polymer's absorption

spectrum, light-to-heat conversion efficiencies, and compatibility with the LCE matrix need to be considered. By tailoring the molecular-level structural design and composition of the conjugated polymer, its photothermal properties can be fine-tuned to match the desired actuation requirements. The photo-to-heat conversion mechanism of CPs is a result of absorbing radiation energy, which leads to the stimulation of electrons from their initial state (S_0) to various vibrational levels within an excited state (S_n). Subsequently, due to the instability of these excited electrons, the energy is released as heat through non-radiative routes (Cui et al., 2023). Alternating D-A strategies with strong electron-withdrawing acceptors has been demonstrated to be an effective method for conjugated polymers with improved light-to-heat conversion efficiencies. In the D-A_1-D-A_2-type alternating backbone structure, the D and A moieties are repeated along the polymer chain, creating a periodic arrangement (Kivala and Diederich, 2009). The D units typically have higher electron-donating ability, while the A units possess stronger electron-accepting characteristics. This alternating arrangement facilitates efficient intramolecular charge transfer and exciton dissociation within the polymer, leading to enhanced NIR light absorption and photophysical processes. In this section, we carefully selected appropriate donor and acceptor units to synthesize CPs from the discussed design strategy. The synthesis experiment, characterization method, and results are reported.

3.2 Materials and Reagents

Tetrakis(triphenylphosphine)-palladium (0) ($Pd[PPh_3]_4$, 99%), phenylboronic acid pinacol ester (97%), and bromobenzene were acquired from Sigma-Aldrich. Toluene, chloroform-d, and tetrahydrofuran (THF) (99.5%, extra dry) were bought from TiV Scientific Limited (Guangzhou, China). Toluene was dried over 4 Å molecular sieves. 4,8-Dibromo-6-(2-ethylhexyl)-[1,2,5]thiadiazolo[3,4f]benzotriazole (TBZ12) (98%) and 2,5-bis(2-octyldodecyl)-3,6-bis(5-(trimethylstannyl)thiophen-2-yl)-2,5-dihydropyrrolo[3,4-c]pyrrole-1,4-dione (DPP58) (98%) were purchased from Derthon Optoelectronic Materials Science & Technology Co., Ltd. (Shenzhen, China). The liquid crystal monomer (LCM), 4-methoxybenzoic acid 4-(6-acryloyloxy-hexyloxy) phenyl ester (ST3866) and crosslinker 1,4-Bis-[4-(3-acryloyloxypropyloxy)benzoyloxy]-2-methylbenzene (RM257) and were purchased from SYNTHON Chemicals GmbH & Co. KG, Germany. The photoinitiator 2-Benzyl-2-dimethylamino-1-(4-morpholinophenyl)-1-butanone (Irgacure 369) was acquired from Sigma-Aldrich. Polyimide (PI) (DL-2590 for planar alignment and DL-4011 for homeotropic alignment) was acquired from Shenzhen Dalton Electronic Material Co., Ltd., China. All the chemicals and solvents were used directly without further purification unless otherwise noted.

3.3 Design Strategy and Synthesis of Photothermal Conjugated Polymers

Planar alternating D-A-structure CPs exhibit many advantages as photothermal materials, including ease of synthesis, high photothermal effect, easy

solution processing, and good biocompatibility. A synthetic strategy based on electron D-A copolymerization can tune the bandgap of the CPs, especially CPs with D-A_1-D-A_2-type alternating backbone structures, which further results in absorption in the NIR region (Kim et al., 2021a). Because the CPs/LCEs mixtures are prepared by organic solution processing, the CPs need to have branched or linear alkyl side chains, which can improve the solubility of CPs in organic solution (Meyer et al., 2019). The good solubility of CPs ensures the homogeneous dispersion in LCE mixtures after evaporating the organic solvent (THF). Among various acceptor moieties for CPs, diketopyrrolopyrrole (DPP) has garnered significant interest. This is primarily due to the electron-deficient nature of the DPP moiety, which contains fused lactam rings that exhibit strong electron-withdrawing properties. These characteristics enable large intramolecular charge transfer within the CP structure (Lin et al., 2012). Its derivatives with rigid planar backbones have been demonstrated to possess high photothermal conversion efficiency and be easily photoexcited in the NIR region (Li et al., 2016, Xiao et al., 2020a). Therefore, in this work, DPP58 containing thiophene as donor and π-bridge, and DPP as acceptor 1, and TBZ12 containing thiadiazolobenzotriazole (TBZ) as acceptor 2, are chosen as the two monomers for the synthesis of the CPs, named DPP58-TBZ12.

The DPP58-TBZ12 CPs were synthesized via palladium-catalyzed Stille cross-coupling polymerization according to a reported method (Men et al., 2020b). The synthesis routine through Stille cross-coupling polymerization is shown in

Figure 3.1. The reaction mixture was prepared in a glove box to eliminate air. Briefly, a solution of electronic donor DPP58 (monomer 1, 119 mg, 0.1 mmol), and electronic acceptor TBZ12 (monomer 2, 44.7 mg, 0.1 mmol) and palladium catalyst $Pd[PPh_3]_4$ (10 mg, 0.008 mmol) was placed in a 25 mL of Schlenk tube. Next, 10 mL of anhydrous toluene was added. All these procedures were completed in a glove box to avoid oxygen. The solution was stirred vigorously at 100 ºC. After 48 h reaction time, 1 mL of phenylboronic acid pinacol ester (8 mg, dissolved in toluene) and 0.1 mL of bromobenzene were dropped into mixtures to remove the end groups separately under the protection of the nitrogen atmosphere. The reaction continued for 20 minutes. After cooling to room temperature, methanol (100 mL) was used to precipitate the resultant in the solution. The precipitates were obtained through filter paper. The crude powder was purified by Soxhlet extraction with methanol and acetone for 24 h. The extraction could clear away low molecular weight polymers and $Pd[PPh_3]_4$ in the products. The resultant product was collected and dried at 45 ºC under a vacuum for 24 h to yield blue DPP58-TBZ12 CPs (205 mg，70% yield). ^{1}H NMR (400 MHz, $CDCl_3$, δ): 9.33-9.11 (br, 4H),7.59-7.38 (br, 4H), 5.01 (br, 2H), 4.27-4.12 (br, 2H), 2.30 (br, 1H), 1.58-0.84 (br, 90H). Molecular weight was measured by GPC as M_n=10240 g/mol; M_w= 11759 g/mol; polydispersity index (PDI)=1.15.

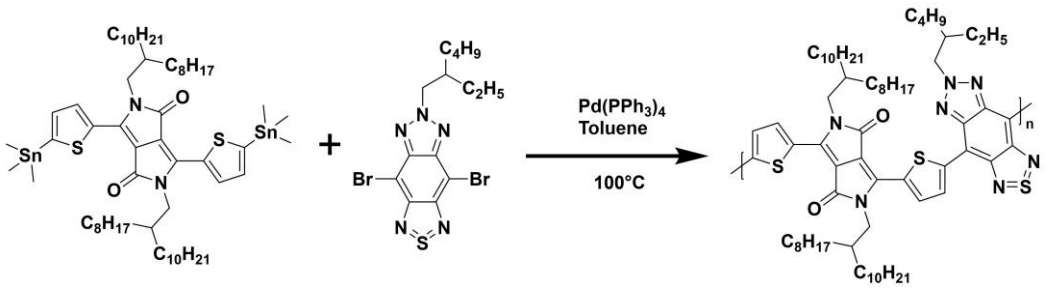

Figure 3.1 Schematic of the synthetic route of conjugated polymers DPP58-TBZ12

3.4 Characterization of DPP58-TBZ12 CPs

To determine the chemical structures of photothermal DPP58-TBZ12 CPs, ^{1}H nuclear magnetic resonance (^{1}H NMR) spectroscopy was carried out on a Bruker Avance-III 400 MHz spectrometer. Chemical shifts were recorded in parts per million (ppm) and were referenced as residual chloroform-d ($CDCl_3$) (δ_H = 7.26 ppm) as the internal standard. Attenuated total reflectance Fourier-transform infrared spectroscopy (ATR-FTIR) measurement was conducted using a Thermo Scientific Nicolet IS50 Spectrometer with an advanced XT-KBr Gold spectrometer at a room temperature in the range of 400-4000 cm^{-1}. Gel permeation chromatography (GPC) (Agilent GPC 50) was used to evaluate the number average molecular weight (Mn), weight average molecular weight (Mw), and polydispersity index (PDI) of the DPP58-TBZ12 CPs. THF was the eluent, and narrowly distributed polystyrene was used as the standard. A Shimadzu UV-vis spectrophotometer (Kyoto, Japan) was used to investigate the UV-vis-NIR absorption spectra of the synthesized CPs.

3.5 NIR Photothermal Properties of DPP58-TBZ12 CPs

The photothermal properties of synthesized DPP58-TBZ12 CPs were measured by an NIR laser setup (LSR808H-2W, Lasever Inc., Ningbo, China) with a wavelength of 808 nm and a laser power of 0.5 W. The beam spot size at the aperture is 4.8 mm × 5.3 mm. The distance between the NIR light source and the CPs dispersion was maintained at 20 cm. The temperature change of samples was recorded using a FLIR C3-X thermal camera (FLIR Systems OU, Estonia). To determine the photothermal conversion efficiency (PCE) of DPP58-TBZ12 CPs, 0.05 mg/mL samples in o-xylene were irradiated by the NIR laser at 0.5 W for 5 minutes to reach a saturation temperature and then cooled down to room temperature with the laser switched off. The temperature of the CPs dispersion was monitored at an interval of 5 s during this cooling period. Heating and cooling cycles were repeated five times to detect the photothermal stability of DPP58-TBZ12 CPs.

The heat loss to the environment can be acquired by observing the temperature decay process following the removal of the NIR light source. Photothermal conversion efficiency (η, %) of DPP58-TBZ12 CPs was calculated by the following equations deriving from Roper's report (Roper et al., 2007):

$$\eta = \frac{hS(T_{max} - T_{amb}) - Q_{dis}}{I\left(1 - 10^{-A_{808}}\right)} \quad (1)$$

where h is the heat transfer coefficient, S is the surface area of the container, T_{max} and T_{amb} are saturation temperature (also the maximum system temperature) of the irradiated sample and the environment temperature. Q_{dis} represents heat

dissipated from light absorbed by the sample container and o-xylene solvent, and it is measured independently using a container containing o-xylene without CPs. I means the incident laser power. A_{808} is the absorbance (0.873) of the CPs dispersion at 808 nm. The value of hS can be calculated from the equation:

$$hS = \frac{mC_{OX}}{\tau_s} \quad (2)$$

where m is the mass of the solution containing the CPs (0.2 g), C_{OX} express the specific heat capacity of the o-xylene solvent (C_{ox} =1.26 J/(g×°C)), and τ_s represents the slope of the linear time data vs negative natural logarithm of driving force temperature.

$$t = -\tau_s \ln(\theta) \quad (3)$$

where θ is introduced to define a parameter.

$$\theta = \frac{T_t - T_{amb}}{T_{max} - T_{amb}} \quad (4)$$

T_{max} and T_{amb} represent the steady-state temperature of the CPs and the environment temperature. T_t is the corresponding temperature of DPP58-TBZ12 CPs during the cooling process.

3.5 Characterization and Results

The chemical structure of the prepared DPP58-TBZ12 CPs was confirmed by ^{1}H NMR spectra and ATR-FTIR. ^{1}H NMR spectra are shown in **Figure 3.2**. All characteristic peaks are corresponding to their related hydrogen atoms according to chemical shift, integral area, and coupling constant. The multiple peaks at 0.84-1.58 ppm were ascribed to the aliphatic protons of the alkyl side chains of DPP58 and TBZ12 units. Characteristic peaks from 7.38 and 7.59 ppm were

corresponding to the aromatic protons in TBZ12. The peaks at 9.11 and 9.33 ppm were related to the protons of the thiophene moieties in DPP58. The observed chemical shift was consistent with the proton position in the conjugated polymer DPP58-TBZ12 structure. The ^{1}H NMR results indicate the D-A DPP58-TBZ12 conjugated polymers were synthesized with success through Stille cross-coupling polymerization.

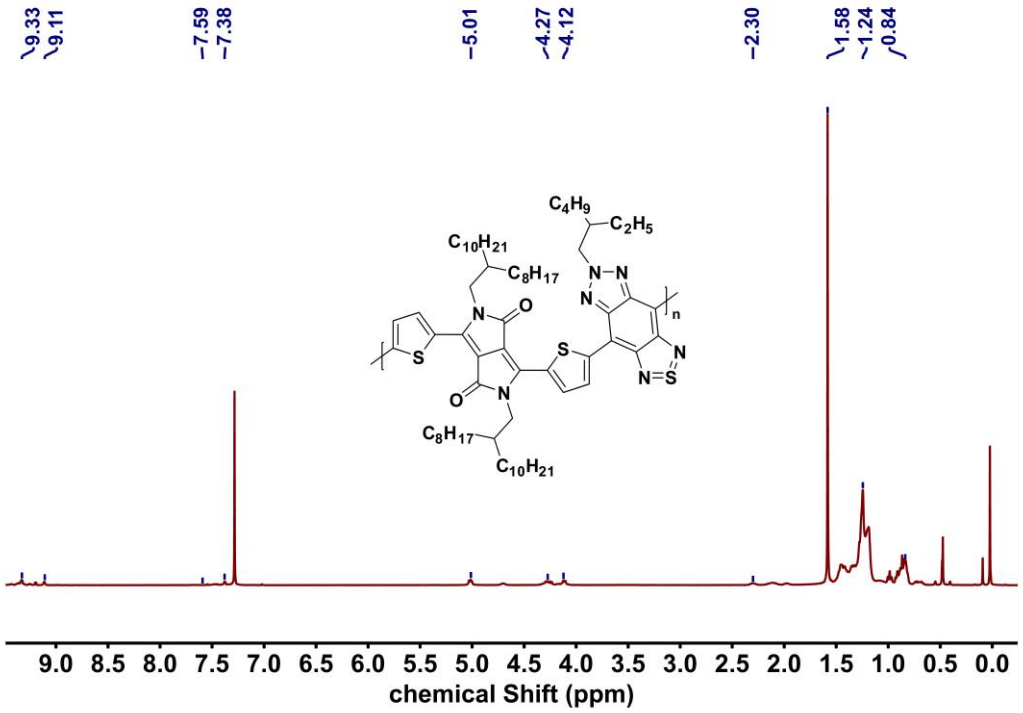

Figure 3.2 ^{1}H NMR spectra (400 MHz) of the DPP58-TBZ12 CPs in $CDCl_3$.

The planar DPP58 monomers contain two electron-rich thiophene rings and an electron-deficient core DPP. The TBZ12 monomers serve as an electron-deficient acceptor. Due to the alternating planar D-A_1-D-A_2 backbone, DPP58-TBZ12 CPs exhibited a low band gap, resulting in a broad absorption range between 600nm and 800nm in THF solution with a peak located around 746 nm.)

as shown in **Figure 3.3**. The absorption behavior of the CPs around the NIR region was beneficial for the preparation of NIR light-responsive photoresists.

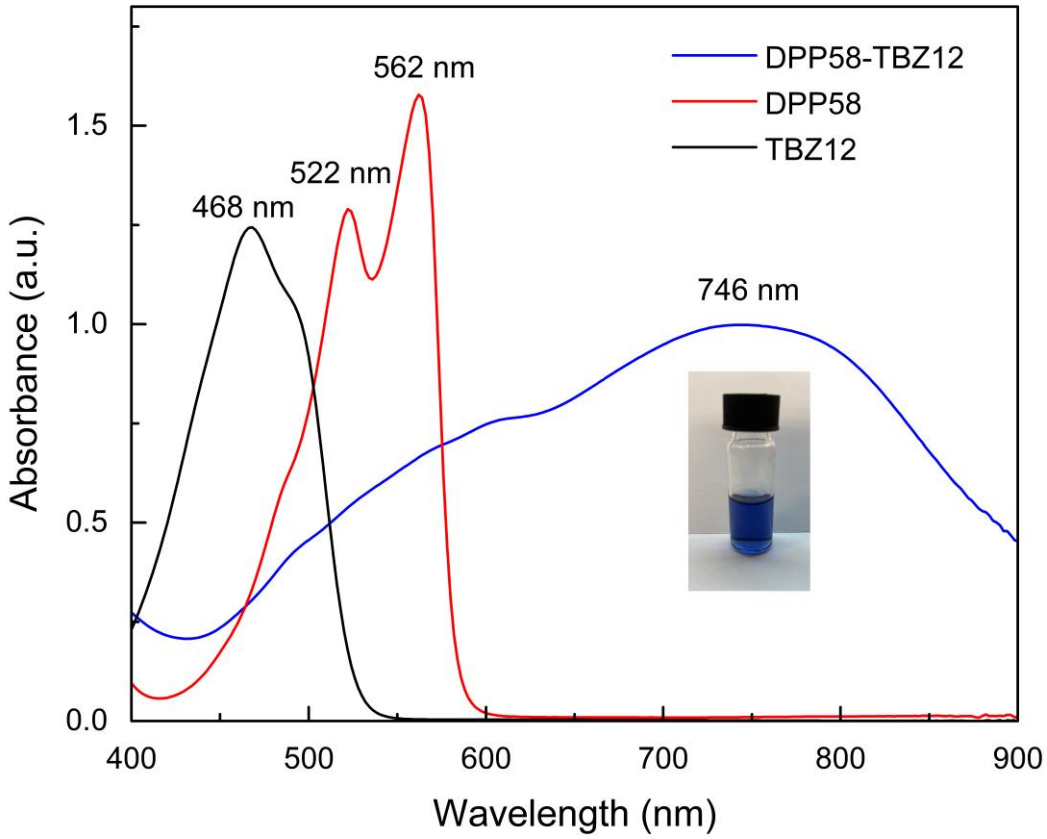

Figure 3.3 UV-Vis-NIR absorption spectra of DPP58, TBZ12, and DPP58-TBZ12 CPs measured at room temperature. (concentration = 0.05 mg/mL, dissolved in THF) (Insert: the photography of 0.05 mg/mL DPP58-TBZ12 CPs in THF solution).

As exhibited in **Figure 3.4 a and b**, no distinct temperature change was observed for o-xylene after 5 min NIR light stimulation. On the contrary, the temperature of the 0.05 mg/mL DPP58-TBZ12 CPs dispersion showed an obvious and quick rise from 18 to 79.2 ºC, which confirmed the effective photothermal conversion ability. According to the experimental results and equations (1) - (4), the time constant for heat transfer from the sample solution was calculated to be

τ_s=69.63 by using the linear time data from the cooling period vs. the negative natural logarithm of driving force temperature (**Figure 3.4 c**). hA was calculated to be 3.6×10^{-3} W/°C. Then a high photothermal conversion efficiency (η) value of DPP58-TBZ12 CPs could be acquired to be 52.7%, compared with other reported photothermal CPs (Chen et al., 2019b, Sun et al., 2018, Du et al., 2019). To evaluate the photothermal stability of the CPs, which is a critical evaluation parameter in NIR photo-actuation, the recyclable temperature change in the presence of the CPs under NIR light on and off is shown in **Figure 3.4 d**. The CPs dispersion was irradiated under 808nm light of 0.5 W for 300 s and cooled down to room temperature by turning off the NIR light. During at least five heating and natural cooling cycles, the maximum temperature of DPP58-TBZ12 CPs was almost constant, demonstrating their admirable photothermal conversion stability.

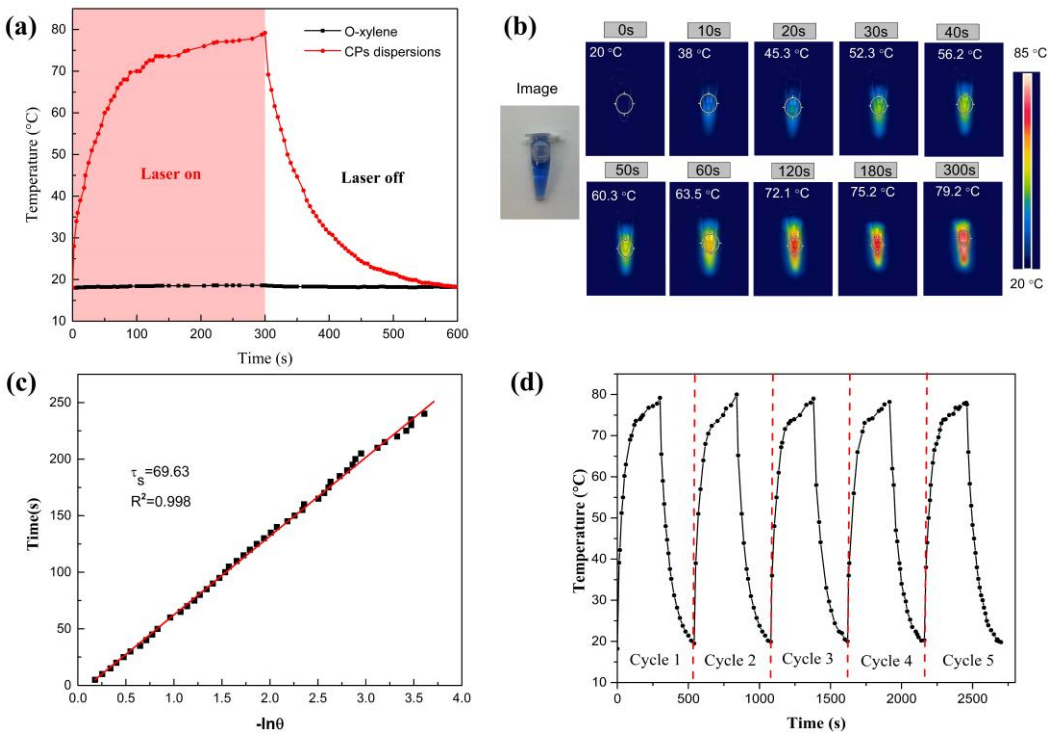

Figure 3.4 (a) Time-dependent temperature change curves of 0.05 mg/mL DPP58-TBZ12 CPs in o-xylene under a NIR laser irradiation (808 nm, 0.5 W), and the laser was shut off after 5 min. (b) Infrared thermal images of 0.05 mg /mL DPP58-TBZ12 CPs solution with laser irradiation at different times. (c) The linear plot of cooling time versus the negative natural logarithm of driving force temperature for determining photothermal conversion efficiency. (d) Stability study of the DPP58-TBZ12 CPs dispersions under five photothermal heating and natural cooling cycles.

3.6 Conclusions

In summary, in this chapter, we successfully synthesized new photothermal CPs π-conjugated backbones, named DPP58-TBZ12. The CPs have strong NIR light absorption (around 746 nm), photostability, and high photothermal conversion efficiency (52.7%). Thanks to the good solubility in the organic

solvent, the homogenous LCE mixtures are prepared for photothermal actuator fabrication. CPs with a low concentration display fast heating speed under NIR light stimulation, which is very beneficial to trigger the phase transition of mesogens.

Chapter 4 2D Film-like NIR Light-triggered LCE Actuators Fabricated by One-pot UV Photopolymerization

4.1 Introduction

Biomimetic actuators inspired by plants and animals have attracted increasing research interest due to their numerous applications in soft robots, actuators, artificial muscle, and biomedical devices (Zeng et al., 2021, Le et al., 2019, Clegg et al., 2019, Pilz da Cunha et al., 2020). For example, self-bending in mimosa leaves and hominid hands and twisting directionality in cucumber plants have inspired enormous intelligent system studies (Shang et al., 2019b, Zhao et al., 2022). Lots of efforts have been committed to developing bionic actuators with morphological control of different dimensions (from 0D to 3D) and sophisticated mechanical locomotion. The development of diverse shape-changing polymer systems significantly advances the creation of untethered soft actuators for complex motion and adaption to environmental confinement (Xiao et al., 2020b, Shang et al., 2019b). They have provided the great potential to integrate actuators, sensors, and intelligent systems into millimeter or even micrometer soft robots. LCEs, combining the entropy elasticity of the polymer network and the anisotropy of the liquid crystalline, are promising candidates for many applications in both air and underwater (Huang et al., 2020, Xiao et al., 2020b, Guan et al., 2022). LCE-based actuators are capable of completing large, reversible, and programmable shape-deformation in response to many stimuli. Programming the rigid, rod-like liquid crystal mesogen orientation in the polymer networks; however, the

macroscopic actuators can deform from flat into 3D structures upon order-disorder phase transition of mesogens. To date, a considerable number of researchers have demonstrated the advantages of LCEs to achieve simple in-plane deformation (e.g., contraction and expansion (Li et al., 2017a, Li et al., 2003)) and complex out-of-plane deformation (e.g., bending (Zhang et al., 2020, Yang et al., 2022a), twisting (Lu et al., 2017, Pang et al., 2019a) and oscillation (Wehner et al., 2016, Kumar et al., 2016)) in response to different stimuli. Interestingly, repeated reversible shape deformation under some incentives on/off cycles can propel the various forms of biomimetic locomotion from natural intelligence (Yang and Shen, 2021, Zhang et al., 2021b).

Among different stimuli, light-driven LCE actuators that operate in solvent-free environments have become a mainstream research direction that features remote, noncontact, ease, and precise spatial-temporal manipulation (Stoychev et al., 2019). A large amount of light-stimulated LCE actuators take advantage of conformational change generated by the photomechanical effects of azobenzene. Azobenzene groups are planar rod-like molecules that are highly sensitive to light. UV light-induced trans (stable stage)-cis (metastable state) azobenzene moieties can generate shape changes in the macroscopic materials (Ahn et al., 2016). Nevertheless, some issues, like two light sources at different wavelengths and slow response speed, related to azobenzene-containing LCEs limit some practical applications (Yang et al., 2015). UV and visible light have low penetration depth in some barriers and adverse health effects. NIR photothermal dopants are another

fascinating actuation inducement for achieving light-driven LCE robots. The functional dopants can absorb NIR light and subsequently release the photon energy through local temperature increases in the LCE matrix. The disorder of aligned mesogens by the temperature (above T_{NI}) in LCEs generates a physical response. To date, various photothermal materials like CNTs (Kim et al., 2019, Yu et al., 2022a), gold nanoparticles (Yang et al., 2022b), graphene (Marotta et al., 2018), and emerging MXene sheets (Yang et al., 2022a) have been functioned for developing homogenous LCE mixtures. However, some notable shortcomings related to these inorganic fillers, like complex and multi-step surface chemical-modification processes for their compatibilities with polymer matrices and opaque color, also exist and limit their applications (Del Pozo et al., 2022b). Thus, organic CPs with excellent photostability, tunable photothermal conversion efficiencies, and low cytotoxicity are good choices as photothermal agents for LCE actuators (Kim et al., 2021a). Conjugated polymers are macromolecular polymers featuring electron donor-acceptor alternating conjugated backbones and a very narrow bandgap. These properties enable CPs to respond to NIR light and convert it to heat energy efficiently through non-radiative relaxation. The compatibility between CPs and LCEs also allows simple mixing for composite preparation in many kinds of organic solvents for long-term stable storage of photo-responsive unpolymerized LCE-based composites without aggregation. Although conjugated polymers are promising resources for photothermal engineering, to the best of our knowledge, there have been very few reports on the attempts to develop soft

CPs/LCEs actuators (Liu et al., 2016).

In this section, we developed a facile approach to prepare a single-layer soft actuator that can perform reversible, various shape morphing and helical twisting locomotion in response to NIR light based on conjugated polymers/liquid crystal elastomer (CPs/LCEs) composites. New diketopyrrolopyrrole-derived alternating donor-acceptor CPs with extraordinary NIR-photothermal effect were synthesized via Stille cross-coupling polymerization, and then homogeneously dispersed in the LCE matrix in an organic solution. The low content of CPs could enable the actuator's remarkable local photothermal effect. Tunable shape deformation styles were obtained by the combination of surface-enforced alignment techniques and different cutting angles with respect to the rubbing direction. Mimicking the Venus flytrap, the bending shape of CPs/LCEs actuators could create close and open states for trapping small objects. The twisting deformation of soft CPs/LCEs actuator could generate incompatible strain to propel the actuator roll forward. Compared with other millimeter-scale NIR light-induced soft actuators reported in literature (Wu et al., 2019, Zhao et al., 2022, Wu et al., 2020b, Wei et al., 2018, Wang et al., 2020a), the CPs/LCEs actuators proposed here exhibit a faster response time (within1 s), more significant deformation potential (180º bending angle) and higher locomotion speed (0.47 mm/s).

4.2 Experiments

4.2.1 Liquid Crystal Cell Preparation with Splay Alignment

The liquid crystal cell assembly was prepared according to reported methods

(surface-enforced alignment techniques) for the later alignment of mesogens in the LCE matrix. Parallel grooves formed by mechanical friction on the polyimide surface can induce the alignment of the mesogens (Li et al., 2020). Glass substrates (2.5 cm × 2.5 cm × 0.7 mm) were cleaned by alternating ultrasonication using acetone and deionized water three times and dried with nitrogen. To prepare a cell with splayed alignment, a glass substrate was spin-coated with PI DL-2590 for parallel alignment of mesogens to the substrate at a speed of 2500rpm for 40 s, dried at a hot plate at 120 ºC for 5 min, and finally rubbed unidirectionally using a velvet cloth. Another substrate was spin-coated with PI DL-4011 for homeotropic alignment at a speed of 2000 rpm for 30 s and dried at a hot plate at 120 ºC for 5 min. High-pressure nitrogen was used to remove the remaining dust particles on the surface of rubbed substrates. To achieve the splayed nematic alignment, a sandwich cell was assembled by a rubbed PI DL-2590 coated substrate on the top and a PI DL-4011 coated glass substrate on its bottom with 60 μm spacers between them. The rubbed polyimide layers, serving as an alignment layer, were formed inside the cell.

4.2.2 Preparation of Soft CPs/LCEs Film with Bioinspired Actuation

To prepare CPs/LCEs film, 75 wt.% RM006 and 24 wt.% RM257, and 1 wt.% Irgacure 369 was dissolved in THF in a vial, followed by the addition of DPP58-TBZ12 CP. After 1 h of stirring, the mixture in the open-cap vial was stirred in a vacuum oven at 70 °C overnight to evaporate the THF solvent completely to yield the pristine LCE mixture and homogenous CPs/LCEs mixtures with 0.1, 0.2, 0.3

wt.% CPs (**Figure 4.1 a and b**). Then, the CPs/LCEs mixture was infiltrated into the liquid crystal cell with splay alignment on a hot plate at 70 ºC through capillary attraction. From the DSC results, all the CPs/LCEs mixture can keep the isotropic phase at 70 ºC during the infiltration process. The liquid crystal cell was subsequently cooled to 40 ºC at a rate of 5 ºC/min to reach a nematic phase with splayed molecular alignment, followed by exposure to a UVGL-58 handheld UV lamp (6 Watt, λ = 365 nm) for 30 min to complete photopolymerization and crosslinking. Finally, the cell was opened by a blade, and free-standing soft CPs/LCEs film was peeled off from the substrates (**Figure 4.1 c and d**). Four strips at different 0° and 45° cutting angles with respect to the planar alignment direction (rubbing direction) were cut out from the sample CPs/LCEs film. Two strips with a size of 15 mm × 3 mm × 0.06 mm at 0° angle were used to demonstrate the bending and Swiss rolling shape deformation when being exposed to NIR light. The strips of 10 mm × 2 mm × 0.06 mm at 45° angle were utilized to display left-hand helical twisting shape morphing and photo-motion ability under NIR laser irradiation, respectively.

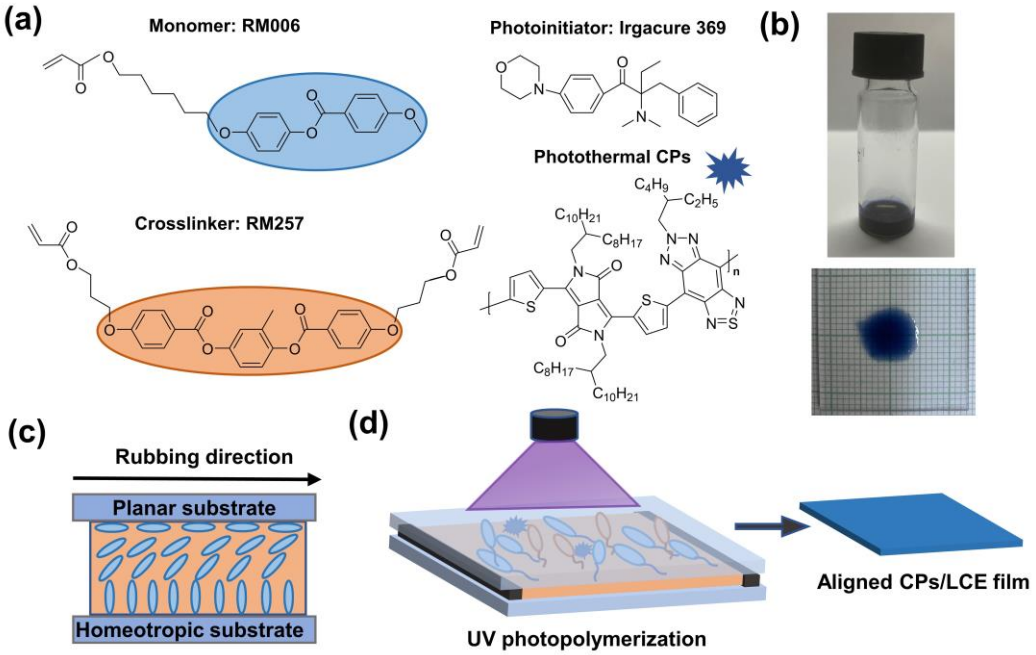

Figure 4.1 (a) Chemical structures of liquid crystal monomers monoacrylate RM006 and crosslinker diacrylate RM 257, photoinitiator Irgacure 369, and photothermal agents DPP58-TBZ12 CPs. (b) Photography of the 0.3 wt.% DPP58-TBZ12 CPs/LCEs composite. (c) Schematic representation of the mesogen alignment across the planar substrate to the homeotropic substrate. (d) Schematic illustration of the CPs/LCEs mixture filled the cell with splay alignment for UV photopolymerization.

4.2.3 Characterization and NIR Light-response

Differential scanning calorimetry (DSC) tests were performed on a Mettler Tolede DSC3. Typically, at least 3 mg of samples were encapsulated in a sealed aluminum pan with another empty pan as the reference. Samples were first heated to 150 ºC, then cooled to 0 ºC and heated to 150 ºC at a rate of 10 ºC/min under a nitrogen atmosphere, and the second heating result was shown. The planar alignment of LC mesogens along the rubbing direction in the CPs/LCEs film was

confirmed by a polarized optical microscope (POM). A spot diameter-tunable 808 nm laser (LSR808h-4W-FC; Lasever Inc., Ningbo, China) was used as the NIR light source. During the following experiments, the NIR light source was situated 20 cm place away from the LCE-based actuators. A Newport 843-R power meter kit was used to adjust the laser power. A FLIR C3-X (FLIR System OU, Estonia) thermal camera was employed to monitor the surface temperature changes of the CPs/LCEs film under 808 nm laser irradiation with different power. Photographs were taken with a phone camera.

4.3 Experimental Results and Discussion

4.3.1 Incorporation Characterization by ATR-FTIR Spectroscopy

The ATR-FTIR spectra for the DPP58-TBZ12 CPs, LCE film, and CPs/LCEs film were conducted in the range of 4000-400 cm^{-1}, as depicted in **Figure 4.2**. Several characteristic peaks of each are identified. The absorption peaks at 2935 cm^{-1} and 2862 cm^{-1} were ascribed to the asymmetrical stretching vibrations of the aliphatic C-H and the symmetrical stretching vibration of the saturated C-H bonds, respectively (Liu et al., 2019). The peaks confirmed the construction of a conjugated skeleton during the polymerization. The strong absorption peaks around 1664 cm^{-1} and 1550 cm^{-1} were related to the C=O and C=C in stretching vibration in DPP58 and TBZ12 rings, respectively. The peak at 1143 cm^{-1} belongs to the stretching vibration of N-N bonds on the TBZ12 ring. The peaks at 1109 cm^{-1}, 1079 $cm^{-1,}$ and 1023 cm^{-1} were assigned to the C-N and N-N stretching vibration in the TBZ12 ring. 846 cm^{-1} was associated with the out-of-plane vibration of the

C-H bonds of the acrylate group.

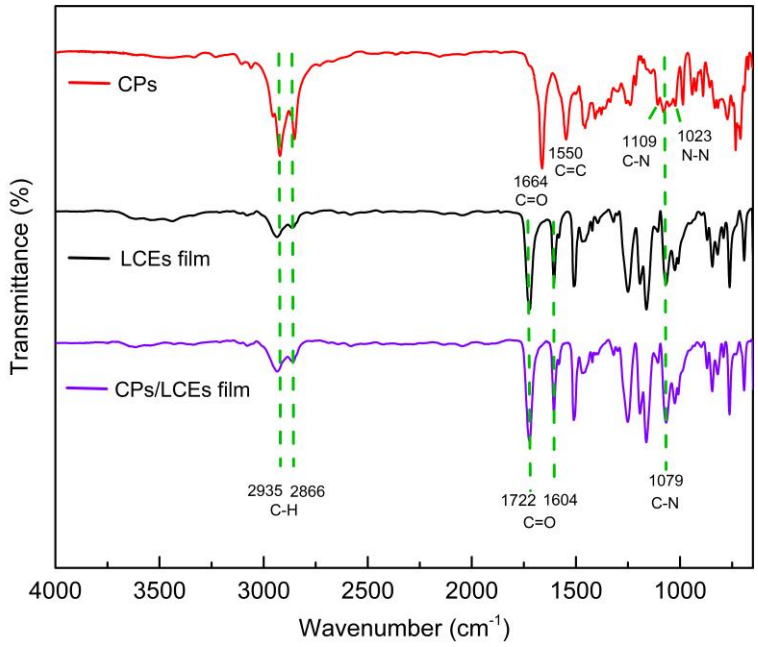

Figure 4.2 ATR-FTIR spectroscopy of the DPP58-TBZ12 CPs, LCE film, and CPs/LCEs film.

4.3.2 NIR Photothermal Properties of CPs/LCEs Actuators

The differential scanning calorimetry (DSC) curves of polymerized pristine LCEs and CPs/LCEs films with different CPs concentrations were recorded to evaluate the thermal properties. As shown in **Figure 4.3**, no glass transition temperature was observed in these mixtures. The addition of DPP58-TBZ12 CPs in LCEs decreases the T_{NI} values from 67.9 to 47.9 ºC. It is believed that the mechanism might lie in the combined effects of the thermal-mechanical response of DPP58-TBZ12 CPs and reduced strength of intermolecular forces (e.g., π–π bonding) between rigid rod-like mesogens because of the insertion of planar DPP58-TBZ12 CPs in the LCE matrixes (Xie et al., 2017). These effects of

DPP58-TBZ12 CPs might result in easier disruption of nematic ordering among mesogens and the resulting lowering of T_{NI}. The effects could be magnified with the increasing CPs content. Similar molecular dimensions and the planar shape of these CPs and LC mesogens did not disturb the mesogen alignments in UV photopolymerization.

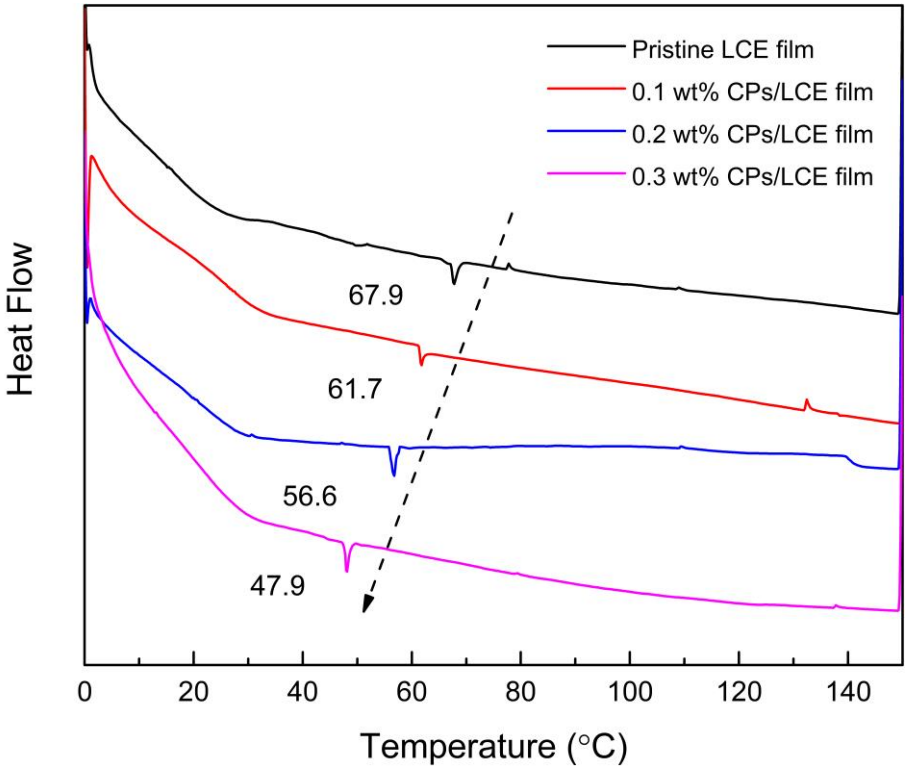

Figure 4.3 DSC curves in the second heating cycle of the CPs/LCEs films with different contents of CPs.

Infrared thermal imaging was employed to evaluate the photothermal effect of DPP58-TBZ12 CPs/LCEs film. To quantitatively assess the photothermal ability of the CPs concentration in the LCEs, curves of temperature changes of the samples with various contents of CPs at different laser intensities were acquired. As shown in **Figure 4a**. When exposed to the NIR laser with a wavelength of 808 nm, the surface temperature on the pure LCE film increases gently with the laser

intensity varying from 0.1 W/cm^2 to 1 W/cm^2. Contrarily, the incorporation of a small account of CPs in the LCEs significantly increases the temperature. The local equilibrium temperature of 0.3 wt.% CPs/LCEs film rises rapidly up to ~162 ºC exposed to NIR laser at 1 W/cm^2. Notably, CPs/LCEs film displays a superfast initial heat rate within 5 s of illumination (**Figure 4.4 b and c**). This superior photothermal effect ensured the ultrafast response of the CPs/LCEs actuator under light irradiation. The locally generated heat above T_{NI} could induce order-disorder phase transition to initiate the shape morphing and thus promote the locomotion of actuators. Herein, we used the CPs/LCEs with 0.3 wt.% CPs for subsequent NIR light-triggered experiments.

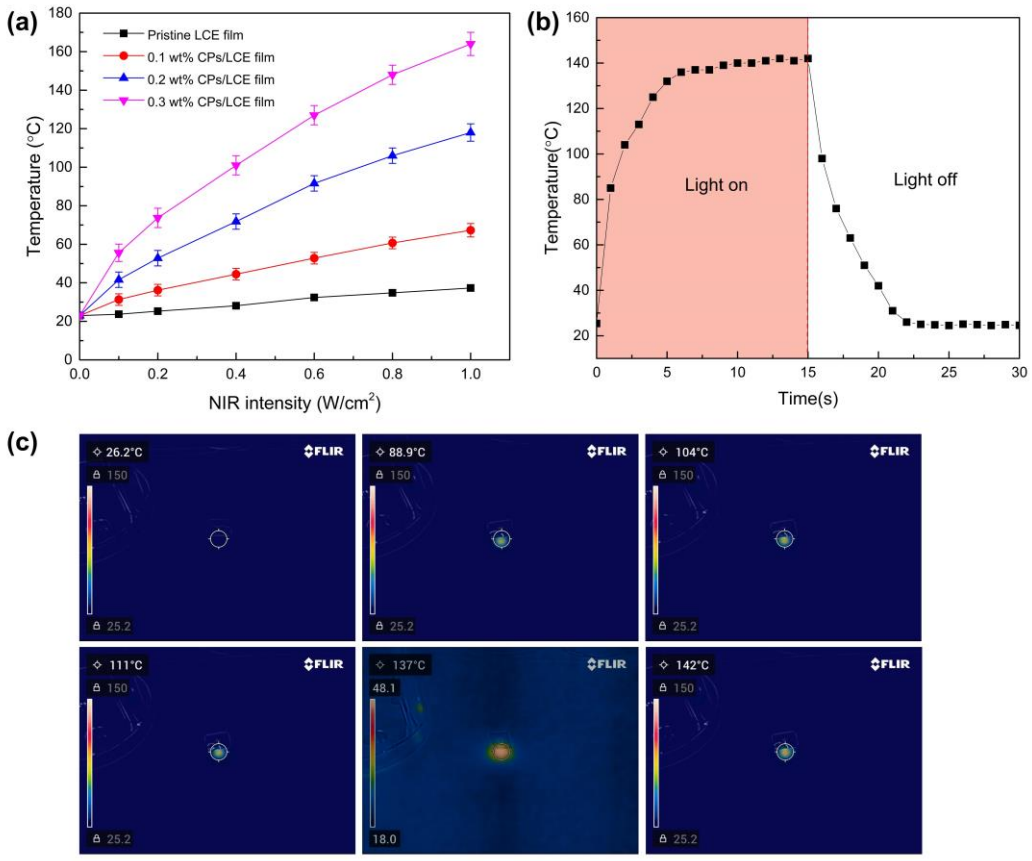

Figure 4.4 (a) The surface temperature change of pristine LCE film and the CPs/LCEs films with different CPs loading under different NIR light

intensities at 808 nm. (b) The temperature change of the 0.3 wt.% CPs/LCEs film when turning on and off the 808nm light with an intensity of ~0.8 W/cm^2. (c) Infrared thermography images of the 0.3 wt.% CPs/LCEs film under 808nm laser at ~0.8 W/cm^2.

4.3.3 NIR Light-induced Deformation of Soft CPs/LCEs Actuators

To achieve diverse shape morphing behavior of soft CPs/LCEs actuators, a homemade liquid crystal cell with a splay alignment was employed. The mesogens within the film were transitioned from the planar surface on the top substrate to homeotropic distribution on the bottom side of the substrate. POM was used to examine the alignment of the mesogens on the rubbed PI layer with planar and homeotropic anchoring. When the rubbing direction of the film was parallel or homotropic to the analyzer, the transmittance was minimized, and the image was a dark tone. If the rubbing direction tilted at an angle of approximately 45° to the analyzer, the transmittance of the film was maximized, and the photo showed a bright color relatively, as displayed in **Figure 4.5**.

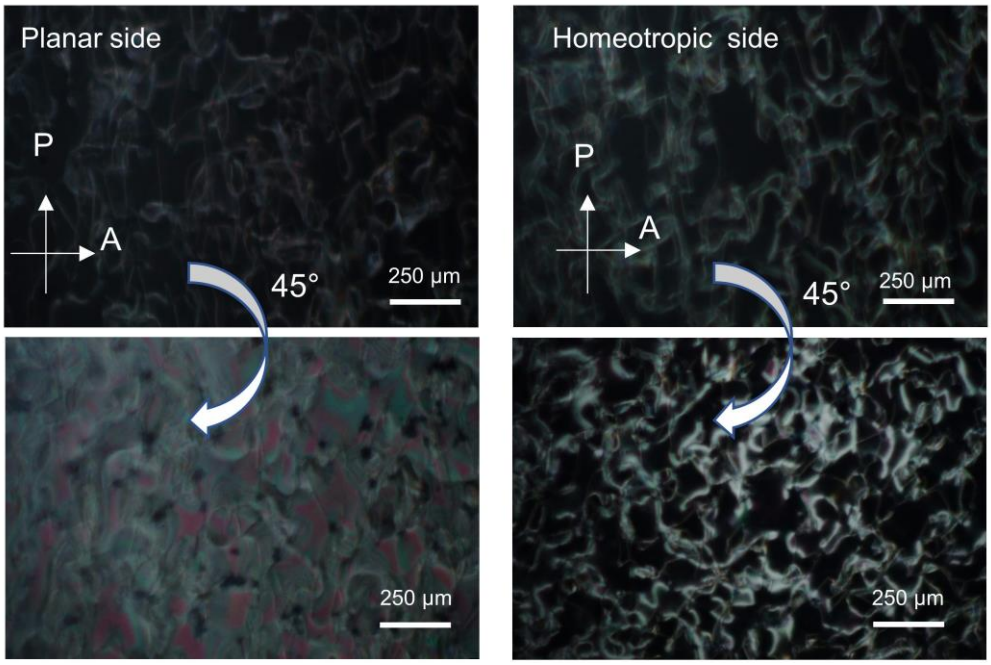

Figure 4.5 POM images of the 0.3 wt.% CPs/LCEs film under cross polarizer and analyzer. P: polarizer, A: analyzer. Scale bar: 250 μm.

The shape changes of the CPs/LCEs rectangle actuators were highly influenced by the cutting angle with respect to the planar alignment direction. A lot of strategies about the cutting angle to the planar alignment direction have been performed for achieving different styles of shape deformation using LCE-based actuators with splay alignment (Del Pozo et al., 2022b, Xiao et al., 2020b, Wani et al., 2019, Wang and Ho, 2022). For deformation demonstration in this study, two kinds of CPs/LCEs rectangle films were cut at 0° and 45° with respect to the planar alignment direction, as shown in **Figure 4.6 a**.

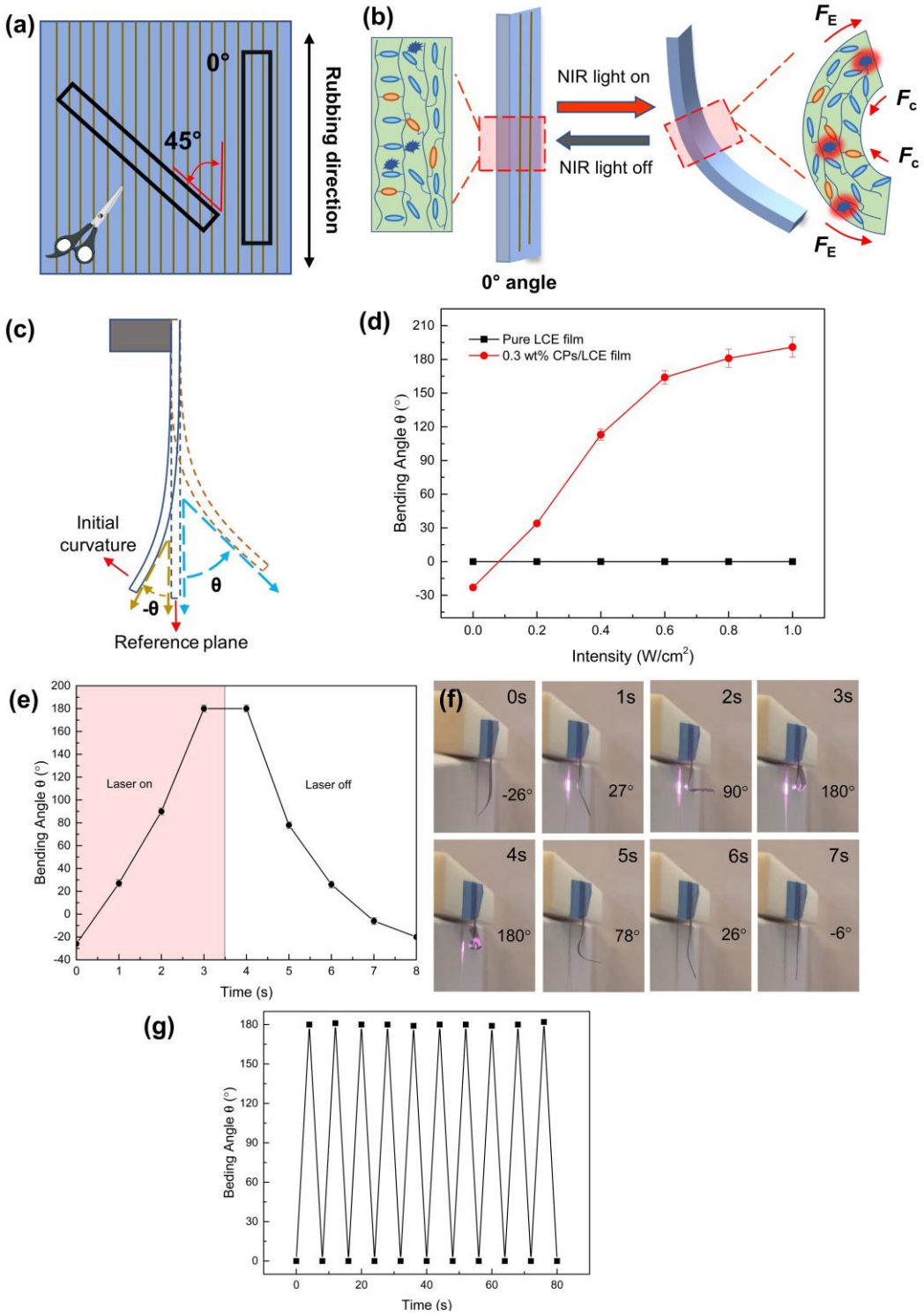

Figure 4.6 (a) Schematic of cutting strategy of preparing 0.3 wt.% CPs/LCEs films at different angles to the rubbing direction. (b) Deformation mechanism illustration of reversible shape-bending of the CPs/LCEs soft actuator with a cutting angle of 0° under NIR light irradiation. The insets show the different

molecule orientations. (c) Measurement method for evaluating bending angle of the 0.3 wt.% CPs/LCEs film. (d)The bending angles of pristine LCE film and the 0.3 wt.% CPs/LCEs actuator under different light intensities at 808 nm. (e) The bending angle change of 0.3 wt.% CPs/LCEs actuator when turning on and off the 808 nm laser at an intensity of ~0.8 W/cm^2. (f) Images of the 0.3 wt.% CPs/LCEs actuator during the NIR light irradiation and removal. (g) Cyclic reversible bending of the 0.3 wt.% CPs/LCEs actuator during ten cycles of turning on/off of the 808 nm laser at 0.8 W/cm^2.

Out-of-plane bending behavior is the most common deformation style of LCE-based actuators. Local bending of the CPs/LCEs film with a size of 15 mm × 3 mm × 0.06 mm was acquired from the sample with a cutting angle of 0°. The principal axis of the rectangular actuator was parallel to the rubbing direction. One film's end was fixed on a holder, as shown in **Figure 4.6 c**. Before NIR laser irradiation, the film exhibited an initial curvature towards the homeotropic substrate because of the anisotropic thermal expansion once cooling from the fabrication temperature to room temperature. A similar observation of the bent LCE-based actuators was also reported by Feng and co-workers (Yang et al., 2022b). Upon local NIR laser illumination, the local temperature above T_{NI} (47.9 ºC) generated by the photothermal effect of CPs led to the order-disorder phase transition of the mesogens throughout the film. Then different forces, including extension force (F_E) on the homeotropic side and contraction force (F_C) on the planar side, were generated accordingly to trigger the out-of-plane bending

towards the planar-oriented surface (**Figure 4.6 b**). When removing the light source, the thin film quickly cooled back to room temperature, and the mesogens returned to an aligned state. The CPs/LCEs film recovered to its initial shape. To better evaluate the relationship between bending angle and NIR light power for subsequent applications, a bending angle (θ) as a function of laser intensity is shown in **Figure 4.6 d**. For the unfilled LCE film, no bending behavior was observed with the increasing laser intensity. Under some laser power dosage and exposure time (about 3s), CPs-doped LCE film started to bend at 0.2 W/cm^2 and reached a maximum angle of 191° at 1 W/cm^2. The higher light intensity can induce higher local temperature rising of CPs in the LCE matrix within the same time, a further greater thermally induced disorder of mesogens. Under irradiation at 0.8 W/cm^2, the film could bend to a maximum of about 180° within 3 s and return to its original state thoroughly upon removing the light source at 8s (**Figure 4.6 e and f**). Further, the morphing repeatability of CPs/LCEs film was investigated. After ten cycles of deformation and recovery process, the film still showed excellent cycle stability (**Figure 4.6 g**). This could be attributed to the superb photostability, photothermal effect, and uniform and stable dispersion of DPP58-TBZ12 CPs in the LCE network.

Another shape change, Swiss rolling, was also achieved by using the film with 0° cutting angle. The film clamped by a tweezer could roll from the unbonded end to the fixed end under the movement of the NIR light spot, as depicted in **Figure 4.7 a**. A part of the CPs/LCEs film was locally stimulated for rolling using

the 808 nm laser spot. When the rolled part moved toward the light spot, continuous rolling behavior happened. Then, 3D Swiss rolling architectures could be created. The left-hand helical twisting behavior of CPs/LCEs film was achieved from the sample with a size of 10 mm × 2 mm × 0.06 mm cut at 45° with respect to the planar alignment, as shown in **Figure 4.7 b**. The mesogen alignment of this film on the planar substrate (top substrate) was tilted to the principal and short side of the rectangular film at 45° angle. When one part of the film was exposed to NIR light, non-uniform shrinkage, and expansion generated incompatible strain between the top and bottom surfaces, which led to the out-of-plane twisted structure. Based on the reversible bending behavior, a bioinspired CPs/LCEs actuator mimicking the Venus flytrap leaf was designed to capture small objects. As shown in **Figure 4.7 c**, when small objects approached the film actuator, one "blade" of the actuator could fold quickly under NIR light irradiation to reach a close state. Then small insects would be captured inside the actuator.

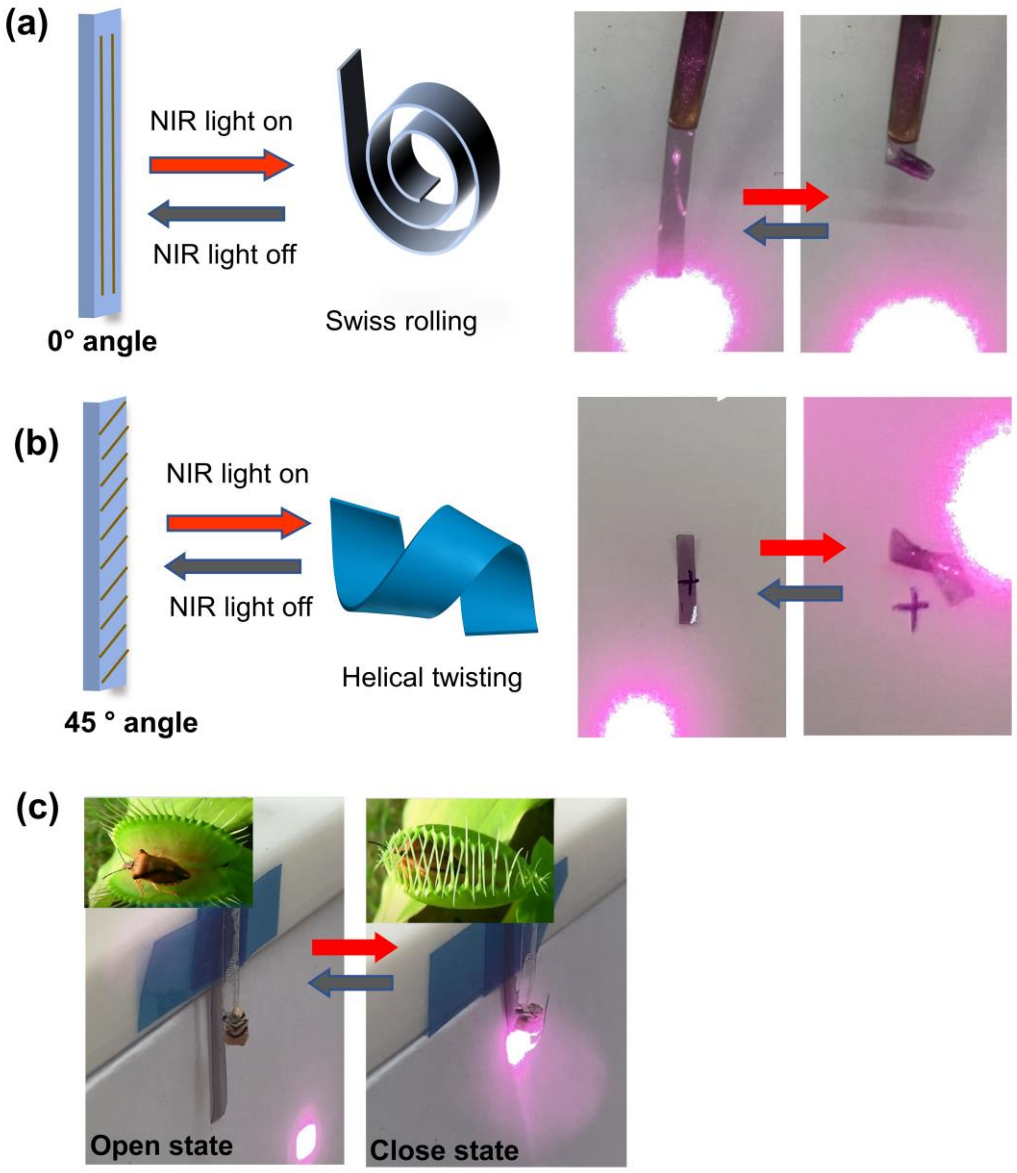

Figure 4.7 Schematic and physical images of (a) Swiss rolling and (b) helical twisting of the 0.3 wt.% CPs/LCEs actuator with cutting angles of 0° and 45° under 808 nm NIR light irradiation of ~0.8 W/cm^2. (c) The Venus flytrap was simulated by using the soft 0.3 wt.% CPs/LCEs film based on bending deformation.

4.3.4 Phototunable Locomotion of Soft CPs/LCEs Actuators

As discussed in the shape deformation, out-of-plane left-hand helical twisting could be generated. Due to unsymmetrical light irradiation, unbalanced shape

deformation in the CPs/LCEs film created a curved tubule. The incompatible strain caused by the unbalanced shape deformation could always exist and transfer under the movement of the NIR light spot if the long axis of the rectangular film is long enough due to the changing temperature. When the light spot was moving, the incompatible strain would be transformed within the actuator along the light-moving direction by the friction between the actuator contact area and substrate. Upon removing the light source, the existing strain propelled the actuator, undergoing out-of-plane twisting to return to a flat state along the long axis of the actuator, as shown in **Figure 4.8a**. Therefore, a forward spatial displacement could be created during this process accordingly (Yang and Shen, 2021). Under successive on/off control of the light spot partially illuminated on the actuator, rolling motion of such kind of untethered actuator could be achieved.

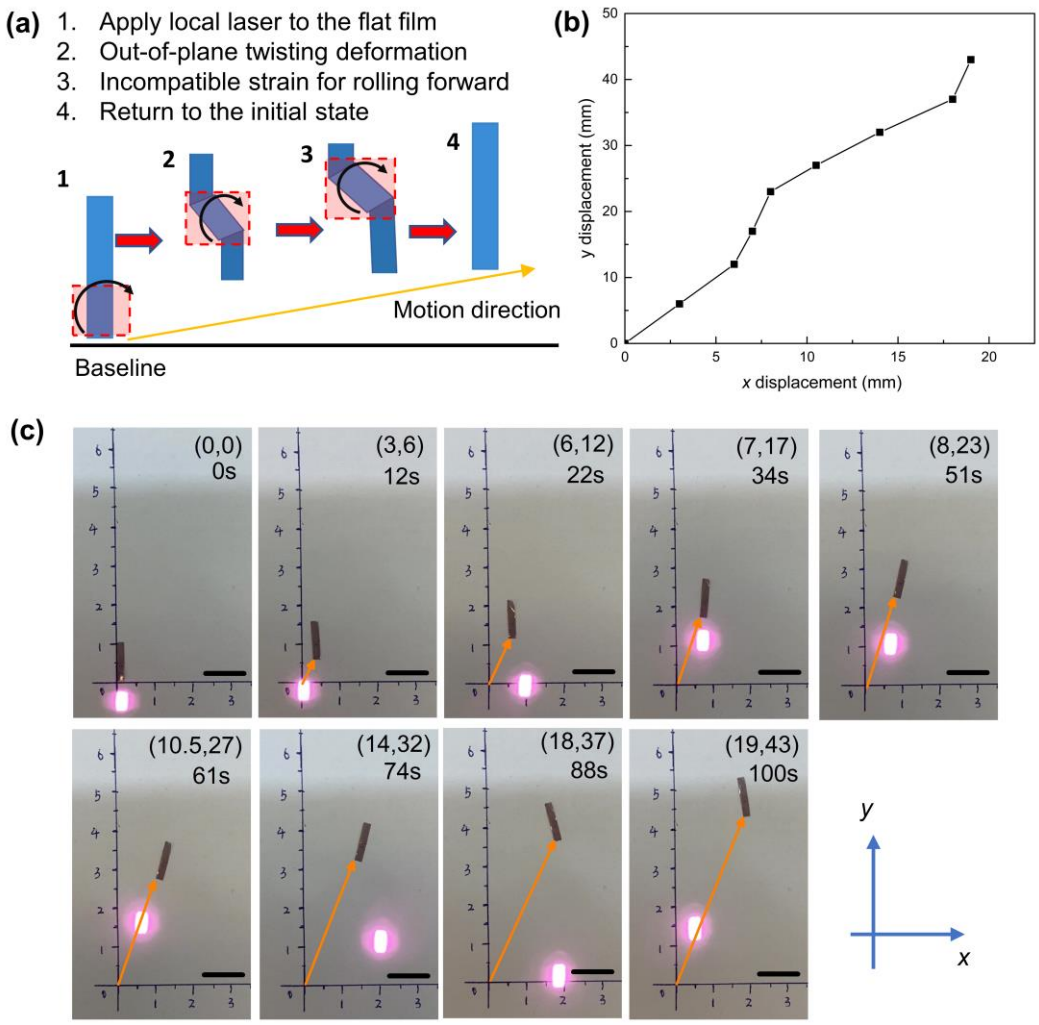

Figure 4.8 Unsymmetrical NIR light expose area enabled friction difference for the forward rolling motion of LCE-based robot. (a) The mechanism of the NIR light-induced motion process. The areas exposed to NIR light irradiation are illustrated by a red block. The black arrows indicate the rolling direction. (b) Corresponding motion routine of the actuator (setting the bottom left corner of the rectangular film as the moving dot). (c) Screenshots of the motion process of 0.3 wt.% CPs/LCEs actuator under successive illumination of ~0.8 W/cm^2 at about 12 s intervals (5 mm tick marks in coordinate paper). The black scale bar is 10 mm. The yellow arrows inside the image mark the motion directions of the film actuator. The location of the actuator after each

complete light illumination procedure was also depicted in the coordinate system.

The CPs/LCEs rectangular film with a size of 10 mm × 2 mm × 0.06 mm was used to demonstrate the photo-motility on one A4 paper with a coordinate system of the x-y plane (shown in **Figure 4.8**) under 808 nm laser at ~0.8 W/cm^2. Locomotion requires the ability of a material to undergo reversible and fast shape transformations. To accurately evaluate the motion ability of the untethered soft robot, we set the bottom left corner of the rectangular film as the moving dot. The homeotropic surface was attached to the A4 paper. In this experiment, slight errors may exist due to hand manipulation inconvenience. Light irradiation on the bottom half of the film caused left-hand twisting, and then the twisted part rolled up to make a homeotropic surface attached to the A4 paper. When the light irradiation traveled to the top half of the film, the incompatible strain was induced, and thus the film recovered to its flat state. After about 8 times of alternating light irradiation cycle, the moving distance of the actuator between the starting situation (0, 0) in the x-y plane and end situation (19, 43) in 100 s was 47 mm with 43 mm in the y-axis and 19 mm in the x-axis (**Figure 4.8 b and c**). The velocity along the motion direction could reach 0.47 mm/s. Although some middle states deviated from the leading moving path, the robot still could go forward at an angle of 66° from the x-axis on the x-y plane by strain propelling. To date, there has been a limited number of research performed to quantitatively analyze the forward motion ability of LCE-based soft robots with simple structures. The NIR light-controllable

motion ability based on helical twisting shape change behavior of the CPs/LCEs film developed in this study has been demonstrated to be more advantageous compared with the reported NIR photo-triggered LCE-based robots, such as walking velocity 0.1 mm/s for a bilayer device (Kohlmeyer and Chen, 2013a), the average speed of 0.12 mm/s (9 mm motion distance in 75 s) for a 13mm-long snake-mimic soft actuator (Wang et al., 2020a), an average speed of 0.16 mm/s (20 mm motion distance in 120 s) for a "U"-shaped strip (Yang et al., 2019), an average rate of 0.06 mm/s for an LCN micro-walker (Jiang et al., 2019), which would lay a good foundation for future development of complex soft athletic robot assembly.

4.4 Conclusions

In this study, we have successfully developed homogenous DPP58-TBZ12 CPs-doped LCE composites and employed them in a bioinspired soft monolayer actuator in a facile method. The incorporation of the organic DPP58-TBZ12 CPs with prominent photothermal effects and photostability has endowed the CPs/LCEs actuator with ultrafast response time, reversible shape changes, and cyclability under NIR light irradiation. By spatially aligning the mesogens in the LCE matrix via surface-enforced alignment techniques and cutting styles of actuators, various 2D-to-3D shape morphing from a single film, including bending, Swiss rolling, and spiral twisting behaviors with ultrafast response time (within 1 s), have been demonstrated under the irradiation of 808 nm laser at ~0.8 W/cm^2. In addition, an NIR light controllable roll-propelling robot was realized with an

average speed of 0.47 mm/s. In future work, we will perform a further investigation on the motion directionality of soft CPs/LCEs robots of different sizes under different laser powers on flat and tilting substrates. It is believed that such alternating D-A CPs/LCEs composite material would provide new impetus for further development of untethered soft-bodied robots with sophisticated spatiotemporal actuation under NIR irradiation which would be utilized in potential cutting-edge applications, including wireless sensors, cargo transportation, biomimetic devices and so on.

Chapter 5 4D Printing of Light-triggered Actuators and Their Potential Biomedical Applications

5.1 Micro-actuators Fabricated by DLW-TPP Technology

5.1.1 Introduction

In Chapter 4, we incorporated CPs in LCEs to prepare ultrafast fim-like actuators by one-pot UV photopolymerization and liquid crystal cells with splay alignments. The film actuators showed tunable deformation and motion under NIR laser irradiation (Huang et al., 2022). However, the structures of the actuators are two-dimensional and simple. More complex structures need to be designed and fabricated. The potential of CPs as dopants has been much less explored to create light-responsive LCE micro-actuators. There has been no report of the complex micro-actuators from NIR-light-responsive CPs-doped LC photoresists via DLW-TPP 4D printing technology.

4D printing has shown remarkable advantages and promising applications in manufacturing stimuli-responsive materials thanks to its capacity to generate complex structures at different scales (Bi and Huang, 2022, Demoly et al., 2021). In the past decades, many studies have been carried out to print time-dependent macroscopic structures with smart materials. However, the 4D printed structures at the microscale remain a challenge because of the difficulty of their fabrication and the shortage of suitable smart materials. DLW-TPP is one of the powerful tools for producing precise and sophisticated structures at the micro and nanometer scale (Liao et al., 2020). Arbitrary freeform structures with a high resolution can be

generated by DLW-TPP (Huang et al., 2020). It has been successfully used to fabricate micro-actuators that are applied in different fields, such as micro-robotics (Zeng et al., 2015, Martella et al., 2017b, Xiong et al., 2018), micro-optics (Ritacco et al., 2021, Guo et al., 2020b), and microfluidics (Barbot et al.).

Hydrogels (Zhang et al., 2019c, Xiong et al., 2018, Wang et al., 2022a) and LCEs (Zeng et al., 2015, Martella et al., 2017b, Martella et al., 2017a, del Pozo et al., 2022a), have greatly advanced the manufacturing of micro-actuators by DLW-TPP. Zheng et al. (Zheng et al., 2020) fabricated two microcantilevers using Poly(N-isopropyl acrylamide) hydrogels with Fe_3O_4 nanoparticles as NIR photothermal fillers. Wang et al. (Wang et al., 2018) reported magnetic field-driven helical 3D microswimmers based on gelatin methacryloyl/Fe_3O_4 nanoparticles, which exhibited a unique swimming behavior under rotation magnetic fields in water. Unfortunately, most hydrogel-based micro-actuators have low elastic modulus and slow response speed even on the order of minutes (Ambulo et al., 2017b, Cheng et al., 2018). LCEs become an appealing choice for realizing responsive microstructures by DLW-TPP technology (Ilami et al., 2021). LCE micro-actuators are mainly controlled by the mesogenic alignment design, which can be programmed before fabrication. Upon exposure to an external stimulus, the LCE micro-actuator loses the nematic state, which leads to contraction behavior along the long mesogen alignment direction and expansion in a perpendicular direction. The most common-used alignment method for DLW-TPP is the

boundary condition of micropatterned channels on the treated LC cell due to the thin thickness (typically < 100 μm) of the microstructures (Wang et al., 2023c).

The small scale of micro-actuators also makes light the most suitable stimulus due to the convenient manipulation via light wavelength and power. Light energy can be converted into mechanical work directly by isomerization change of photochromic molecules (Zeng et al., 2015, Hsu et al., 2022) or indirectly through the photothermal effect of functional dopants (Chen et al., 2019a). Azobenzene-doped LCEs were enormously applied in the macro-scale actuators until Zeng et al. (Zeng et al., 2015) fabricated a UV-light-fueled microscopic walker by DLW-TPP. However, the periodical switching operation of dual-wavelength light for reversible deformation is not viable for many practical applications (Wang et al., 2020b, Wang et al., 2012). LCEs that use the photothermal effect of photothermal dopants to generate actuation display an obvious advantage. It should be noted that it is a critical issue to solve the dispersion quality and concentration of the dopants in photoresists. For instance, gold nanoparticles were treated with 3-mercaptopropionic acid by Chen et al. (Chen et al., 2019a), and multi-walled carbon nanotubes were also acid-modified by Xiong et al. (Xiong et al., 2016) for developing DLW-TPP-compatible LC photoresists. Inorganic nanomaterials must undergo surface chemical modification with functional groups before incorporation into LCEs. Nevertheless, poor compatibility makes most inorganic dopants prone to self-aggregate into larger ones and separate from the LC mixtures easily. For most LCE-based actuators, a high concentration of inorganic dopants is

required for a favorable photothermal effect, which affects the printing process (Del Pozo et al., 2022b). Therefore, high photothermal conversion efficiency (PCE), low doping ratio, and good dispersion of dopants in LC photoresists become crucial factors to be carefully considered in choosing the photothermal dopants for photothermal actuation of LCE micro-actuators.

In this chapter, we develop a new light-responsive LC photoresist suitable for DLW-TPP technology to produce NIR light-responsive micro-actuators. A novel low bandgap DPP58-TBZ12 CPs with alternating D-A backbone structures was fabricated as photothermal fillers in the LCE matrix. The DPP58-TBZ12 CPs exhibited a broad NIR absorption range and high photothermal conversion efficiency. And they could be easily incorporated in the printable LC photoresists by organic solvent. The effect of CPs content on the thermal property of the LC photoresist, printing parameter, and printing range during the DLW-TPP was investigated in detail. Adding a small amount of the CPs (0.3 wt.%) in LCEs could not only lower the nematic-to-isotropic transition temperature value (T_{NI}) which was beneficial for 4D DLW-TPP microfabrication, but also yielded a fast response and large-scale actuation of the micro-actuators upon NIR light stimulation thanks to the superior photothermal effect of the DPP58-TBZ12 CPs. To the best of our knowledge, this is the first report of using CPs/LC photoresists with room temperature liquid crystal phases to manufacture micro-actuators by DLW-TPP technology without a heating stage.

5.1.2 Experimental

5.1.2.1. NIR Light-responsive Photoresists Design Concept for DLW-TPP

An LC photoresist for DLW-TPP needs a stable LC phase at room temperature without an extra heating stage, which ensures the successful printing of simple or complex structures of a few hundred nanometers or micrometers that take different printing times. To date, reactive LC photoresists with room-temperature liquid crystal phases are rare. The LC phases of most reported LC mixtures exist above room temperature, and LC mixtures crystallize easily in the ambient environment in a short time. Thus, it is challenging to prepare DLW-TPP-compatible LC photoresists. Particularly, LC mixtures with light (UV-vis and NIR)-responsive dopants have seldom been developed. Due to their simpler synthesis, flexible side-chain elastomers are often modified with mesogenic moieties attached to an aliphatic spacer. These elastomers typically exhibit lower isomerization temperatures because of their greater chain flexibility and decoupling of the mesogens from the polymer backbone. According to our previous studies (Chen et al., 2019a, Huang et al., 2022), ST3866 with monoacrylate mesogens was selected as the LC monomer to provide flexibility for the network. To fabricate stable LCE structures, RM257 (T_{NI} = 129 ºC) containing diacrylate mesogens was chosen as the crosslinker to form the network and fix the alignment. Irgacure 369 was chosen as the photoinitiators. It has been used in other studies to generate radicals in acrylate-based photoresists. It is known that LC photoresists of higher T_{NI} may

suffer some degrees of crystallization, which is unbeneficial to the DLW-TPP microfabrication (Guo et al., 2020a, Liu and Broer, 2014). The weight percentage between the monomer and crosslinker was investigated to determine the T_{NI} of different LC photoresists.

The photothermal dopants should not destroy the mesogenic alignment and should be transparent or semitransparent to the femtosecond laser (Del Pozo et al., 2022b). Alternating donor-acceptor (D-A) conjugated polymers exhibit many advantages as photothermal materials, including ease of synthesis, unique temperature tunability from NIR light, lightweight, and good biocompatibility. It has been demonstrated that D-A_1-D-A_2-type CPs possess a lower band gap energy, resulting in absorption in the NIR region. Diketopyrrolopyrrole (DPP) represents an electron-acceptor due to its electron-deficient nature, which makes it suitable for use as a bridging moiety in D-A-type CPs. Therefore, in this work, DPP58 containing thiophene as donor and DPP as acceptor 1, and TBZ12 containing thiadiazolobenzotriazole as acceptor 2, are chosen as the two monomers for the synthesis of the CPs, named DPP58-TBZ12. The conjugated polymer DPP58-TBZ12 was then incorporated into the LC photoresists as an effective photothermal agent responsive to NIR light irradiation. DPP58-TBZ12 CPs and LC photoresists show good solubility in THF, which makes it easy to obtain homogenous mixtures after evaporating the THF solvent. Because the thickness of the microstructures by DLW-TPP is less than 100 μm, the method for mesogenic

alignments was achieved by the micropattern-boundary conditions of unidirectional rubbing PI-coated glass.

5.1.2.2 Preparation of the DPP58-TBZ12 CPs/LC Photoresists

The CPs/LC photoresists were prepared according to the following process. Different amount of as-synthesized conjugated polymers DPP58-TBZ12 was ultrasonically dissolved into THF solution in a vial. Then 75 wt.% ST3866 as the LC monomers, 24 wt.% RM257 as crosslinkers and 1 wt.% Irgacure 369 as the free radical photoinitiator (chemical structure shown in **Figure 5.1 a**) was added to the solution. The mixtures stored in an open vial were stirred gently in a vacuum oven at 65 ºC for 12 h to remove the solvent thoroughly. These LC photoresists were produced with different contents of DPP58-TBZ12: 0, 0.1, 0.3, 0.5 wt.% for subsequent photopolymerization of 3D microstructures. **Figure 5.1 b** exhibits that the DPP58-TBZ12 CPs are well-dispersed in the LC photoresists. After storage in a dark place for 7 days, crystallization occurred somewhat in the pristine LC photoresist. The CPs-doped photoresist maintained good stability and high dispersion without evident aggregates of CPs and crystallization behavior, making these photoresists suitable for printing. It is significant to note that the high dispersion capability and good compatibility of DPP58-TBZ12 CPs within LCEs can ensure the successful printing of NIR light-responsive micro-actuators by DLW-TPP.

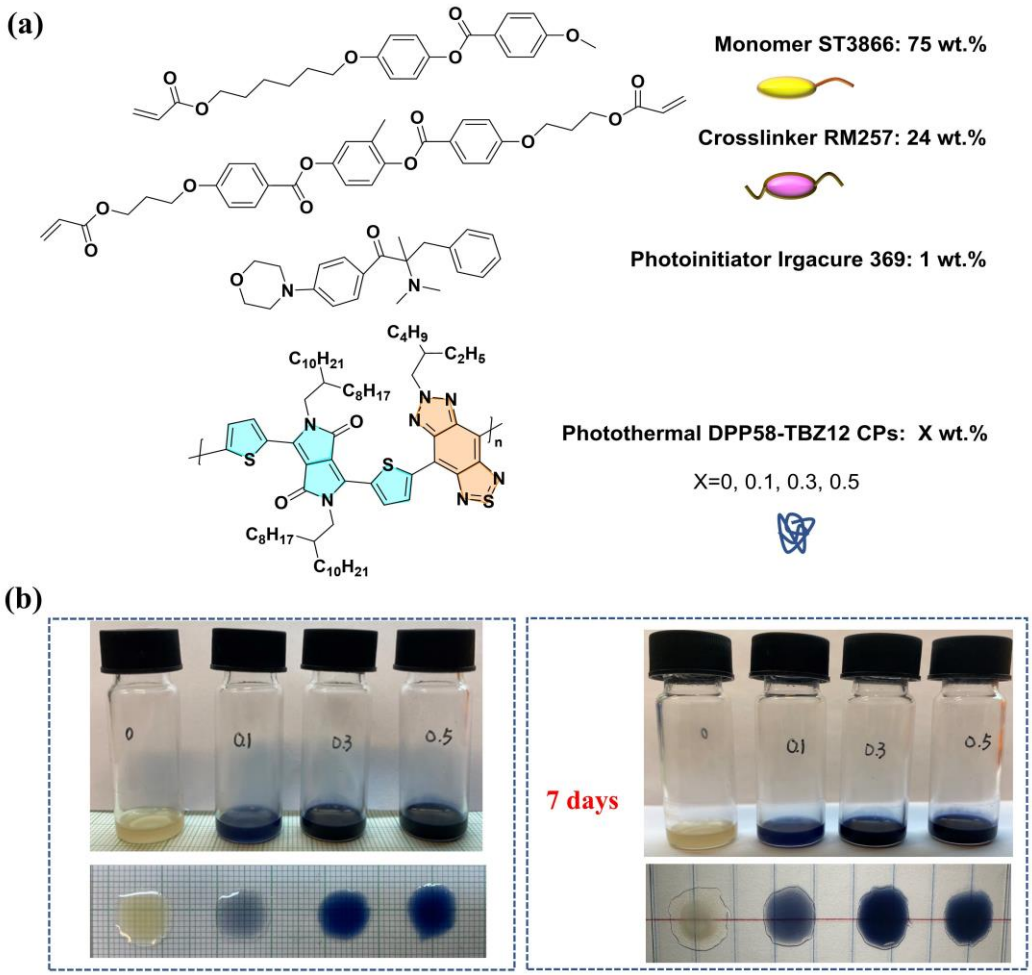

Figure 5.1 (a) Chemical structures of LC monomer ST3866, crosslinker RM257, photoinitiator Irgacure 369, and photothermal dopant DPP58-TBZ12 CPs. (b) Images of the prepared LC photoresists with 0, 0.1 wt.%, 0.3 wt.%, and 0.5 wt.% DPP58-TBZ12 CPs on the first and seventh days.

5.1.2.3 Liquid Crystal Cells Construction

The sandwich-like liquid crystal cell was assembled based on widely used approaches to achieve the uniaxial alignment of the mesogens (Chen et al., 2019a). In detail, two glasses used for LC cells were washed by successive immersion in acetone and methanol. PI was spin-coated on the glass substrate for planar surface alignment (parallel to the substrate) at 1500 rpm for 40 s, followed by curing on a

120 ºC stage for 3 min. A velvet cloth was employed to mechanically rub the PI-coated glasses to obtain a micro-grooved surface for the mesogen alignment. Finally, a homemade LC cell was constructed by carefully assembling two rubbed PI-coated substrates with antiparallel alignment direction on two inner sides gapped via spherical spacers (55 µm diameter) in UV-curable glue. The prepared photoresists were heated to reach the isotropic phase at 60 ºC above their T_{NI}. Subsequently, they were injected into the homemade aligned LC cells from the edge through capillary force to avoid flow-induced alignment (**Figure 5.2 a**). The LC cells were then cooled to room temperature at a controlled rate (5 °C/min). Finally, an LC cell filled by ordered nematic phase photoresists was constructed well for DLW-TPP. Notably, a low cooling rate is vital to reduce the number of disclinations (Guo et al., 2020b). The alignment of mesogens was checked with a polarized optical microscope. Finally, user-designed 3D microstructures or other samples were produced by DLW-TPP or UV light exposure (1.2 mW/cm^2, 365 nm).

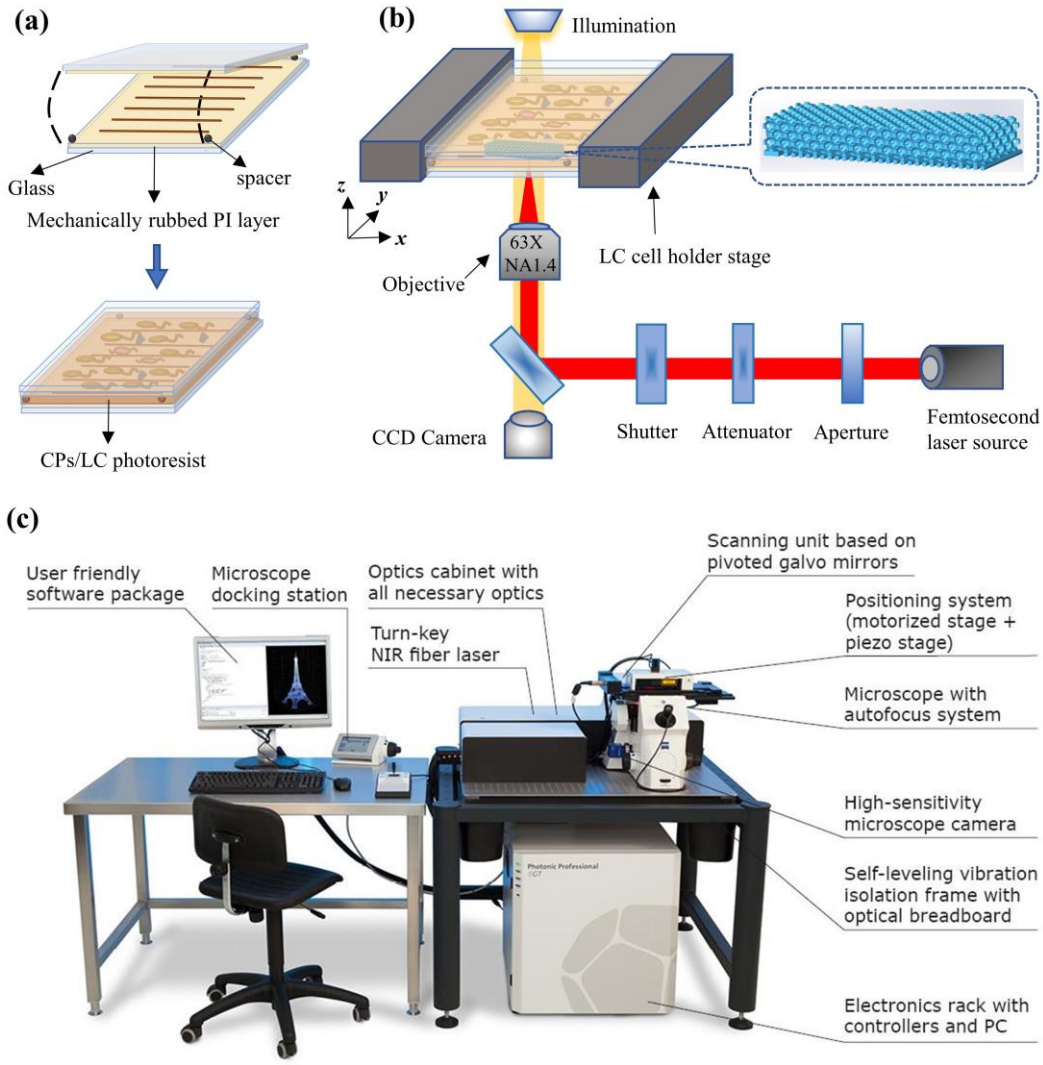

Figure 5.2 (a) Schematic illustration of liquid crystal cell assembly and a typical liquid crystal cell filled by DPP58-TBZ12 CPs/LC photoresists. (b) The schematic diagram of oil immersion configuration in DLW-TPP setup for fabricating microstructures. (c) A commercially available DLW-TPP system (Nanoscribe Photonic Professional, GmbH, Germany).

5.1.2.4 DLW-TPP Setup

A commercially available DLW-TPP system (Nanoscribe Photonic Professional, GmbH, Germany) was employed to fabricate 3D microstructures (**Figure 5.2 b**). A Ti: sapphire femtosecond laser with a central wavelength of 780

nm (pulse duration of ~ 100 fs, a repetition rate of 80 MHz, and a maximum power of 180 mW) was used in this equipment. The laser beam was focused into the CPs/LC photoresists using a 63x oil-immersion objective lens (Zeiss, NA=1.4). The schematic diagram of the DLW-TPP setup is shown in **Figure 5.2 c**. At a power scaling of 1, the average laser output in the focus area was 50 mW. All 3D microstructures were designed by computer-aided design software (Solidworks). The sample cell was fixed on the *XYZ* positioning stage controlled by combined modes (galvo mode for *x- and y-axes* and piezo mode for the *z-axis*). After bottom-up DLW-TPP microfabrication, the cell was separated, and the glass substrate with microstructures was dipped in acetone for 6 minutes to remove the unpolymerized photoresist. The desired self-standing 3D micro-actuators on the glass substrates were achieved by drying with gentle nitrogen flow.

5.1.2.5 Characterizations and Measurements

The nematic-to-isotropic transition temperature (T_{NI}) of the LC photoresists was determined by differential scanning calorimetry (DSC) (Mettler Tolede, DSC3). LC or CPs/LC photoresists of at least 3mg were aced into aluminum pans. Subsequently, samples were heated and cooled from 20 ºC to 120 ºC at a ramping rate of 10 ºC min^{-1} under nitrogen protection. Two cycles were performed, and the results in the second cycle were recorded. Thermogravimetric analysis (TGA) was conducted on a Mettler Toledo TGA/DSC 3+ at a heating rate of 10 ºC min^{-1} from 25 to 650 ºC. UV-polymerized pristine LCE and CPs/LCEs films were chosen as the TGA samples. Investigation of the main printing parameter window for newly developed photoresists was critical for the morphology and integrity of 4D printing structures and manufacturing time. Laser powers varying from 3.5 to 21 mW and

scanning speeds ranging from 2 to 24 mm/s were assessed in the DLW-TPP process. A field-emission scanning electron microscope (SEM) (Tescan VEGA3, Czech Republic) was applied to observe and analyze the fabricated 3D DPP58-TBZ12 CPs/LCEs microstructures at an acceleration voltage of 20 kV after sputter-coating them with 10 nm gold layer. A polarized optical microscope (POM) (Zeiss Axiolab 5) with a hot stage was used to observe the bright field images of LC mixtures and cross-polarized microscope images of LCE microstructures.

NIR light-induced actuation of DPP58-TBZ12 CPs/LCEs micro-actuators was performed using the NIR laser setup of 808 nm (LSR808H-2W, Lasever Inc., Ningbo, China). The beam spot size of the NIR laser is 4.8 mm × 5.3 mm. The output laser powers could be adjusted from 0.1 W to 5 W. The corresponding power intensity can be adjusted from 4 to 197 mW/mm^2. The deformed micro-actuators were recorded by a CCD camera with an optical microscope.

5.1.3 Results and Discussions

5.1.3.1 Thermal properties of DPP58-TBZ12 CPs/LC photoresists

Before the addition of NIR-absorbing species, the T_{NI} values of LC photoresists with the different weight ratios of ST3866:RM257 were investigated. DSC results show that the T_{NI} values of the LC photoresists decrease with the increasing weight ratio of the diacrylate crosslinker RM257, as listed in **Table 5.1**. They exhibited a wide temperature range to keep the nematic phase. In comparison, the LC photoresist 3 with a low crosslinker concentration was chosen because of the low T_{NI} for room-temperature 4D printing and the relatively low stiffness of the polymeric network for actuation upon stimulation. **Figure 5.3 a** presents the results of DSC measurement in the second heating process after erasing the

thermal memory of the pre-polymerized LC and DPP58-TBZ12 CPs/LC photoresists. The heat flux with temperature for these pre-polymerized mixtures only displayed the nematic-isotropic transition. The T_{NI} of unfilled LC and CPs/LC photoresists with 0.1, 0.3, 0.5 wt.% of DPP58-TBZ12 CPs are 55.1, 51.4, 48.0, and 45.2 ºC, respectively. T_{NI} of blank nematic LC photoresists is about 55.1 ºC, while those of the DPP58-TBZ12 CPs/LC photoresists are lower. The DSC results indicated that the T_{NI} value of CPs/LC photoresists dropped largely with the content increase of DPP58-TBZ12 CPs. Because photopolymerization and crosslinking of LC photoresists are required to occur in the nematic state for later NIR photothermal actuation, the temperature for performing DLW-TPP should be in the range of the nematic phase temperature. The room temperature below the T_{NI} satisfies the printing temperature requirement of DLW-TPP for these photoresists.

The crossed polarized micrographs of 0.3 wt.% CPs/LC photoresists at 25 and 60 ºC depicted the nematic and isotropic phases, respectively. A clear schlieren texture was visible when the LC mixtures were cooled to room temperature that was below the transition temperature T_{NI} (48.0 ºC) (**Figure 5.3 b**). The mechanism might be attributed to two reasons: (a) diminished strength of intermolecular forces between rigid rod-shaped mesogens due to the insertion of planar CPs; (b) the thermal-mechanical response of the planar CPs (Sugiyama et al., 2018, McCracken et al., 2021, Hebner et al., 2021). These effects of the DPP58-TBZ12 CPs might lead to a more manageable disturbance of nematic arrangement between mesogens and lower T_{NI} values. It is worth noting that the LC photoresists containing the CPs with lower T_{NI} have longer and more stable periods in a defect-free nematic phase at room temperature. The influence of DPP58-TBZ12 CPs on the T_{NI} of LC

mixtures also may alleviate some degree of crystallization during the DLW-TPP fabrication. TGA was carried out to examine the mass loss of the UV-photopolymerized samples of pristine LCE and CPs/LCEs films. The TGA curves exhibit that the pristine and the DPP58-TBZ12 CPs incorporated LCE films had high thermal stabilities. The decomposition of these films did not occur until the temperature reached approximately 340 °C (**Figure 5.3 c**).

Table 5.1 Phase transition temperature for LC photoresists (wt.% of the total mixture)

Photoresists	Monomer ST3866	Crosslinker RM257	Photoinitiator Irgacure 369	T_{NI} (ºC)
LC Photoresist 1	35	64	1	77.7
LC Photoresist 2	55	44	1	65.6
LC Photoresist 3	75	24	1	55.1

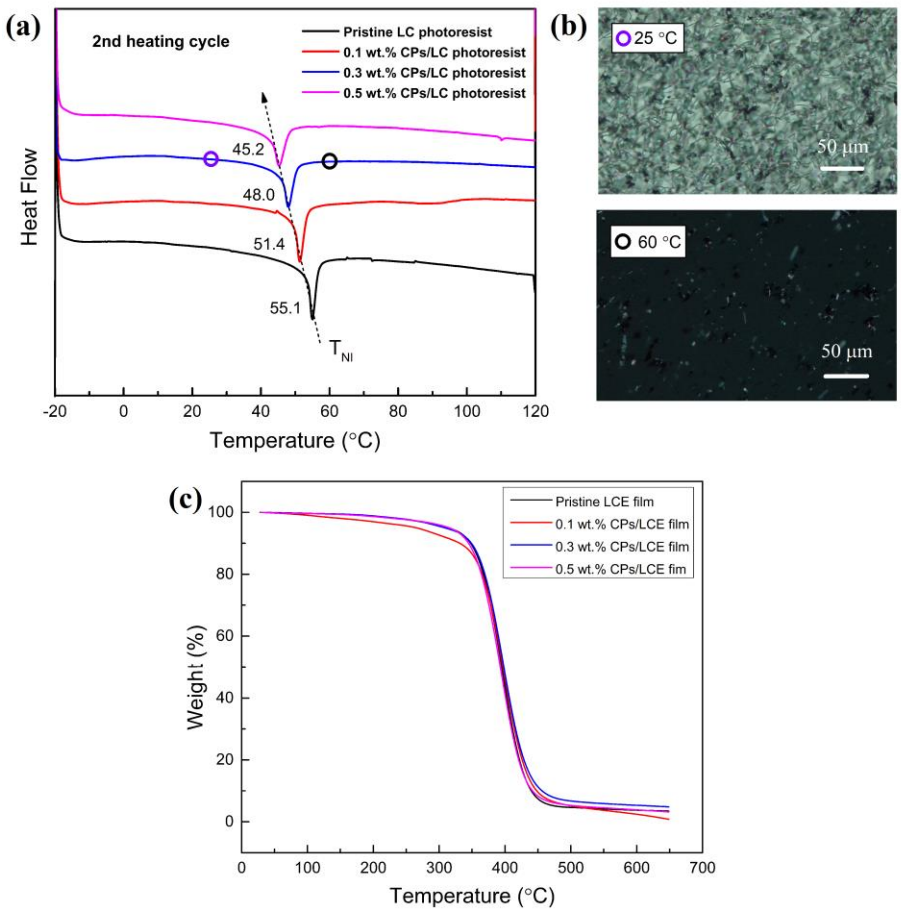

Figure 5.3 (a) DSC thermograms of pristine LC photoresists and DPP58-TBZ12 CPs/LC photoresists during the second heating cycle at a rate of 10 ºC/min under the protection of nitrogen. (b) Crossed polarized micrographs of the 0.3 wt. % CPs/LC photoresist taken below (25 °C, top) and above (60 °C, bottom) the T_{NI} between uncoated glasses. (c) TGA results of the pristine LCE and CPs/LCEs films with different doping ratios of the CPs.

5.1.3.2 Printing Parameters of DLW-TPP for DPP58-TBZ12 CPs/LC Photoresists

The printing capacity of DLW-TPP in the micro and nanoscale enables the complexity and diversity of the designed structures. The developed CPs/LC photoresists allow a wide range of printing parameters, especially laser power and

scan speed. It is significant to tune these two main printing parameters to ensure the final quality and manufacturing efficiency of the printing structures. Laser power determines the throughput of photons in the focal volume within the photoresist, while the scanning speed regulates the photon dose (Chen et al., 2019a). A suitable laser power should meet the requirements that it can initiate the polymerization and does not exceed the burning threshold to generate structures matched with the designed 3D model. A low laser power leads to incomplete polymerization and crosslink of the LCEs, further leading to collapsed structures. In addition, the photothermal effect of the CPs in the printing process also needs to be considered in determining the suitable laser power. The filled DPP58-TBZ12 CPs could absorb the femtosecond laser energy and likely result in localized burning and bubbling of the photoresist in a very short time during the manufacturing process, particularly evident with slow scan speed. Although the laser power is very low, unwanted heat energy could still make the printing layers swell and influence the fidelity of the designed model.

In this case, a porous inverse opal structure unit with 3.7 μm of radius pore size was designed as the model for the parameter selection of as-prepared DPP58-TBZ12 CPs/LC photoresists (**Figure 5.4 a**). In the DLW-TPP manufacturing process, a hatching distance of 0.2 μm and a slicing distance of 0.3 μm was adopted. The laser power varied between 3.5, 7, 10.5, 14, 17.5, and 21 mW, and the scanning speed was adjusted between 2, 4, 6, 8, 10, 14, 16, 20, and 24 mm/s. LC photoresists incorporated with 0.3 wt.% and 0.5 wt.% CPs were employed to explore the influence of photothermal filler amounts. Two matrixes with 54 micro inverse opal units were printed with different parameters. Suitable printing windows with appropriate laser power and scanning speed define acceptable

structures with well-recognizable clarity visually. The side effect of heat energy was aggravated by increasing the addition of DPP58-TBZ12 CPs in photoresists during the DLW-TPP process, which made the printing window narrow for printing parameters selection (**Figure 5.4 b and c**). Although the CPs absorb 746 nm laser light, expansion during the printing process can be avoided by choosing suitable printing parameters in the wide printing window. From these results of printing parameters and concentration of CPs, a laser power of 7 mW and a scanning speed of 10 mm s^{-1} were adopted as suitable experimental printing parameters for generating CPs/LCEs microstructures. LC photoresists with 0.3 wt.% CPs were chosen as the material for 4D DLW-TPP technology.

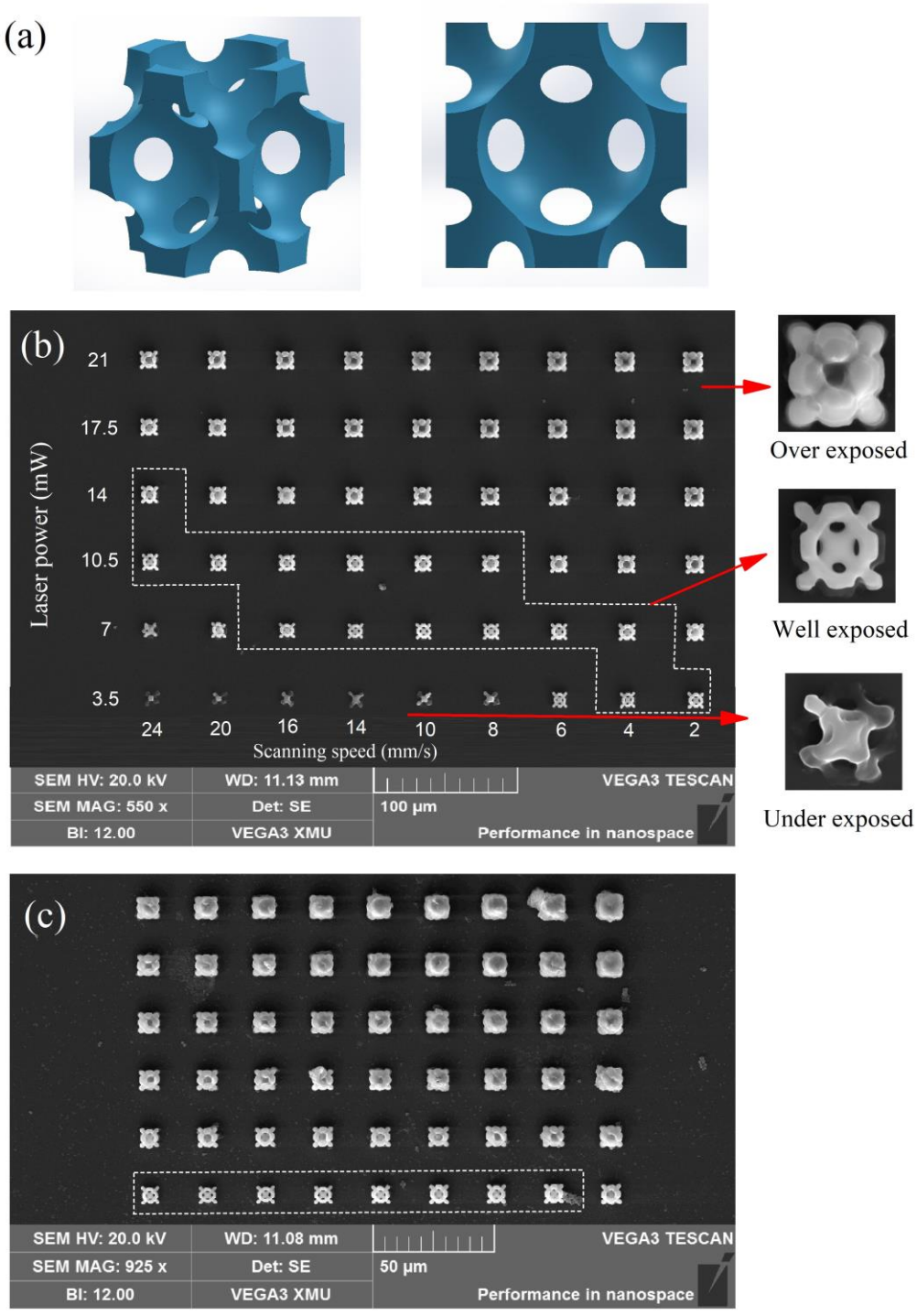

Figure 5.4 (a) 3D model design of an inverse opal structure unit with 3.7 µm of radius. (b) Scanning electron microscopic (SEM) images of 0.3 wt.% CPs/LCEs microstructures fabricated using DLW-TPP technology at varying laser powers (from 3.5 to 21 mW at an interval of 3.5 mW) and varying

scanning speeds (2, 4, 6, 8, 10, 14, 16, 20, 24 mm/s). Under-exposed, well-exposed, and over-exposed microstructures were also displayed to determine printing windows. (c) SEM images of 0.5 wt.% CPs/LCEs microstructures fabricated using DLW-TPP with the same varying laser powers and scanning speeds.

5.1.3.3 Confirmation of the Mesogen Alignment in the Printed Microstructures

To demonstrate the NIR light-induced actuation capabilities of a micro-actuator fabricated with the developed photoresists, a porous NIR light-driven LCE micro-actuator (150 μm × 50 μm × 20 μm) composed of two layers of 3D inverse opal structure with 3.7 μm radius was fabricated by DLW-TPP using the 0.3 wt.% CPs/LC photoresist (**Figure 5.5 a**). The SEM image of the printed structure is shown in **Figure 5.5 b**, which is consistent with the designed model. The alignment of the rigid mesogens on the PI-coated substrate was verified through the polarized optical microscope (POM) with the printed microstructures placed between crossed polarizers. There is a clear difference in the molecular orientation-induced birefringence of the CPs/LCEs microstructures under polarized light. The porous scaffold appeared dark when the rubbing direction aligned parallel to either the polarizer or analyzer (**Figure 5.5 c**). In contrast, the scaffold turned bright when the rubbing direction was rotated at 45° to the polarizer (**Figure 5.5 d**). The difference demonstrates that the printed microstructures comprise the homogeneous orientation of the mesogens along the rubbing direction.

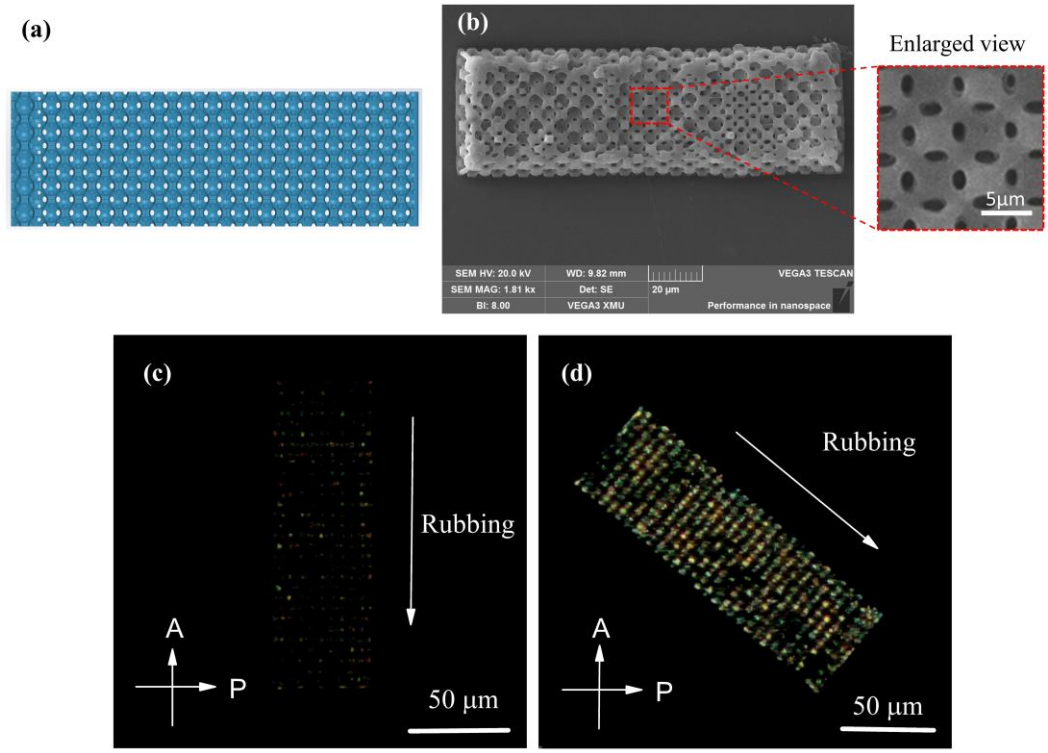

Figure 5.5 (a) Top view of the designed micro-actuator composed of two layers of 3D inverse opal structure with 3.7 μm of radius. (b) SEM image of porous 0.3 wt.% CPs/LCEs microstructure. The inset is the enlarged view of the structures. (c-d) Polarized optical microscope pictures of the printed CPs/LCEs microstructures with the rubbing direction along the analyzer "A" and rotated by 45° to the polarizer "P". The white arrows show the rubbing direction in the PI-coated glass. Scale bar: 50 μm.

5.1.3.4 NIR Photothermal Actuation of the Micro-actuators

The micro-actuator showed a large anisotropic shape change upon NIR light irradiation, which contracted and expanded along parallel ($l_{/\!/}$) and perpendicular ($l_{\perp}$) to the alignment direction, respectively. The anisotropic photothermal response in different directions is characteristic of uniaxially aligned polymerized

networks. Interface adhesion between the micro-actuator and the glasses has a great influence on axial deformation. Therefore, specific cylindric supporters with 3 μm of diameter are designed to reduce the adhesion of the micro-actuator for light-induced actuation after development. The photo-triggered actuation was investigated by placing the developed micro-actuators on the glass substrate. Upon NIR light irradiation with the wavelength of 808 nm, the local temperature will increase quickly to disorder the mesogen arrangement of the LCEs due to the photothermal conversion ability of the DPP58-TBZ12 CPs (**Figure 5.6 a**). The whole printed micro-actuator can be carefully detached from the glass substrate by a micromanipulation setup. It is clear to observe that the micro-actuator contracts along the alignment direction under the irradiation with the NIR laser (**Figure 5.6 b**). To systematically characterize the response performance of the printed LCE-based microstructures, maximum actuation strains of the micro-actuator on the glass substrate along $l_{/\!/}$ as the function of NIR laser powers are shown in **Figure 5.6 c**. The actuation strain (ε) is defined as

$$\varepsilon = \frac{L - l}{L} \times 100\% \quad (5)$$

where L is the length of the micro-actuator in the original state, whereas l is the length of the deformed micro-actuator in the actuated state. As shown in **Figure 5.6 d**, the pristine LCE micro-actuator without CPs showed neglectable actuation strains under different laser power intensities when the NIR laser power intensity rose from 47 to 173 mW/mm^2 at an interval of about 16 mW/mm^2. In contrast, the CPs/LCEs micro-actuator exhibited remarkable contraction strain values. Small actuation strain increases were observed as the NIR laser power intensity increased

from 142 to 173 mW/mm^2. When the NIR laser power intensity was 173 mW/mm^2, the actuation strains of the CPs/LCEs micro-actuator reached the maximum values, 25.0% for the $l_{/\!/}$ direction and 13.6% for the $l_{\perp}$ direction (**Figure 5.6 d**). A laser power intensity of 173 mW/mm^2 is advised as a suitable external stimulation value to assess the NIR photothermal actuation performance.

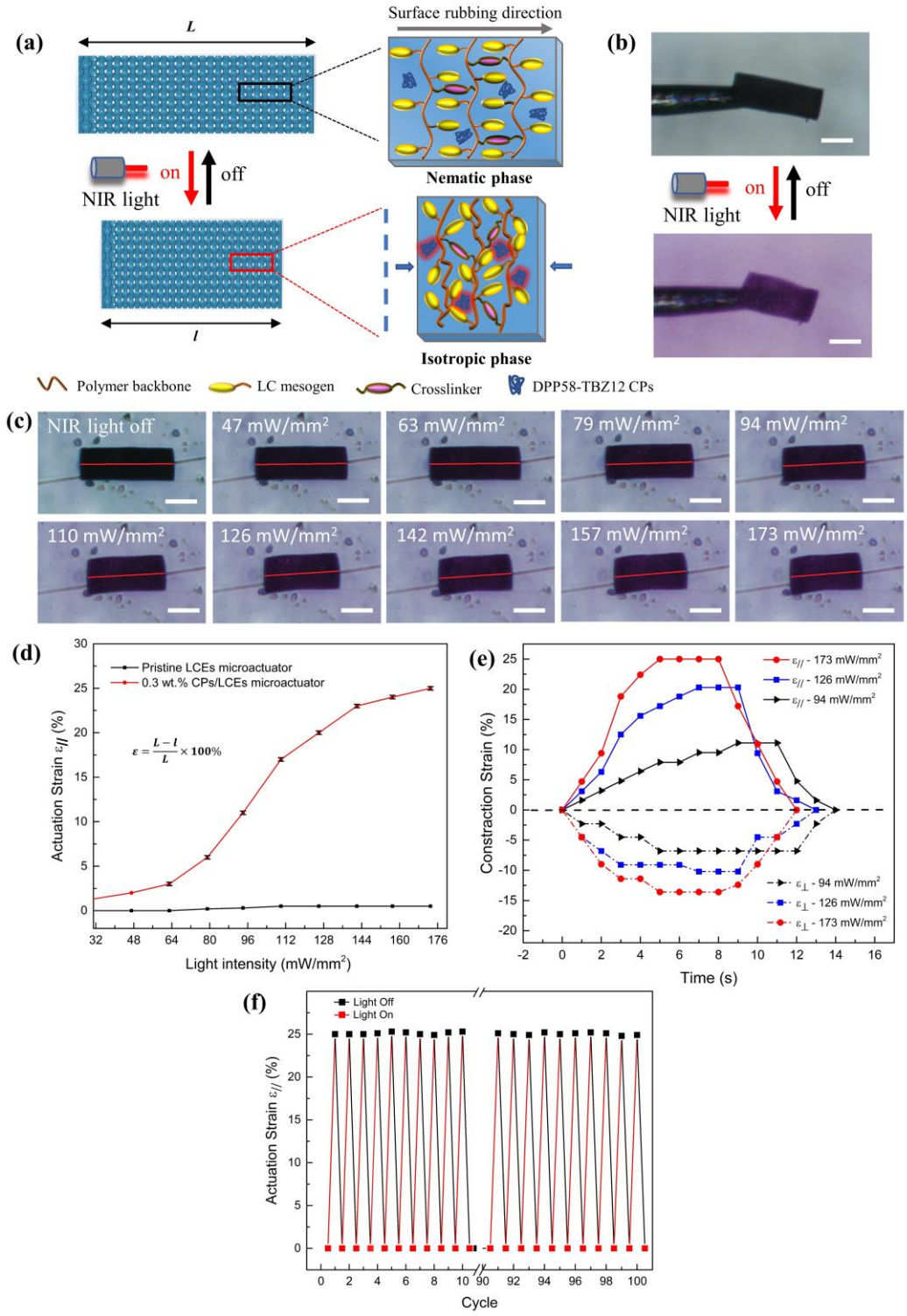

Figure 5.6 (a) Schematic illustration shows reversible photothermal actuation styles of CPs/LCEs micro-actuators under an on-off switching of NIR light, and corresponding reversible rearrangement mechanism of mesogens in LCEs. (b) A micro-actuator is held on a steel tip in the air and illuminated by

a NIR laser. Scale bar: 50 μm. (c) Photographs of micro-actuators in the equilibrium state under different NIR laser power intensities. Scale bar: 50 μm. (d) Maximum Actuation strain of the CPs/LCEs micro-actuator exposed to different laser power intensities. Error bars represent standard deviations of three measurements. (e) Actuation strain in the parallel and perpendicular directions as the function of time for the CPs/LCEs micro-actuator under different laser power intensities. (f) Reversible contraction strain of the micro-actuator triggered by the NIR light (808 nm, 173 mW/mm^2) on/off (ON: 5 s; OFF: 4 s).

For the study on the effect of NIR laser power intensity on the response sensitivity of the soft micro-actuator, **Figure 5.6 e** shows the deformation and recovery time of the CPs/LCEs micro-actuator under NIR laser intensity of 94, 126, and 173 mW/mm^2. The micro-actuator displayed significantly different actuation performances at different laser power intensities. The contraction strains were 11, 20, and 25% when the power intensities were 94, 126, and 173 mW/mm2, respectively. The micro-actuator could respond to the NIR laser quickly within 1s. The micro-actuator could reach the maximum photo-induced actuation strain in 5s under the NIR laser intensity of 173 mW/mm^2. Larger laser power intensity could trigger a shorter response time of the CPs/LCEs micro-actuator, which might be attributed to a higher local heating speed.

The photothermal actuation response of the porous CPs/LCEs microstructures to NIR light is fully reversible and reproducible for many actuation

cycles. Periodic continuous NIR light on (5 s)/off (5 s) cycles were carried out to investigate the durability of the CPs/LCEs micro-actuator, and the results are shown in **Figure 5.6 f**. The actuator maintained the original uniaxial actuation strain ($\varepsilon \approx 25.0\%$) without obvious distortion after 100 cycles, indicating excellent anti-fatigue properties of the CPs/LCEs microstructure sample. The ability of micro-actuators to undergo significant reversible contraction strain is crucial in various functional devices and soft robotics applications. A larger contraction strain indicates the broader working range of the CPs/LCEs micro-actuators by controlling the external stimuli.

It is worth mentioning that the maximum contractile strain (25%) of the CPs/LCEs micro-actuator is higher than that of the previously reported DLW-TPP-printed light-responsive LCE-based micro-actuators (20% for gold nanoparticles-incorporated LCE woodpile microstructure under NIR laser (Chen et al., 2019a), 20% for azobenzene-doped LCE microstructure under 532 nm laser excitation (Zeng et al., 2015), and 19% for azobenzene-filled LCE micro-block under a green laser light (Martella et al., 2017a)). With TPP-compatible CPs/LC photoresists, the fabrication of the light-responsive micro-actuators via DLW-TPP has been realized, and their excellent actuation performance under NIR light irradiation has also been demonstrated.

5.1.4 Conclusions

In summary, we have developed a new light-responsive LC photoresist that can be used in the precise construction of 3D micrometer-sized actuators via direct

laser writing based on two-photon polymerization. Different component ratios of LC photoresists are carefully designed and tuned for room-temperature DLW-TPP. Conjugated polymers DPP58-TBZ12 with NIR absorption, high photothermal conversion efficiency (52.7%), and photostability were successfully synthesized via Stille cross-coupling polymerization to serve as the photothermal dopants. The organic CPs with D-A alternating backbone structures could be uniformly incorporated into LC photoresists to achieve the light response of the LC photoresists. The CPs/LC photoresists could maintain the room temperature liquid crystal phase stable for at least 7 days. The incorporation of CPs also lowered the T_{NI} value of the LC photoresists largely to alleviate some degrees of crystallization at room temperature, making them compatible with the commercial DLW-TPP without the need of a heating stage. By carefully tuning the photoresist formulation and printing parameters (laser power and scanning speed), we demonstrate that the 4D microprinted porous CPs/LCEs micro-actuator with as low as 0.3 wt.% CPs can achieve 25% actuation strain upon stimulation to NIR light (808 nm) of 173 mW/mm^2. The results demonstrate that the developed CPs/LC photoresists are promising materials for TPP-printable actuating micro-objects. This work enriches the choice library of DLW-TPP-compatible LC photoresists for fabricating responsive micro-actuators at room temperature. It is worth mentioning that the CPs/LC photoresists can also be applied to other 4D printing techniques like UV-assisted direct-ink-writing-based printing to manufacture macroscale structures, which paves the way toward the multi-scale 3D actuators with promising potential

in the fields of functional separation membranes, and soft robotic systems and beyond.

5.2 Potential Biomedical Applications of Light-triggered Micro-actuators

5.2.1 Dynamic Cell Culture Platform for Cell Alignment

Controlled cell alignment plays a pivotal role in the microarchitecture and functionality of human tissues. The arrangement and orientation of cells within skeletal and cardiac tissues are critical for their biological, mechanical, and electrical properties. Proper cell alignment ensures efficient signal transmission, coordinated movement, and optimal tissue function. Additionally, it contributes to the mechanical strength and stability of tissues, facilitates electrical conductivity in tissues reliant on electrical signaling, and supports tissue regeneration and repair processes. Furthermore, controlling cell alignment is crucial in tissue engineering to mimic the native tissue structure and function, enabling the development of functionally engineered tissues. In this regard, understanding the necessity to control cell alignment is essential for advancing our knowledge of tissue biology, promoting tissue regeneration, and improving therapeutic approaches.

To study and replicate the biological function of cells, it is crucial to recreate their 3D microstructures in engineered tissues in the laboratory. The accurate reproduction of tissue morphogenesis in vitro is essential to developing engineered human tissues that possess the same characteristics as their native counterparts. Engineered tissue constructs are created by incorporating cells into scaffolds that mimic the natural 3D cellular environment. The topographical patterns and

mechanical properties of these 3D scaffolds play a crucial role in guiding the structural and functional development of immortalized cardiac and skeletal muscle cell lines (Simitzi et al., 2017).

LCEs are particularly recommended as active materials for fabricating dynamic cell culture platforms. This is because LCEs possess structural flexibility, mechanical strength, and the ability to undergo reversible contractile and extensile deformations. The dynamic shape deformation property of LCEs makes them suitable for simulating the dynamic microenvironment of cell growth.

In this work, we aim to combine the developed LCE-based microstructures with large actuation strains to investigate the dynamic interplay between the properties of extracellular matrix and biological cells. Firstly, 2D cell culture platforms with micro- and nanopatterns are fabricated by DLW-TPP to evaluate the effects of surface topography on cell alignment. Next, NIR light-responsive LCE-based micro-scaffolds with nano-features will be generated as the dynamic platforms for training cardiac cell lines to acquire and improve cell alignment and cell contraction force.

5.2.2 2D Cell Culture Platform Fabricated by DLW-TPP

Two different types of substrates (micro-patterned substrates and micro-nano-patterned substrates) using IP-L photoresist were fabricated by DLW-TPP. The glass coverslip was cleaned with acetone and distilled water to remove any residual dust or organics and dried with nitrogen. To improve the adhesion of the structure on the glass coverslip, 3-(Trimethoxysilyl) propyl methacrylate (Sigma Aldrich) is

used to strengthen the adhesion. Then, the DLW-TPP technique was used to produce two different types of substrates (micro-patterned substrates and micro-nano-patterned substrates) using the IP-L photoresist. After the printing process, the patterned substrate was developed by propylene glycol methyl ether acetate (PGMEA) and isopropyl alcohol (IPA) to free the desired structures from the unexposed polymer. Morphologies of the substrates were characterized using SEM.

Before seeding cells on the substrates, the substrates were cleaned with ethanol and sterilized water, and dried at room temperature. Fibroblast cell line MG63 (less than seven passages; ATCC) was cultured under a 5% CO_2 atmosphere at 37°C in the Dulbecco's modified eagle medium (DMEM), 10% (v/v) fetal bovine serum (FBS), and 1% (v/v) penicillin/Streptomycin(P/S). Once the cells reached about 80% confluence, the cells were first trypsinized, counted, and then resuspended in the DMEM with a density of 5×10^4 cells/mL. 1.5 mL of the cell suspension was placed onto a substrate in the Petri dish, and then the system was left undisturbed at 37 °C to allow the MG63 fibroblast cells to attach to the inner region of the grooves. The cells were cultured for 2 days. A schematic procedure to engineer MG63 cells on IP-L substrates is shown in **Figure 5.7**. Then, cells are observed under a microscopy imaging system.

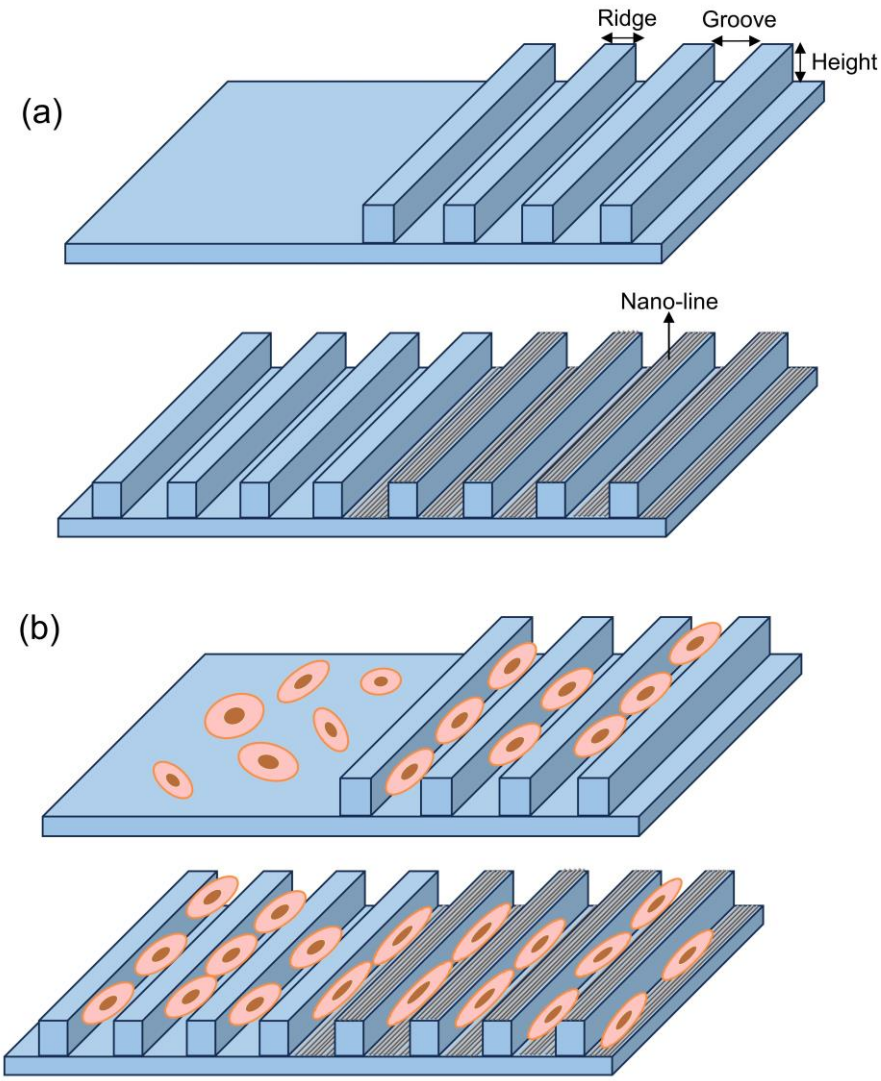

Figure 5.7 Schematic procedure to engineer MG63 cells on IP-L substrates: (a) Construction of substrate containing flat part and micro-patterned part, the substrate containing micro-patterned part and micro-nano-patterned part. (b) Schematic sketch of cell morphology on different substrates.

A micro-pattern with 20 μm width and 5μm height and a micro-nano-pattern are shown in **Figure 5.8 a-c**. The cell growth was observed under a microscope and shown in **Figure 5.8 d-i**. After 3-day cell culture, The MG63 cells on the flat substrate (non-patterned) showed random morphology and free differentiation route with a larger cell body. By contrast, cells on the patterned substrates

presented regular alignment along the microgroove direction. What is more, micro-grooved substrate with nano-lines can induce elongated cell shape and longer actin fibers compared with the micro-grooves (**Figure 5.8 f and i**). nanoline-grooved substrates promoted an elongated cell morphology. It has been demonstrated that DLW-TPP is a promising method for offering the possibility of fabricating a structure with micro- and nano-features. The biosurface can provide space constraint for cell elongation. Both micro- and nano-structures were found to guide the cell alignment, while the nano-pattern can induce cell elongation to a great extent in this study.

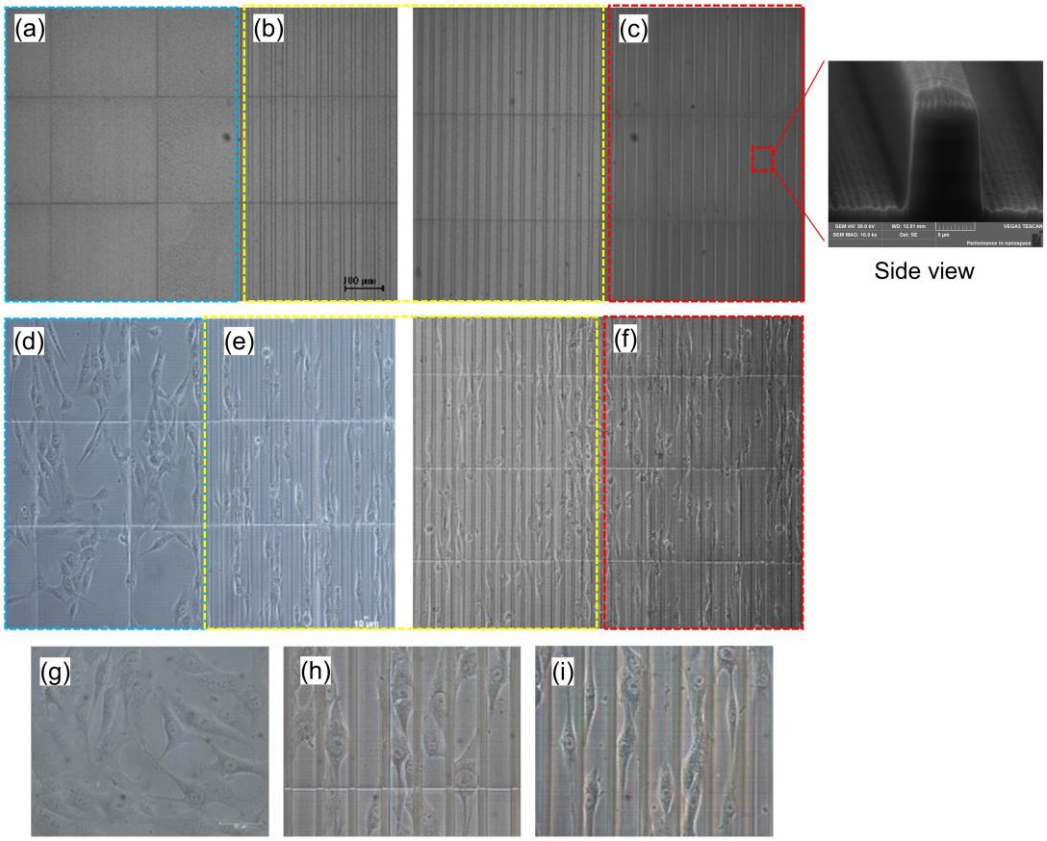

Figure 5.8 Surface topography and cell alignment on different types of micro-patterned substrates. (a, b, c) flat, micro-grooved, and micro-/nano-featured substrates, (d, e, f) the cells on the substrate after 3-day culture, (g, h, i)

Enlarged microscope images of cells on flat, micropatterned, micro-nano-patterned substrate.

5.2.3 LCE-based Micro-scaffolds for Cell Alignment Regulation

One drawback of many reported light-responsive LCEs is that they require relatively high temperatures, typically exceeding 80 °C, to achieve significant actuation strains of 10% to 15% (Ambulo et al., 2020). This temperature requirement poses a challenge in practical applications, especially in the context of tissue engineering. Subjecting surrounding cells to such high temperatures could result in thermal damage, rendering the use of high transition temperature LCEs impractical and potentially harmful.

Therefore, finding alternative LCE materials with lower transition temperatures becomes crucial. Lower transition temperature LCEs would allow for actuation strains to be achieved without subjecting the surrounding cells to excessively high temperatures. By utilizing LCEs with lower transition temperatures, it becomes possible to design and create dynamic cell culture platforms that can accurately mimic the movement and function of organs without compromising the integrity and safety of the surrounding tissues. Meanwhile, in properly designed culture environments, the heat capacity of the water can moderate the temperature changes observed by the cells.

Recently, mild heat stimulation (up to approximately 43 °C) generated from remote NIR light has emerged as an innovative alternative for inducing activation in skeletal and cardiac muscles. This approach involves the application of gentle heat to elicit muscle contractions and responses, providing a promising alternative to traditional methods of muscle stimulation due to the non-invasive and non-electrical, precise and localized properties (Lodola et al., 2019, Oyama et al., 2012,

Marino et al., 2017). Thin conjugated polymer films as transducers are demonstrated to improve the contraction rate *in vitro* cardiomyocyte culture under infrared light (Lodola et al., 2019).

The thermal energy generated by the NIR photothermal LCE-based micro-actuators can also achieve thermal stimulation on the surface. Integrated with the micro-nano-pattern and reversible contraction behavior, the NIR light-triggered microstructures have great potential for the manipulation culture of cardiac cells. The most important issue is to acquire a mild surface temperature under the reversible contraction deformation.

Chapter 6 Conclusion, Contribution, and Suggestions for Future Work

6.1 Overall Conclusion

The work in this thesis is almost the first attempt to develop a method combining the synthesis of novel conjugated polymers (CPs) and CPs/LCEs, programming for alignment of liquid crystal mesogens, photopolymerization techniques, and optimization of printing parameters for enhancing the performance of the LCE-based actuators. Novel conjugated polymers DPP58-TBZ12 have been successfully designed and synthesized as well as incorporated into LCEs, which display outstanding photothermal conversion efficiency and photostability. It has been demonstrated that the developed CPs/LCEs material has been fabricated into both 2D thin film-like macro-actuators and 3D porous micro-actuators via one-pot UV photopolymerization and direct laser writing-based two-photon polymerization (DLW-TPP), respectively. The shape deformation modes and the alignment directions have been carefully investigated. The printing parameters, including the laser power and scanning speed, have been optimized in the DLW-TPP microfabrication. The results demonstrate the potential of the prepared photoresponsive CPs/LCEs and the actuators. The major findings of the research are summarized as follows:

(1) Novel organic photothermal dopants, DPP58-TBZ12 CPs, are fabricated via palladium-catalysed Stille cross-coupling polymerization. Based on the design strategy of CPs with planar alternating D-A structured backbones, monomer DPP58 containing thiophene as donor and diketopyrrolopyrrole as acceptor 1, and monomer TBZ12 containing thiadiazolobenzotriazole as accepter 2 are used. The photothermal conversion efficiency can reach 52.7%.

The CPs also show good solubility in THF solvent, which is beneficial for the subsequent preparation of photo-responsive CPs/LCEs mixtures.

(2) The DPP58-TBZ12 CPs were incorporated in the LCEs to create 2D CPs/LCEs millimeter-scale actuators by one-pot UV photopolymerization. These CPs with planar molecular structures exhibited good dispersion in the LCE mixture, which is advantageous in saving on the cost and simplifying the preparation process. A low content (0.3 wt.%) of the conjugated polymers in the LCE matrix could result in an ultrafast increase in local temperature under 808 nm NIR irradiation. Using surface-patterned glass substrates, a single film with splay alignments was allowed to be fabricated via the one-pot UV photopolymerization. The 60 μm-thick CPs/LCEs film actuators exhibited a superior photothermal effect, repeatable shape change, and ultrafast response time with actuation within 1 s upon 808 nm laser irradiation. By carefully choosing the cutting angle between the alignment direction and the long axis of the rectangular film-like actuators, tunable shape deformation, including bending, “Swiss” rolling, and helical twisting, could be realized under unsymmetrical NIR light illumination. The film could bend up to 180° within 3 s and recover to its initial shape within 4 s. Moreover, the CPs/LCEs actuator could be pulsed to roll toward one direction at an average motion speed of 0.47 mm/s under NIR light based on successive left-hand helical twisting. The development of NIR light-driven soft actuators would offer a promising path toward micromachine and untethered soft robotics.

(3) In addition to the fabrication of the macro-actuators, the CPs were doped into LC photoresists to fabricate micro-actuators by the DLW-TPP technology. The most important thing is to tune the weight ratio of different components to

acquire CPs/LC photoresists with room-temperature liquid crystal phases for realizing the fabrication of the micro-actuators. The incorporation of CPP58-TBZ12 CPs lowers the nematic-to-isotropic transition temperature (T_{NI}) of the LC photoresists, which is beneficial for enabling room-temperature DLW-TPP microfabrication. The T_{NI} value decreases from 51.4 to 45.2 ºC with the concentration increasing from 0.1 to 0.5 wt.%. The lowered T_{NI} can also effectively alleviate the occurrence of crystalline behaviors of the photoresists before and during the DLW-TPP printing process. The concentration of CPs influences the printing windows because of the high photothermal conversion efficiency. The concentration of CPs should enable a broad printing window to select suitable printing parameters. The printing parameters, including laser power and scanning speed, were investigated for the developed LC photoresists. A well-defined CPs/LCEs micro-actuator with CPs as low as 0.3 wt.% was successfully printed to achieve a large 25.0% actuation strain in 5 s upon NIR light stimulation. This work provides new photothermal CPs/LC photoresists for the state-of-the-art DLW-TPP technology. The high contraction strain and cyclability of the 4D printed microactuators have demonstrated the great potential of the developed photoresists in the DLW-TPP microfabrication.

(4) The actuation performance of the macro-actuators and micro-actuators was compared with that of the reported LCE-based actuators in terms of the response time, locomotion speed, or contraction/expansion strain. These evaluation values of the CPs/LCEs actuators have been greatly improved. For example, the response time of the macro-actuators was ultrafast, and the velocity (0.47 mm/s) of the macro-actuator was higher than that (0.16 mm/s)

of the dye-containing LCE macro-actuator (Yang et al., 2019). The contraction strain (25.0%) of the CPs/LCEs micro-actuators was larger than that (20%) of the reported gold nanorods/LCEs micro-scaffold (Chen et al., 2019a). These were attributed to the high photothermal conversion efficiency and fast heating speed of DPP58-TBZ12 CPs under NIR light. The properties clearly demonstrated that the developed NIR light-responsive CPs/LCEs were advantageous in the manufacturing of actuators with different dimensions and scales. Different deformation modes of the CPs/LCEs actuators were also demonstrated successfully by designing the mesogen alignment in the LCE networks.

6.2 Statement of Originality and Contribution to Knowledge

The work in this thesis is almost the first attempt to develop novel photothermal DPP58-TBZ12 CPs for the fabrication of light-triggered CPs/LCEs actuators with enhanced response performance and multimodal deformation. As compared with the properties of other photothermal agents, an LCE matrix with incorporation of the CPs was effective in triggering the phase transition, which avoids the incompatibility between the photothermal agents and LCEs while maintaining the homogenous distribution in the LCEs.

This is the first attempt to realize different actuation modes of 2D CPs/LCEs film actuators with controllable deformation and ultrafast response speed by controlling the alignment angle to the long axis of the film actuators. The LCEs-based film actuators could contribute to the development of multimodal deformation and battery-free soft robots. Controllable locomotion can be realized in a single robot based on these multimodal shape deformations.

It is the first time to develop new CPs/LC photoresists with room-temperature liquid crystal phases for enabling the fabrication of 3D micro-actuators via DLW-TPP. The 3D NIR light-triggered CPs/LCEs micro-actuator has achieved a large actuation strain. This breakthrough and DLW-TPP optimized manufacturing strategy have laid down a solid foundation for further development of other high-precision 3D porous micro-actuators.

6.3 Suggestions for Future Work

The introduction of CPs in LCEs can effectively avoid the obvious aggregation and compatibility issues of inorganic dopants. Meanwhile, the CPs/LCEs mixtures show the advantages of fabricating soft actuators with facile controllability, multiple functionalities, and recyclability. Despite these achievements, soft robotics based on light-responsive LCE actuators is still in its infancy, with many challenges left to be addressed. The following aspects will be conducted in future work:

(1) The developed micro-actuators are not fully applied in practical applications. The main challenge lies in the fact that the transition temperature of LCEs between the nematic and isotropic phases is relatively high, typically exceeding 50 °C. This poses a problem for biomedical applications where the body temperature is around 35 °C, as the high transition temperature is unsuitable. Consequently, it becomes necessary to adjust the weight ratio of components in LCE materials to achieve a lower transition temperature that is more compatible with biomedical applications. In the next work, we will try to understand how the molecular structure of CPs influences the transition temperature of LCEs and design other CPs. To fulfill the potential application of the NIR light-responsive photoresists and DLW-TPP microfabrication,

CPs/LCEs micro-actuators with structural features, contraction force, and mild heating simulation will be developed to achieve the goal of inducing cell culture.

(2) In addition, suitable finite element simulations of spatial alignment orientation of liquid crystal mesogens have not been established to predict and guide the structure design with specific deformation. The influence of the photothermal conjugated polymers on the material's mechanical properties is also less investigated. Our future works will establish theoretical models to guide the fabrication of 3D macroscopic CPs/LCEs structures using UV-assisted direct ink writing technology. Meanwhile, the mechanical properties and generated force will be evaluated for further applications.

References

AHN, S. K., WARE, T. H., LEE, K. M., TONDIGLIA, V. P. & WHITE, T. J. 2016. Photoinduced Topographical Feature Development in Blueprinted Azobenzene‐Functionalized Liquid Crystalline Elastomers. *Advanced Functional Materials,* 26**,** 5819-5826.

AMBULO, C. P., BURROUGHS, J. J., BOOTHBY, J. M., KIM, H., SHANKAR, M. R. & WARE, T. H. 2017a. Four-dimensional Printing of Liquid Crystal Elastomers. *ACS Applied Materials & Interfaces,* 9**,** 37332-37339.

AMBULO, C. P., BURROUGHS, J. J., BOOTHBY, J. M., KIM, H., SHANKAR, M. R. & WARE, T. H. 2017b. Four-dimensional Printing of Liquid Crystal Elastomers. *ACS Appl Mater Interfaces,* 9**,** 37332-37339.

AMBULO, C. P., TASMIM, S., WANG, S., ABDELRAHMAN, M. K., ZIMMERN, P. E. & WARE, T. H. 2020. Processing advances in liquid crystal elastomers provide a path to biomedical applications. *J Appl Phys,* 128**,** 140901.

APSITE, I., SALEHI, S. & IONOV, L. 2022. Materials for Smart Soft Actuator Systems. *Chem Rev,* 122**,** 1349-1415.

BARBOT, A., POWER, M., SEICHEPINE, F. & YANG, G.-Z. Liquid seal for compact micropiston actuation at the capillary tip. *Science Advances,* 6**,** eaba5660.

BARNES, M., SAJADI, S. M., PAREKH, S., RAHMAN, M. M., AJAYAN, P. M. & VERDUZCO, R. 2020. Reactive 3D Printing of Shape-Programmable

Liquid Crystal Elastomer Actuators. *ACS Applied Materials & Interfaces,* 12**,** 28692-28699.

BAUMAN, G. E., MCCRACKEN, J. M. & WHITE, T. J. J. A. C. I. E. 2022. Actuation of liquid crystalline elastomers at or below ambient temperature. 61**,** e202202577.

BI, H., YE, G., YANG, H., SUN, H., REN, Z., GUO, R., XU, M., CAI, L. & HUANG, Z. 2020. Near infrared-induced shape memory polymer composites with dopamine-modified multiwall carbon nanotubes via 3D-printing. *European Polymer Journal,* 136.

BI, X. & HUANG, R. 2022. 3D printing of natural fiber and composites: A state-of-the-art review. *Materials & Design,* 222**,** 111065.

BOOTHBY, J. M., KIM, H. & WARE, T. H. 2017. Shape changes in chemoresponsive liquid crystal elastomers. *Sensors and Actuators B: Chemical,* 240**,** 511-518.

CEAMANOS, L., KAHVECI, Z., LÓPEZ-VALDEOLIVAS, M., LIU, D., BROER, D. J. & SÁNCHEZ-SOMOLINOS, C. 2020. Four-Dimensional Printed Liquid Crystalline Elastomer Actuators with Fast Photoinduced Mechanical Response toward Light-Driven Robotic Functions. *ACS Applied Materials & Interfaces,* 12**,** 44195-44204.

CEAMANOS, L., MULDER, D. J., KAHVECI, Z., LÓPEZ-VALDEOLIVAS, M., SCHENNING, A. P. & SÁNCHEZ-SOMOLINOS, C. J. J. O. M. C. B. 2023. Photomechanical response under physiological conditions of

azobenzene-containing 4D-printed liquid crystal elastomer actuators. 11**,** 4083-4094.

CHEN, L., DONG, Y., TANG, C. Y., ZHONG, L., LAW, W. C., TSUI, G. C. P., YANG, Y. & XIE, X. 2019a. Development of Direct-Laser-Printable Light-Powered Nanocomposites. *ACS Appl Mater Interfaces,* 11**,** 19541-19553.

CHEN, M., GAO, M., BAI, L., ZHENG, H., QI, H. J. & ZHOU, K. 2022a. Recent Advances in 4D Printing of Liquid Crystal Elastomers. *Advanced Materials,* n/a**,** 2209566.

CHEN, M., GAO, M., BAI, L., ZHENG, H., QI, H. J. & ZHOU, K. 2022b. Recent Advances in 4D Printing of Liquid Crystal Elastomers. *Adv Mater***,** e2209566.

CHEN, P., MA, Y., ZHENG, Z., WU, C., WANG, Y. & LIANG, G. 2019b. Facile syntheses of conjugated polymers for photothermal tumour therapy. *Nat Commun,* 10**,** 1192.

CHENG, Y., REN, K., YANG, D. & WEI, J. 2018. Bilayer-type fluorescence hydrogels with intelligent response serve as temperature/pH driven soft actuators. *Sensors and Actuators B: Chemical,* 255**,** 3117-3126.

CLEGG, J. R., WAGNER, A. M., SHIN, S. R., HASSAN, S., KHADEMHOSSEINI, A. & PEPPAS, N. A. 2019. Modular Fabrication of Intelligent Material-Tissue Interfaces for Bioinspired and Biomimetic Devices. *Prog Mater Sci,* 106.

CUI, X., RUAN, Q., ZHUO, X., XIA, X., HU, J., FU, R., LI, Y., WANG, J. & XU,

H. 2023. Photothermal Nanomaterials: A Powerful Light-to-Heat Converter. *Chem Rev,* 123**,** 6891-6952.

DAVIDSON, E. C., KOTIKIAN, A., LI, S., AIZENBERG, J. & LEWIS, J. A. 2020. 3D Printable and Reconfigurable Liquid Crystal Elastomers with Light-Induced Shape Memory via Dynamic Bond Exchange. *Advanced Materials,* 32**,** 1905682.

DE HAAN, L. T., SÁNCHEZ‐SOMOLINOS, C., BASTIAANSEN, C. M., SCHENNING, A. P. & BROER, D. J. J. A. C. I. E. 2012. Engineering of complex order and the macroscopic deformation of liquid crystal polymer networks. 51**,** 12469-12472.

DEL POZO, M., DELANEY, C., BASTIAANSEN, C. W. M., DIAMOND, D., SCHENNING, A. & FLOREA, L. 2020. Direct Laser Writing of Four-Dimensional Structural Color Microactuators Using a Photonic Photoresist. *ACS Nano,* 14**,** 9832-9839.

DEL POZO, M., DELANEY, C., PILZ DA CUNHA, M., DEBIJE, M. G., FLOREA, L. & SCHENNING, A. P. H. J. 2021. Temperature‐Responsive 4D Liquid Crystal Microactuators Fabricated by Direct Laser Writing by Two‐Photon Polymerization. *Small Structures,* 3.

DEL POZO, M., DELANEY, C., PILZ DA CUNHA, M., DEBIJE, M. G., FLOREA, L. & SCHENNING, A. P. H. J. 2022a. Temperature-Responsive 4D Liquid Crystal Microactuators Fabricated by Direct Laser Writing by Two-Photon Polymerization. *Small Structures,* 3**,** 2100158.

DEL POZO, M., SOL, J., SCHENNING, A. & DEBIJE, M. G. 2022b. 4D Printing of Liquid Crystals: What's Right for Me? *Adv Mater,* 34**,** e2104390.

DEMOLY, F., DUNN, M. L., WOOD, K. L., QI, H. J. & ANDRÉ, J.-C. 2021. The status, barriers, challenges, and future in design for 4D printing. *Materials & Design,* 212**,** 110193.

DENG, Z., ZHANG, H., PRIIMAGI, A. & ZENG, H. 2022. Light-Fueled Nonreciprocal Self-Oscillators for Fluidic Transportation and Coupling. *Advanced Materials,* n/a**,** 2209683.

DONG, L. & ZHAO, Y. 2018. Photothermally driven liquid crystal polymer actuators. *Materials Chemistry Frontiers,* 2**,** 1932-1943.

DRADRACH, K., ZMYSLONY, M., DENG, Z., PRIIMAGI, A., BIGGINS, J. & WASYLCZYK, P. 2023. Light-driven peristaltic pumping by an actuating splay-bend strip. *Nat Commun,* 14**,** 1877.

DU, Y., DING, Y., GE, F., WANG, X., MA, S., LU, H., ZHANG, G. & QIU, L. 2019. A regular ternary conjugated polymer bearing π-extended diketopyrrole and isoindigo acceptor units for field-effect transistors and photothermal conversion. *Dyes and Pigments,* 164**,** 27-34.

EL-ATAB, N., MISHRA, R. B., AL-MODAF, F., JOHARJI, L., ALSHARIF, A. A., ALAMOUDI, H., DIAZ, M., QAISER, N. & HUSSAIN, M. M. 2020. Soft Actuators for Soft Robotic Applications: A Review. *Advanced Intelligent Systems,* 2.

FARAJI RAD, Z., PREWETT, P. D. & DAVIES, G. J. 2021. High-resolution two-

photon polymerization: the most versatile technique for the fabrication of microneedle arrays. *Microsyst Nanoeng,* 7**,** 71.

FINKELMANN, H., KOCK, H.-J. & REHAGE, G. 1981. Investigations on liquid crystalline polysiloxanes 3. Liquid crystalline elastomers — a new type of liquid crystalline material. *Die Makromolekulare Chemie, Rapid Communications,* 2**,** 317-322.

FRANCIS, W., DUNNE, A., DELANEY, C., FLOREA, L. & DIAMOND, D. 2017. Spiropyran based hydrogels actuators—Walking in the light. *Sensors and Actuators B: Chemical,* 250**,** 608-616.

GAO, M., ZHU, L., PEH, C. K. & HO, G. W. 2019. Solar absorber material and system designs for photothermal water vaporization towards clean water and energy production. *Energy & Environmental Science,* 12**,** 841-864.

GE, F., YANG, R., TONG, X., CAMEREL, F. & ZHAO, Y. J. A. C. 2018. A multifunctional dye‐doped liquid crystal polymer actuator: light‐guided transportation, turning in locomotion, and autonomous motion. 130**,** 11932-11937.

GE, Q., SAKHAEI, A. H., LEE, H., DUNN, C. K., FANG, N. X. & DUNN, M. L. 2016. Multimaterial 4D Printing with Tailorable Shape Memory Polymers. *Scientific Reports,* 6**,** 31110.

GELEBART, A. H., JAN MULDER, D., VARGA, M., KONYA, A., VANTOMME, G., MEIJER, E. W., SELINGER, R. L. B. & BROER, D. J. 2017. Making waves in a photoactive polymer film. *Nature,* 546**,** 632-636.

GUAN, Z., WANG, L. & BAE, J. 2022. Advances in 4D printing of liquid crystalline elastomers: materials, techniques, and applications. *Mater Horiz*.

GUIN, T., HINTON, H. E., BURGESON, E., BOWLAND, C. C., KEARNEY, L. T., LI, Y., IVANOV, I., NGUYEN, N. A. & NASKAR, A. K. 2020. Tunable Electromechanical Liquid Crystal Elastomer Actuators. *Advanced Intelligent Systems,* 2.

GUO, L.-X., LIU, M.-H., SAYED, S. M., LIN, B.-P., KELLER, P., ZHANG, X.-Q., SUN, Y. & YANG, H. J. C. S. 2016a. A calamitic mesogenic near-infrared absorbing croconaine dye/liquid crystalline elastomer composite. 7**,** 4400-4406.

GUO, L. X., LIU, M. H., SAYED, S. M., LIN, B. P., KELLER, P., ZHANG, X. Q., SUN, Y. & YANG, H. 2016b. A calamitic mesogenic near-infrared absorbing croconaine dye/liquid crystalline elastomer composite. *Chem Sci,* 7**,** 4400-4406.

GUO, Y., SHAHSAVAN, H. & SITTI, M. 2020a. 3D Microstructures of Liquid Crystal Networks with Programmed Voxelated Director Fields. *Adv Mater,* 32**,** e2002753.

GUO, Y., SHAHSAVAN, H. & SITTI, M. 2020b. Microscale Polarization Color Pixels from Liquid Crystal Elastomers. *Advanced Optical Materials,* 8.

GUPTA, N., CHAN, Y.-H., SAHA, S. & LIU, M.-H. 2020. Recent Development in Near-Infrared Photothermal Therapy Based on Semiconducting Polymer

Dots. *ACS Applied Polymer Materials,* 2**,** 4195-4221.

HE, Q., WANG, Z., WANG, Y., MINORI, A., TOLLEY, M. T. & CAI, S. 2019. Electrically controlled liquid crystal elastomer–based soft tubular actuator with multimodal actuation. 5**,** eaax5746.

HEBNER, T. S., BOWMAN, C. N. & WHITE, T. J. 2021. The contribution of intermolecular forces to phototropic actuation of liquid crystalline elastomers. *Polymer Chemistry,* 12**,** 1581-1587.

HSU, L. Y., MAINIK, P., MÜNCHINGER, A., LINDENTHAL, S., SPRATTE, T., WELLE, A., ZAUMSEIL, J., SELHUBER‐UNKEL, C., WEGENER, M. & BLASCO, E. 2022. A Facile Approach for 4D Microprinting of Multi‐Photoresponsive Actuators. *Advanced Materials Technologies*.

HU, G., ZHANG, B., KELLY, S. M., CUI, J., ZHANG, K., HU, W., MIN, D., DING, S. & HUANG, W. 2022. Photopolymerisable liquid crystals for additive manufacturing. *Additive Manufacturing,* 55.

HU, J., WANG, W. & YU, H. 2019. Endowing Soft Photo‐Actuators with Intelligence. *Advanced Intelligent Systems,* 1.

HUANG, Z., CHI-PONG TSUI, G., DENG, Y. & TANG, C.-Y. 2020. Two-photon polymerization nanolithography technology for fabrication of stimulus-responsive micro/nano-structures for biomedical applications. *Nanotechnology Reviews,* 9**,** 1118-1136.

HUANG, Z., TSUI, G. C.-P., DENG, Y., TANG, C.-Y., YANG, M., ZHANG, M. & WONG, W.-Y. 2022. Bioinspired near-infrared light-induced ultrafast

soft actuators with tunable deformation and motion based on conjugated polymers/liquid crystal elastomers. *Journal of Materials Chemistry C,* 10**,** 12731-12740.

HUANG, Z., TSUI, G. C.-P., YEUNG, K.-W., LI, C., TANG, C.-Y., YANG, M., ZHANG, M. & WONG, W.-Y. 2023. 4D direct laser writing of photo-triggered liquid crystal elastomer microactuators with large actuation strain. *Materials & Design,* 232.

IAMSAARD, S., ASSHOFF, S. J., MATT, B., KUDERNAC, T., CORNELISSEN, J. J., FLETCHER, S. P. & KATSONIS, N. 2014. Conversion of light into macroscopic helical motion. *Nat Chem,* 6**,** 229-35.

ILAMI, M., BAGHERI, H., AHMED, R., SKOWRONEK, E. O. & MARVI, H. 2021. Materials, Actuators, and Sensors for Soft Bioinspired Robots. *Adv Mater,* 33**,** e2003139.

IONOV, L. 2015a. Polymeric actuators. *Langmuir,* 31**,** 5015-24.

IONOV, L. 2015b. Polymeric Actuators. *Langmuir,* 31**,** 5015-5024.

JI, Y., HUANG, Y. Y., RUNGSAWANG, R. & TERENTJEV, E. M. J. A. M. 2010. Dispersion and alignment of carbon nanotubes in liquid crystalline polymers and elastomers. 22**,** 3436-3440.

JIANG, Z. C., XIAO, Y. Y., TONG, X. & ZHAO, Y. 2019. Selective Decrosslinking in Liquid Crystal Polymer Actuators for Optical Reconfiguration of Origami and Light-Fueled Locomotion. *Angew Chem Int Ed Engl,* 58**,** 5332-5337.

KIM, H., LEE, J. A., AMBULO, C. P., LEE, H. B., KIM, S. H., NAIK, V. V., HAINES, C. S., ALIEV, A. E., OVALLE‐ROBLES, R., BAUGHMAN, R. H. & WARE, T. H. 2019. Intelligently Actuating Liquid Crystal Elastomer‐Carbon Nanotube Composites. *Advanced Functional Materials,* 29.

KIM, H. J., KIM, B., AUH, Y. & KIM, E. 2021a. Conjugated Organic Photothermal Films for Spatiotemporal Thermal Engineering. *Adv Mater***,** e2005940.

KIM, K., GUO, Y., BAE, J., CHOI, S., SONG, H. Y., PARK, S., HYUN, K. & AHN, S. K. 2021b. 4D Printing of Hygroscopic Liquid Crystal Elastomer Actuators. *Small,* 17**,** e2100910.

KIVALA, M. & DIEDERICH, F. 2009. Acetylene-Derived Strong Organic Acceptors for Planar and Nonplanar Push−Pull Chromophores. *Accounts of Chemical Research,* 42**,** 235-248.

KOHLMEYER, R. R. & CHEN, J. 2013a. Wavelength-selective, IR light-driven hinges based on liquid crystalline elastomer composites. *Angew Chem Int Ed Engl,* 52**,** 9234-7.

KOHLMEYER, R. R. & CHEN, J. J. A. C. I. E. 2013b. Wavelength‐selective, IR light‐driven hinges based on liquid crystalline elastomer composites. 52**,** 9234-9237.

KOTIKIAN, A., MCMAHAN, C., DAVIDSON, E. C., MUHAMMAD, J. M., WEEKS, R. D., DARAIO, C. & LEWIS, J. A. 2019. Untethered soft

robotic matter with passive control of shape morphing and propulsion. *Science Robotics,* 4**,** eaax7044.

KOTIKIAN, A., TRUBY, R. L., BOLEY, J. W., WHITE, T. J. & LEWIS, J. A. 2018a. 3D Printing of Liquid Crystal Elastomeric Actuators with Spatially Programed Nematic Order. *Adv Mater,* 30.

KOTIKIAN, A., TRUBY, R. L., BOLEY, J. W., WHITE, T. J. & LEWIS, J. A. 2018b. 3D Printing of Liquid Crystal Elastomeric Actuators with Spatially Programed Nematic Order. *Advanced Materials,* 30**,** 1706164.

KUMAR, K., KNIE, C., BLEGER, D., PELETIER, M. A., FRIEDRICH, H., HECHT, S., BROER, D. J., DEBIJE, M. G. & SCHENNING, A. P. 2016. A chaotic self-oscillating sunlight-driven polymer actuator. *Nat Commun,* 7**,** 11975.

LAN, R., SUN, J., SHEN, C., HUANG, R., ZHANG, Z., ZHANG, L., WANG, L. & YANG, H. 2020. Near-Infrared Photodriven Self-Sustained Oscillation of Liquid-Crystalline Network Film with Predesignated Polydopamine Coating. *Adv Mater,* 32**,** e1906319.

LE, X., LU, W., ZHANG, J. & CHEN, T. 2019. Recent Progress in Biomimetic Anisotropic Hydrogel Actuators. *Adv Sci (Weinh),* 6**,** 1801584.

LEANZA, S., WU, S., SUN, X., QI, H. J. & ZHAO, R. R. J. A. M. 2023. Active Materials for Functional Origami. 2302066.

LENDLEIN, A. & GOULD, O. E. J. N. R. M. 2019. Reprogrammable recovery and actuation behaviour of shape-memory polymers. 4**,** 116-133.

LENG, J., LAN, X., LIU, Y. & DU, S. 2011. Shape-memory polymers and their composites: Stimulus methods and applications. *Progress in Materials Science,* 56**,** 1077-1135.

LEWIS, J. A. 2006. Direct Ink Writing of 3D Functional Materials. *Advanced Functional Materials,* 16**,** 2193-2204.

LI, M., PAL, A., AGHAKHANI, A., PENA-FRANCESCH, A. & SITTI, M. J. N. R. M. 2022. Soft actuators for real-world applications. 7**,** 235-249.

LI, M. H., KELLER, P., LI, B., WANG, X. & BRUNET, M. 2003. Light-Driven Side-On Nematic Elastomer Actuators. *Advanced Materials,* 15**,** 569-572.

LI, S., WANG, X., HU, R., CHEN, H., LI, M., WANG, J., WANG, Y., LIU, L., LV, F., LIANG, X.-J. & WANG, S. 2016. Near-Infrared (NIR)-Absorbing Conjugated Polymer Dots as Highly Effective Photothermal Materials for In Vivo Cancer Therapy. *Chemistry of Materials,* 28**,** 8669-8675.

LI, Y., LIU, Y. & LUO, D. 2020. Polarization Dependent Light‐Driven Liquid Crystal Elastomer Actuators Based on Photothermal Effect. *Advanced Optical Materials,* 9.

LI, Y., YU, H., YU, K., GUO, X. & WANG, X. 2021. Reconfigurable Three-Dimensional Mesotructures of Spatially Programmed Liquid Crystal Elastomers and Their Ferromagnetic Composites. *Advanced Functional Materials,* 31**,** 2100338.

LI, Z., YANG, Y., WANG, Z., ZHANG, X., CHEN, Q., QIAN, X., LIU, N., WEI, Y. & JI, Y. 2017a. Polydopamine nanoparticles doped in liquid crystal

elastomers for producing dynamic 3D structures. *Journal of Materials Chemistry A,* 5**,** 6740-6746.

LI, Z., YANG, Y., WANG, Z., ZHANG, X., CHEN, Q., QIAN, X., LIU, N., WEI, Y. & JI, Y. J. J. O. M. C. A. 2017b. Polydopamine nanoparticles doped in liquid crystal elastomers for producing dynamic 3D structures. 5**,** 6740-6746.

LIAO, C., WUETHRICH, A. & TRAU, M. 2020. A material odyssey for 3D nano/microstructures: two photon polymerization based nanolithography in bioapplications. *Applied Materials Today,* 19.

LIN, H.-W., LEE, W.-Y. & CHEN, W.-C. 2012. Selenophene-DPP donor–acceptor conjugated polymer for high performance ambipolar field effect transistor and nonvolatile memory applications. *J. Mater. Chem.,* 22**,** 2120-2128.

LIU, D. & BROER, D. J. 2014. Liquid crystal polymer networks: preparation, properties, and applications of films with patterned molecular alignment. *Langmuir,* 30**,** 13499-509.

LIU, L., LIU, M. H., DENG, L. L., LIN, B. P. & YANG, H. 2017. Near-Infrared Chromophore Functionalized Soft Actuator with Ultrafast Photoresponsive Speed and Superior Mechanical Property. *J Am Chem Soc,* 139**,** 11333-11336.

LIU, W., GUO, L.-X., LIN, B.-P., ZHANG, X.-Q., SUN, Y. & YANG, H. 2016. Near-Infrared Responsive Liquid Crystalline Elastomers Containing Photothermal Conjugated Polymers. *Macromolecules,* 49**,** 4023-4030.

LIU, X., KONG, L., DU, H., ZHANG, Y., ZHAO, J. & XIE, Y. 2019. Synthesis and electrochromic properties of electrochromic polymers based on propylenedioxythiophene, diketopyrrolopyrrole and benzodithiophene units. *Organic Electronics,* 64**,** 223-235.

LIU, Z., BISOYI, H. K., HUANG, Y., WANG, M., YANG, H. & LI, Q. 2022. Thermo- and Mechanochromic Camouflage and Self-Healing in Biomimetic Soft Actuators Based on Liquid Crystal Elastomers. *Angewandte Chemie International Edition,* 61**,** e202115755.

LODOLA, F., VURRO, V., CRASTO, S., DI PASQUALE, E. & LANZANI, G. 2019. Optical Pacing of Human-Induced Pluripotent Stem Cell-Derived Cardiomyocytes Mediated by a Conjugated Polymer Interface. *Adv Healthc Mater,* 8**,** e1900198.

LÓPEZ-VALDEOLIVAS, M., LIU, D., BROER, D. J. & SÁNCHEZ-SOMOLINOS, C. 2018. 4D Printed Actuators with Soft-Robotic Functions. *Macromolecular Rapid Communications,* 39**,** 1700710.

LU, X., AMBULO, C. P., WANG, S., RIVERA-TARAZONA, L. K., KIM, H., SEARLES, K. & WARE, T. H. 2021. 4D-Printing of Photoswitchable Actuators. *Angew Chem Int Ed Engl,* 60**,** 5536-5543.

LU, X., GUO, S., TONG, X., XIA, H. & ZHAO, Y. 2017. Tunable Photocontrolled Motions Using Stored Strain Energy in Malleable Azobenzene Liquid Crystalline Polymer Actuators. *Adv Mater,* 29.

LU, X., SUN, L., JIANG, P. & BAO, X. 2019. Progress of Photodetectors Based

on the Photothermoelectric Effect. *Adv Mater,* 31**,** e1902044.

MA, C., LU, W., YANG, X., HE, J., LE, X., WANG, L., ZHANG, J., SERPE, M. J., HUANG, Y. & CHEN, T. 2018. Bioinspired Anisotropic Hydrogel Actuators with On–Off Switchable and Color-Tunable Fluorescence Behaviors. *Advanced Functional Materials,* 28**,** 1704568.

MA, S., LI, X., HUANG, S., HU, J. & YU, H. 2019. A Light-Activated Polymer Composite Enables On-Demand Photocontrolled Motion: Transportation at the Liquid/Air Interface. *Angewandte Chemie International Edition,* 58**,** 2655-2659.

MA, Z. C., ZHANG, Y. L., HAN, B., HU, X. Y., LI, C. H., CHEN, Q. D. & SUN, H. B. 2020. Femtosecond laser programmed artificial musculoskeletal systems. *Nat Commun,* 11**,** 4536.

MAO, Y., DING, Z., YUAN, C., AI, S., ISAKOV, M., WU, J., WANG, T., DUNN, M. L. & QI, H. J. 2016. 3D Printed Reversible Shape Changing Components with Stimuli Responsive Materials. *Scientific Reports,* 6**,** 24761.

MARINO, A., ARAI, S., HOU, Y., DEGL'INNOCENTI, A., CAPPELLO, V., MAZZOLAI, B., CHANG, Y.-T., MATTOLI, V., SUZUKI, M. & CIOFANI, G. J. A. N. 2017. Gold nanoshell-mediated remote myotube activation. 11**,** 2494-2508.

MAROTTA, A., LAMA, G. C., AMBROGI, V., CERRUTI, P., GIAMBERINI, M. & GENTILE, G. 2018. Shape memory behavior of liquid-crystalline

elastomer/graphene oxide nanocomposites. *Composites Science and Technology,* 159**,** 251-258.

MARTELLA, D., ANTONIOLI, D., NOCENTINI, S., WIERSMA, D. S., GALLI, G., LAUS, M. & PARMEGGIANI, C. 2017a. Light activated non-reciprocal motion in liquid crystalline networks by designed microactuator architecture. *RSC Advances,* 7**,** 19940-19947.

MARTELLA, D., NOCENTINI, S., NUZHDIN, D., PARMEGGIANI, C. & WIERSMA, D. S. 2017b. Photonic Microhand with Autonomous Action. *Adv Mater,* 29.

MCCRACKEN, J. M., DONOVAN, B. R., LYNCH, K. M. & WHITE, T. J. 2021. Molecular Engineering of Mesogenic Constituents Within Liquid Crystalline Elastomers to Sharpen Thermotropic Actuation. *Advanced Functional Materials,* 31.

MEN, X., CHEN, H., SUN, C., LIU, Y., WANG, R., ZHANG, X., WU, C. & YUAN, Z. 2020a. Thermosensitive Polymer Dot Nanocomposites for Trimodal Computed Tomography/Photoacoustic/Fluorescence Imaging-Guided Synergistic Chemo-Photothermal Therapy. *ACS Appl Mater Interfaces,* 12**,** 51174-51184.

MEN, X., WANG, F., CHEN, H., LIU, Y., MEN, X., YUAN, Y., ZHANG, Z., GAO, D., WU, C. & YUAN, Z. 2020b. Ultrasmall Semiconducting Polymer Dots with Rapid Clearance for Second Near‐Infrared Photoacoustic Imaging and Photothermal Cancer Therapy. *Advanced Functional Materials,* 30.

MERKEL, D. R., TRAUGUTT, N. A., VISVANATHAN, R., YAKACKI, C. M. & FRICK, C. P. 2018. Thermomechanical properties of monodomain nematic main-chain liquid crystal elastomers. *Soft Matter,* 14**,** 6024-6036.

MEYER, D. L., SCHMIDT-MEINZER, N., MATT, C., REIN, S., LOMBECK, F., SOMMER, M. & BISKUP, T. 2019. Side-Chain Engineering of Conjugated Polymers: Distinguishing Its Impact on Film Morphology and Electronic Structure. *The Journal of Physical Chemistry C,* 123**,** 20071-20083.

O'HALLORAN, S., PANDIT, A., HEISE, A. & KELLETT, A. 2022. Two-Photon Polymerization: Fundamentals, Materials, and Chemical Modification Strategies. *Adv Sci (Weinh)***,** e2204072.

OYAMA, K., MIZUNO, A., SHINTANI, S. A., ITOH, H., SERIZAWA, T., FUKUDA, N., SUZUKI, M., ISHIWATA, S. I. J. B. & COMMUNICATIONS, B. R. 2012. Microscopic heat pulses induce contraction of cardiomyocytes without calcium transients. 417**,** 607-612.

PALAGI, S., MARK, A. G., REIGH, S. Y., MELDE, K., QIU, T., ZENG, H., PARMEGGIANI, C., MARTELLA, D., SANCHEZ-CASTILLO, A., KAPERNAUM, N., GIESSELMANN, F., WIERSMA, D. S., LAUGA, E. & FISCHER, P. 2016. Structured light enables biomimetic swimming and versatile locomotion of photoresponsive soft microrobots. *Nature Materials,* 15**,** 647-653.

PANG, X., LV, J. A., ZHU, C., QIN, L. & YU, Y. 2019a. Photodeformable

Azobenzene-Containing Liquid Crystal Polymers and Soft Actuators. *Adv Mater,* 31**,** e1904224.

PANG, X., LV, J. A., ZHU, C., QIN, L. & YU, Y. J. A. M. 2019b. Photodeformable azobenzene‐containing liquid crystal polymers and soft actuators. 31**,** 1904224.

PENG, X., WU, S., SUN, X., YUE, L., MONTGOMERY, S. M., DEMOLY, F., ZHOU, K., ZHAO, R. R. & QI, H. J. 2022. 4D Printing of Freestanding Liquid Crystal Elastomers via Hybrid Additive Manufacturing. *Adv Mater,* 34**,** e2204890.

PILATE, F., TONCHEVA, A., DUBOIS, P. & RAQUEZ, J.-M. 2016. Shape-memory polymers for multiple applications in the materials world. *European Polymer Journal,* 80**,** 268-294.

PILZ DA CUNHA, M., DEBIJE, M. G. & SCHENNING, A. 2020. Bioinspired light-driven soft robots based on liquid crystal polymers. *Chem Soc Rev,* 49**,** 6568-6578.

PIROTTE, G., VERSTAPPEN, P., VANDERZANDE, D. & MAES, W. 2018. On the “True” Structure of Push-Pull-Type Low-Bandgap Polymers for Organic Electronics. *Advanced Electronic Materials,* 4.

QIN, L., LIU, X. & YU, Y. 2021. Soft Actuators of Liquid Crystal Polymers Fueled by Light from Ultraviolet to Near Infrared. *Advanced Optical Materials,* 9.

RITACCO, T., ACETI, D. M., DE DOMENICO, G., GIOCONDO, M., MAZZULLA, A., CIPPARRONE, G. & PAGLIUSI, P. 2021. Tuning

Cholesteric Selective Reflection In Situ Upon Two‐Photon Polymerization Enables Structural Multicolor 4D Microfabrication. *Advanced Optical Materials,* 10.

ROCHA, V. G., SAIZ, E., TIRICHENKO, I. S. & GARCÍA-TUÑÓN, E. 2020. Direct ink writing advances in multi-material structures for a sustainable future. *Journal of Materials Chemistry A,* 8**,** 15646-15657.

ROPER, D. K., AHN, W. & HOEPFNER, M. 2007. Microscale Heat Transfer Transduced by Surface Plasmon Resonant Gold Nanoparticles. *The Journal of Physical Chemistry C,* 111**,** 3636-3641.

RYABCHUN, A., LANCIA, F. & KATSONIS, N. 2023. Light-Responsive Springs from Electropatterned Liquid Crystal Polymer Networks. *Advanced Optical Materials,* n/a**,** 2300358.

SAADI, M., MAGUIRE, A., POTTACKAL, N. T., THAKUR, M. S. H., IKRAM, M. M., HART, A. J., AJAYAN, P. M. & RAHMAN, M. M. 2022a. Direct Ink Writing: A 3D Printing Technology for Diverse Materials. *Adv Mater,* 34**,** e2108855.

SAADI, M. A. S. R., MAGUIRE, A., POTTACKAL, N. T., THAKUR, M. S. H., IKRAM, M. M., HART, A. J., AJAYAN, P. M. & RAHMAN, M. M. 2022b. Direct Ink Writing: A 3D Printing Technology for Diverse Materials. *Advanced Materials,* 34**,** 2108855.

SAFRANSKI, D. L. & GALL, K. 2008. Effect of chemical structure and crosslinking density on the thermo-mechanical properties and toughness of

(meth)acrylate shape memory polymer networks. *Polymer,* 49**,** 4446-4455.

SEO, Y., KIM, S., LEE, H. S., PARK, J., LEE, K., JUN, I., SEO, H., KIM, Y. J., YOO, Y., CHOI, B. C., SEOK, H. K., KIM, Y. C., OK, M. R., CHOI, J., JOO, C. K. & JEON, H. 2020. Femtosecond laser induced nano-textured micropatterning to regulate cell functions on implanted biomaterials. *Acta Biomater*.

SHAHA, R. K., TORBATI, A. H. & FRICK, C. P. 2021. Body-temperature shape-shifting liquid crystal elastomers. *Journal of Applied Polymer Science,* 138**,** 50136.

SHAHSAVAN, H., AGHAKHANI, A., ZENG, H., GUO, Y., DAVIDSON, Z. S., PRIIMAGI, A. & SITTI, M. 2020. Bioinspired underwater locomotion of light-driven liquid crystal gels. *Proc Natl Acad Sci U S A,* 117**,** 5125-5133.

SHANG, J., LE, X., ZHANG, J., CHEN, T. & THEATO, P. 2019a. Trends in polymeric shape memory hydrogels and hydrogel actuators. *Polymer Chemistry,* 10**,** 1036-1055.

SHANG, Y., WANG, J., IKEDA, T. & JIANG, L. 2019b. Bio-inspired liquid crystal actuator materials. *Journal of Materials Chemistry C,* 7**,** 3413-3428.

SHI, P., ZHAO, Y., LIU, Z. & HE, X. 2022. Liquid crystal elastomer composite-based photo-oscillator for microrobots. *Journal of Composite Materials,* 57**,** 633-643.

SIMITZI, C., RANELLA, A. & STRATAKIS, E. 2017. Controlling the morphology and outgrowth of nerve and neuroglial cells: The effect of

surface topography. *Acta Biomater,* 51**,** 21-52.

STOYCHEV, G., KIRILLOVA, A. & IONOV, L. 2019. Light‐Responsive Shape‐Changing Polymers. *Advanced Optical Materials,* 7.

SUGIYAMA, F., KLEINSCHMIDT, A. T., KAYSER, L. V., RODRIQUEZ, D., FINN, M., 3RD, ALKHADRA, M. A., WAN, J. M., RAMIREZ, J., CHIANG, A. S., ROOT, S. E., SAVAGATRUP, S. & LIPOMI, D. J. 2018. Effects of flexibility and branching of side chains on the mechanical properties of low-bandgap conjugated polymers. *Polym Chem,* 9**,** 4354-4363.

SUN, C., ZHANG, S., REN, Y., ZHANG, J., SHEN, J., QIN, S., HU, W., ZHU, S., YANG, H. & YANG, D. 2022a. Force-Induced Synergetic Pigmentary and Structural Color Change of Liquid Crystalline Elastomer with Nanoparticle-Enhanced Mechanosensitivity. *Advanced Science,* 9**,** 2205325.

SUN, T., DOU, J. H., LIU, S., WANG, X., ZHENG, X., WANG, Y., PEI, J. & XIE, Z. 2018. Second Near-Infrared Conjugated Polymer Nanoparticles for Photoacoustic Imaging and Photothermal Therapy. *ACS Appl Mater Interfaces,* 10**,** 7919-7926.

SUN, X., WEI, J. & YU, Y. 2022b. Photoinduced deformation of amorphous polyimide enabled by an improved azobenzene isomerization efficiency. *Polymer Chemistry,* 13**,** 5447-5452.

TABRIZI, M., WARE, T. H. & SHANKAR, M. R. 2019. Voxelated Molecular

Patterning in Three-Dimensional Freeforms. *ACS Appl Mater Interfaces,* 11**,** 28236-28245.

TER SCHIPHORST, J., SAEZ, J., DIAMOND, D., BENITO-LOPEZ, F. & SCHENNING, A. 2018. Light-responsive polymers for microfluidic applications. *Lab Chip,* 18**,** 699-709.

TIAN, H., WANG, Z., CHEN, Y., SHAO, J., GAO, T., CAI, S. J. A. A. M. & INTERFACES 2018. Polydopamine-coated main-chain liquid crystal elastomer as optically driven artificial muscle. 10**,** 8307-8316.

TSANG, A. C. H., ZHANG, J., HUI, K. N., HUI, K. S. & HUANG, H. 2022. Recent Development and Applications of Advanced Materials via Direct Ink Writing. *Advanced Materials Technologies,* 7**,** 2101358.

WANG, J. Y., JIN, F., DONG, X. Z., LIU, J. & ZHENG, M. L. 2022a. Flytrap Inspired pH‐Driven 3D Hydrogel Actuator by Femtosecond Laser Microfabrication. *Advanced Materials Technologies*.

WANG, M., HU, X. B., ZUO, B., HUANG, S., CHEN, X. M. & YANG, H. 2020a. Liquid crystal elastomer actuator with serpentine locomotion. *Chem Commun (Camb),* 56**,** 7597-7600.

WANG, M., HUANG, X. & YANG, H. 2023a. Photothermal‐Responsive Crosslinked Liquid Crystal Polymers. *Macromolecular Materials and Engineering*.

WANG, W., SUN, X., WU, W., PENG, H. & YU, Y. 2012. Photoinduced deformation of crosslinked liquid-crystalline polymer film oriented by a

highly aligned carbon nanotube sheet. *Angew Chem Int Ed Engl,* 51**,** 4644-7.

WANG, X.-Q. & HO, G. W. 2022. Design of untethered soft material micromachine for life-like locomotion. *Materials Today,* 53**,** 197-216.

WANG, X., BEHL, M., LENDLEIN, A. & BALK, M. 2023b. Responses to single and multiple temperature-, medium-, and pH-stimuli triggering reversible shape shifts in hydrogel actuators. *Materials & Design,* 225.

WANG, X., QIN, X.-H., HU, C., TERZOPOULOU, A., CHEN, X.-Z., HUANG, T.-Y., MANIURA-WEBER, K., PANÉ, S. & NELSON, B. J. 2018. 3D Printed Enzymatically Biodegradable Soft Helical Microswimmers. *Advanced Functional Materials,* 28.

WANG, Y., DANG, A., ZHANG, Z., YIN, R., GAO, Y., FENG, L. & YANG, S. 2020b. Repeatable and Reprogrammable Shape Morphing from Photoresponsive Gold Nanorod/Liquid Crystal Elastomers. *Adv Mater,* 32**,** e2004270.

WANG, Y., MENG, H.-M., SONG, G., LI, Z. & ZHANG, X.-B. 2020c. Conjugated-Polymer-Based Nanomaterials for Photothermal Therapy. *ACS Applied Polymer Materials,* 2**,** 4258-4272.

WANG, Y., WANG, Y., WEI, Q. & ZHANG, J. 2022b. Light-responsive shape memory polymer composites. *European Polymer Journal,* 173.

WANG, Y., YIN, R., JIN, L., LIU, M., GAO, Y., RANEY, J. & YANG, S. 2023c. 3D-Printed Photoresponsive Liquid Crystal Elastomer Composites for

Free-Form Actuation. *Advanced Functional Materials,* 33**,** 2210614.

WANG, Z., BOECHLER, N. & CAI, S. 2022c. Anisotropic mechanical behavior of 3D printed liquid crystal elastomer. *Additive Manufacturing,* 52.

WANG, Z., GUO, Y., CAI, S. & YANG, J. 2022d. Three-Dimensional Printing of Liquid Crystal Elastomers and Their Applications. *ACS Applied Polymer Materials,* 4**,** 3153-3168.

WANG, Z., WANG, Z., ZHENG, Y., HE, Q., WANG, Y. & CAI, S. Three-dimensional printing of functionally graded liquid crystal elastomer. *Science Advances,* 6**,** eabc0034.

WANI, O. M., VERPAALEN, R., ZENG, H., PRIIMAGI, A. & SCHENNING, A. 2019. An Artificial Nocturnal Flower via Humidity-Gated Photoactuation in Liquid Crystal Networks. *Adv Mater,* 31**,** e1805985.

WANI, O. M., ZENG, H. & PRIIMAGI, A. 2017. A light-driven artificial flytrap. *Nat Commun,* 8**,** 15546.

WANI, O. M., ZENG, H., WASYLCZYK, P. & PRIIMAGI, A. J. A. O. M. 2018. Programming photoresponse in liquid crystal polymer actuators with laser projector. 6**,** 1700949.

WARE, T. H., MCCONNEY, M. E., WIE, J. J., TONDIGLIA, V. P. & WHITE, T. J. 2015. Voxelated liquid crystal elastomers. *Science,* 347**,** 982-984.

WEHNER, M., TRUBY, R. L., FITZGERALD, D. J., MOSADEGH, B., WHITESIDES, G. M., LEWIS, J. A. & WOOD, R. J. 2016. An integrated design and fabrication strategy for entirely soft, autonomous robots. *Nature,*

536**,** 451-5.

WEI, W., GAO, J., YANG, J., WEI, J. & GUO, J. 2018. A NIR light-triggered pyroelectric-dominated generator based on a liquid crystal elastomer composite actuator for photoelectric conversion and self-powered sensing. *RSC Adv,* 8**,** 40856-40865.

WEI, X., WU, Q., CHEN, L., SUN, Y., CHEN, L., ZHANG, C., LI, S., MA, C. & JIANG, S. 2023. Remotely Controlled Light/Electric/Magnetic Multiresponsive Hydrogel for Fast Actuations. *ACS Appl Mater Interfaces*.

WU, J., YAO, S., ZHANG, H., MAN, W., BAI, Z., ZHANG, F., WANG, X., FANG, D. & ZHANG, Y. 2021. Liquid Crystal Elastomer Metamaterials with Giant Biaxial Thermal Shrinkage for Enhancing Skin Regeneration. *Advanced Materials,* 33**,** 2106175.

WU, Y., YANG, Y., QIAN, X., CHEN, Q., WEI, Y. & JI, Y. 2020a. Liquid-Crystalline Soft Actuators with Switchable Thermal Reprogrammability. *Angew Chem Int Ed Engl,* 59**,** 4778-4784.

WU, Z., CHENG, P., ZHAO, W., FANG, J., XU, T. & CHEN, D. 2020b. Allyl sulfide-based visible light-induced dynamically reshaped liquid crystalline elastomer/SWCNT nanocomposites capable of multimode NIR photomechanical actuations. *New Journal of Chemistry,* 44**,** 10902-10910.

WU, Z., LIU, L., CHENG, P., FANG, J., XU, T. & CHEN, D. 2019. Reusable gold nanorod/liquid crystalline elastomer (GNR/LCE) composite films with UV-triggered dynamic crosslinks capable of micropatterning and NIR

actuation. *Journal of Materials Chemistry C,* 7**,** 14245-14254.

XIAO, L., CHEN, X., YANG, X., SUN, J. & GENG, J. J. A. A. P. M. 2020a. Recent advances in polymer-based photothermal materials for biological applications. 2**,** 4273-4288.

XIAO, Y.-Y., JIANG, Z.-C. & ZHAO, Y. 2020b. Liquid Crystal Polymer‐Based Soft Robots. *Advanced Intelligent Systems,* 2.

XIAO, Y. Y., JIANG, Z. C., TONG, X. & ZHAO, Y. 2019. Biomimetic Locomotion of Electrically Powered "Janus" Soft Robots Using a Liquid Crystal Polymer. *Adv Mater,* 31**,** e1903452.

XIE, R., COLBY, R. H. & GOMEZ, E. D. 2017. Connecting the Mechanical and Conductive Properties of Conjugated Polymers. *Advanced Electronic Materials,* 4.

XIONG, W., LIU, Y., JIANG, L. J., ZHOU, Y. S., LI, D. W., JIANG, L., SILVAIN, J. F. & LU, Y. F. 2016. Laser-Directed Assembly of Aligned Carbon Nanotubes in Three Dimensions for Multifunctional Device Fabrication. *Adv Mater,* 28**,** 2002-9.

XIONG, Z., ZHENG, C., JIN, F., WEI, R., ZHAO, Y., GAO, X., XIA, Y., DONG, X., ZHENG, M. & DUAN, X. 2018. Magnetic-field-driven ultra-small 3D hydrogel microstructures: Preparation of gel photoresist and two-photon polymerization microfabrication. *Sensors and Actuators B: Chemical,* 274**,** 541-550.

YAKACKI, C. M., SAED, M., NAIR, D. P., GONG, T., REED, S. M. &

BOWMAN, C. N. 2015. Tailorable and programmable liquid-crystalline elastomers using a two-stage thiol–acrylate reaction. *RSC Advances,* 5**,** 18997-19001.

YAMADA, M., KONDO, M., MAMIYA, J., YU, Y., KINOSHITA, M., BARRETT, C. J. & IKEDA, T. 2008. Photomobile polymer materials: towards light-driven plastic motors. *Angew Chem Int Ed Engl,* 47**,** 4986-8.

YANG, M., XU, Y., ZHANG, X., BISOYI, H. K., XUE, P., YANG, Y., YANG, X., VALENZUELA, C., CHEN, Y. & WANG, L. J. A. F. M. 2022a. Bioinspired Phototropic MXene‐Reinforced Soft Tubular Actuators for Omnidirectional Light‐Tracking and Adaptive Photovoltaics. 2201884.

YANG, Q., PENG, C., REN, J., ZHAO, W., ZHENG, W., ZHANG, C., HU, Y. & ZHANG, X. 2019. A Near‐Infrared Photoactuator Based on Shape Memory Semicrystalline Polymers toward Light‐Fueled Crane, Grasper, and Walker. *Advanced Optical Materials,* 7.

YANG, X., CHEN, Y., ZHANG, X., XUE, P., LV, P., YANG, Y., WANG, L. & FENG, W. 2022b. Bioinspired light-fueled water-walking soft robots based on liquid crystal network actuators with polymerizable miniaturized gold nanorods. *Nano Today,* 43.

YANG, Y. & SHEN, Y. 2021. Light‐Driven Carbon‐Based Soft Materials: Principle, Robotization, and Application. *Advanced Optical Materials,* 9.

YANG, Y., ZHAN, W., PENG, R., HE, C., PANG, X., SHI, D., JIANG, T. & LIN, Z. 2015. Graphene-Enabled Superior and Tunable Photomechanical

Actuation in Liquid Crystalline Elastomer Nanocomposites. *Adv Mater,* 27**,** 6376-81.

YAO, X., CHEN, H., QIN, H. & CONG, H. P. 2023. Nanocomposite Hydrogel Actuators with Ordered Structures: From Nanoscale Control to Macroscale Deformations. *Small Methods***,** e2300414.

YEUNG, K.-W., DONG, Y., CHEN, L., TANG, C.-Y., LAW, W.-C., TSUI, G. C.-P. & ENGSTRØM, D. S. J. N. R. 2020. Printability of photo-sensitive nanocomposites using two-photon polymerization. 9**,** 418-426.

YOU, R., CHOI, Y. S., SHIN, M. J., SEO, M. K. & YOON, D. K. 2019. Reconfigurable Periodic Liquid Crystal Defect Array via Modulation of Electric Field. *Advanced Materials Technologies,* 4.

YU, Y., LI, L., LIU, E., HAN, X., WANG, J., XIE, Y.-X. & LU, C. 2022a. Light-driven core-shell fiber actuator based on carbon nanotubes/liquid crystal elastomer for artificial muscle and phototropic locomotion. *Carbon,* 187**,** 97-107.

YU, Z., WANG, Y., ZHENG, J., SUN, S., FU, Y., CHEN, D., CAI, W., WANG, D., ZHOU, H. & LI, D. 2022b. Fast-Response Bioinspired Near-Infrared Light-Driven Soft Robot Based on Two-Stage Deformation. *ACS Appl Mater Interfaces,* 14**,** 16649-16657.

YUK, H., LIN, S., MA, C., TAKAFFOLI, M., FANG, N. X. & ZHAO, X. 2017. Hydraulic hydrogel actuators and robots optically and sonically camouflaged in water. *Nature Communications,* 8**,** 14230.

ZENG, H., WANG, Y., JIANG, T., XIA, H., GU, X. & CHEN, H. 2021. Recent progress of biomimetic motions-from microscopic micro/nanomotors to macroscopic actuators and soft robotics. *RSC Adv,* 11**,** 27406-27419.

ZENG, H., WANI, O. M., WASYLCZYK, P., KACZMAREK, R. & PRIIMAGI, A. 2017. Self-Regulating Iris Based on Light-Actuated Liquid Crystal Elastomer. *Adv Mater,* 29.

ZENG, H., WANI, O. M., WASYLCZYK, P. & PRIIMAGI, A. 2018. Light-Driven, Caterpillar-Inspired Miniature Inching Robot. *Macromol Rapid Commun,* 39.

ZENG, H., WASYLCZYK, P., PARMEGGIANI, C., MARTELLA, D., BURRESI, M. & WIERSMA, D. S. 2015. Light-Fueled Microscopic Walkers. *Adv Mater,* 27**,** 3883-7.

ZHAI, F., FENG, Y., LI, Z., XIE, Y., GE, J., WANG, H., QIU, W. & FENG, W. 2021. 4D-printed untethered self-propelling soft robot with tactile perception: Rolling, racing, and exploring. *Matter,* 4**,** 3313-3326.

ZHANG, A., WANG, F., CHEN, L., WEI, X., XUE, M., YANG, F. & JIANG, S. 2021a. 3D printing hydrogels for actuators: A review. *Chinese Chemical Letters,* 32**,** 2923-2932.

ZHANG, C., LU, X., FEI, G., WANG, Z., XIA, H. & ZHAO, Y. 2019a. 4D Printing of a Liquid Crystal Elastomer with a Controllable Orientation Gradient. *ACS Applied Materials & Interfaces,* 11**,** 44774-44782.

ZHANG, J., GUO, Y., HU, W., SOON, R. H., DAVIDSON, Z. S. & SITTI, M.

2021b. Liquid Crystal Elastomer-Based Magnetic Composite Films for Reconfigurable Shape-Morphing Soft Miniature Machines. *Adv Mater,* 33**,** e2006191.

ZHANG, Q. M. & SERPE, M. J. 2017. Stimuli-Responsive Polymers for Actuation. *Chemphyschem,* 18**,** 1451-1465.

ZHANG, W., NAN, Y., WU, Z., SHEN, Y. & LUO, D. 2022. Photothermal-Driven Liquid Crystal Elastomers: Materials, Alignment and Applications. *Molecules,* 27.

ZHANG, Y.-S., JIANG, S.-A., LIN, J.-D. & LEE, C.-R. 2020. Bio-inspired design of active photo-mechano-chemically dual-responsive photonic film based on cholesteric liquid crystal elastomers. *Journal of Materials Chemistry C,* 8**,** 5517-5524.

ZHANG, Y., ZHOU, S., CHONG, K. C., WANG, S. & LIU, B. 2019b. Near-infrared light-induced shape memory, self-healable and anti-bacterial elastomers prepared by incorporation of a diketopyrrolopyrrole-based conjugated polymer. *Materials Chemistry Frontiers,* 3**,** 836-841.

ZHANG, Y. L., TIAN, Y., WANG, H., MA, Z. C., HAN, D. D., NIU, L. G., CHEN, Q. D. & SUN, H. B. 2019c. Dual-3D Femtosecond Laser Nanofabrication Enables Dynamic Actuation. *ACS Nano,* 13**,** 4041-4048.

ZHAO, D. & LIU, Y. 2020. A prototype for light-electric harvester based on light sensitive liquid crystal elastomer cantilever. *Energy,* 198**,** 117351.

ZHAO, J., ZHANG, L. & HU, J. 2021a. Varied Alignment Methods and Versatile

Actuations for Liquid Crystal Elastomers: A Review. *Advanced Intelligent Systems,* 4.

ZHAO, T., ZHANG, Y., FAN, Y., WANG, J., JIANG, H. & LV, J.-A. 2022. Light-modulated liquid crystal elastomer actuator with multimodal shape morphing and multifunction. *Journal of Materials Chemistry C,* 10**,** 3796-3803.

ZHAO, Y., LO, C.-Y., RUAN, L., PI, C.-H., KIM, C., ALSAID, Y., FRENKEL, I., RICO, R., TSAO, T.-C. & HE, X. 2021b. Somatosensory actuator based on stretchable conductive photothermally responsive hydrogel. *Science Robotics,* 6**,** eabd5483.

ZHAO, Y., LO, C.-Y., RUAN, L., PI, C.-H., KIM, C., ALSAID, Y., FRENKEL, I., RICO, R., TSAO, T.-C. & HE, X. J. S. R. 2021c. Somatosensory actuator based on stretchable conductive photothermally responsive hydrogel. 6**,** eabd5483.

ZHENG, C., JIN, F., ZHAO, Y., ZHENG, M., LIU, J., DONG, X., XIONG, Z., XIA, Y. & DUAN, X. 2020. Light-driven micron-scale 3D hydrogel actuator produced by two-photon polymerization microfabrication. *Sensors and Actuators B: Chemical,* 304.

ZHENG, W. J., AN, N., YANG, J. H., ZHOU, J. & CHEN, Y. M. 2015. Tough Al-alginate/Poly(N-isopropylacrylamide) Hydrogel with Tunable LCST for Soft Robotics. *ACS Applied Materials & Interfaces,* 7**,** 1758-1764.